University of Granada

Physics and Space Sciences

Doctoral Thesis

Osteblastic cell response of biomimetic coatings formed on titanium surfaces mediated by self-assembled films

Authoress:

Alda Yadira

Sánchez-Treviño

Supervisors:

Dr. Miguel A.

Rodríguez-Valverde

Dr. Miguel A.

Cabrerizo-Vílchez

Editor: Editorial de la Universidad de Granada
Autor: Alda Yadira Sánchez Treviño
D.L.: GR 1880-2014
ISBN: 978-84-9083-064-2

La doctoranda Dª Alda Yadira Sánchez-Treviño y los directores de la tesis D. Miguel A. Rodríguez-Valverde y D. Miguel A. Cabrerizo-Vílchez, garantizamos, al firmar esta tesis doctoral, que el trabajo ha sido realizado por la doctoranda bajo la dirección de los directores de la tesis y hasta donde nuestro conocimiento alcanza, en la realización del trabajo, se han respetado los derechos de otros autores a ser citados, cuando se han utilizado sus resultados o publicaciones en la realización del trabajo.

Granada, February 17, 2014

Director de la Tesis	Director de la Tesis	Doctoranda
		
M.A. Rodríguez-Valverde	M.A. Cabrerizo-Vílchez	A.Y. Sánchez-Treviño

Contents

Acknowledgments

This work was supported by the "Ministerio Español de Ciencia e Innovación" (BES-2009-025032 project MAT2007-66117 and project MAT2011-23339) and the "Junta de Andalucía" (projects P08-FQM-4325 and P09-FQM-4698). Yadira and her supervisors are very grateful to the Biocolloid and Fluid Physics group (http://biocol.ugr.es/) and to the Department of Applied Physics (http://fisicaaplicada.ugr.es/) of the University of Granada (http://www.ugr.es/).

Yadira and her supervisors also thank to Dr. Carlos Manuel Rodríguez Navarro of

the Department of Mineralogy and Petrology for the XRD analysis, José Antonio Martín, Daniel Blasco Avellaneda, Miguel A. Fernández, and Dr. Carmen L. Moraila of the Applied Physics Department for the help in the experimental work, and Dr. Elvira de Luna Bertos, Dr. Javier Ramos Torrecillas, Dr. Olga García Martínez and Dr. Concepción Ruiz from the Department Nursing for the cell cultures. Also we thank to Dr. Isabel Sánchez Almazo, Laura Méndez Liñán and Elena Villafranca Sánchez from CIC-UGR for the ESEM and XPS analysis. We thank to Dr. Marco Morra and Dr. Clara Cassinelli from Nobil Bio Ricerche and Dr. Sandra Elizabeth Rodil Posada, Dr. Phaedra Suriel Silva Bermudez and Johan Restrepo from the PlasNaMat group of the UNAM for enrichment and contribution during the two short - term stages during this research. Finally, Yadira is also grateful to Dr. Alberto Martín Molina, Dr. Julia Maldonado Valderrama and Germán Luque Caballero for the recognition by the experimental work in AFM, to Dr. Juan I. Rosales of the Department of Stomatology for fruitful discussions, and Dr. Miguel Ángel Rodríguez Valverde and Dr. Miguel Ángel Cabrerizo Vílchez for their supervision and help.

CASTELLANO

Agradezco la oportunidad que tuve de venir a Granada a realizar esta tesis profesional y de vida, de la que he aprendido mucho y madurado más en esos dos ámbitos. Me agradezco a mi misma el valor, esfuerzo y la constancia demostrada para lograr este objetivo. Agradezco inmensamente el apoyo de mis abuelos Conchita y Felipe para poder cruzar el Atlántico, así como el de mi madre Ana María y hermana Liz y a los miembros de la familia Treviño por el cariño que me han dado.

La amistad brindada por Carmen María, Rosa, Sabrina, Marisel, Carlos, Marcos, esos pequeños momentos me alentaron mucho cuando lo necesité. A mis italiana(o)s querida(o)s que me trataron maravillosamente en esa estancia en 2011 en Portacomaro: Marco, Clara, Giovanna, Daniele, Nunzia, Abi, Vale, Sabri. A mis mexicana(o)s Fabi, Idah, Zula, Pao,

Raúl, Erika y todas esas personas que hicieron el 2012 en Granada divertido, más llevadero y me mostraron la cara buena de las personas.

A mis pumas de la UNAM multiculturales por esa estancia tan única, divertida, llena de aprendizaje y cariñosa, esa calidez brindada significó un impulso muy grande en mi vida, muchas gracias Liz, Osmary, Roberto, Beti, Johan, Andrés, Argelia, Bart, Víctor, Juan Carlos, Iván, Ernesto, Marco, Giovanni, Óscar.

Agradezco el apoyo moral, aceptación y el cariño de mis bellas amigas danzarinas que un poco tarde entraron en mi vida, sin su apoyo no hubiera logrado dar el último paso: Isabel, María Ángeles, Maria Dolores, Candi. Así como esa complicidad y buen ambiente de esas clases sabatinas para reponer energía que no hubieran sido posibles sin las demás niñas: Ague, Sandra, Rosalía, Carmen, Sheila, María.

A todas esas personas que me brindaron cosas buenas durante estos años en España, personas que recién conozco pero me han aportado cosas positivas (Núria, Hak, Fede), así como a personas cálidas y humanas que forman parte del departamento de física aplicada de la UGR: María Tirado, Conrado, José Antonio, Arturo Moncho, Miguel Heredía, José Callejas, Delfi, Paola, Germán, Alberto, Kasia, Ricardo, Leonor, Juan Luis, Fernando Vereda, Ana Belén, Ángel Delgado, Modesto, Jorge Portí y no menos importante a mis jefes y tutores Miguel Ángel y Cabrerizo por el apoyo, la guía y el aprendizaje que han dejado en mi.

Summary

Titanium is considered a well - established material for dental implantology but an improved healing response for early loading is still open. Biomimetic strategies are proposed to solve this problem from bioinspired coatings formed on the titanium surface. Our aim was to decrease the induction time during the biomimetic precipitation on cpTi surfaces modified with alkylphosphonate molecules. During this time, ions and complexes from a supersaturated physiological solution (SBF) are adsorbed onto the titanium surface leading to the formation of a bone - like apatite layer. In this dissertation we studied the biomimetic coatings formed over ultra - polished cpTi surfaces modified with different alkylphosphonate molecules with terminal groups with different affinity for apatite nucleation. We found that we were able to form Self Assembled Films (SAFs) rather than SAMs with mixed structures with different heterogeneity degree and that polymorphism was usually observed in the coating for the same molecule in different samples with a morphology that evolves as the

immersion time in SBF. Also we found, in our biomimetic coverages, the amorphous nature of HA as happens in natural bone and teeth previous to the formation of apatite crystals, the fluid retention capacity for each SAF and the optimal end group for our purpose based on our cell results and cristallinity degree. The framework of the current research is the BIOTIMP project (http://wdb.ugr.es/local/biotimp).

CASTELLANO

El titanio es considerado un material bien establecido para la implantología dental, sin embargo, la respuesta mejorada de curación para la carga temprana es un tema que aún sigue abierto. Se han propuesto estrategias biomiméticas para resolver este problema de recubrimientos bioinspirados formados sobre superficies de titanio. Nuestro objetivo fué disminuir el tiempo de inducción durante la precipitación biomimética en superficies de titanio comercialmente puro (cpTi) modificadas con moléculas de alquilfosfonatos. Durante este tiempo, los iones y complejos de una solución fisiológica sobresaturada (SBF), se adsorbieron sobre la superficie de titanio conduciendo a la formación de una apatita parecida a la existente en el hueso. En esta tesis se estudiaron los recubrimientos biomiméticos formados sobre superficies ultrapulidas de cpTi modificadas con diferentes moléculas alquilfosfonato con grupos terminales que poseen diferente afinidad para la nucleación de apatita. Hemos sido capaces de formar películas auto - ensambladas (SAFs), en lugar de SAMs, con estructuras mixtas con diferente grado de heterogeneidad; además el polimorfismo se observó generalmente en los recubrimientos biomiméticos para una misma molécula pero en diferentes muestras, con una morfología que evolucionó conforme al tiempo de inmersión en SBF. También encontramos, en nuestros recubrimientos biomiméticos, la naturaleza

amorfa de la HA como ocurre en el hueso natural y los dientes anterior a la formación de cristales de apatita, la capacidad de retención de líquidos para cada SAF y el grupo final óptimo para nuestro propósito basado en nuestros resultados de estudios celulares y grado de cristalinidad. El marco de la presente investigación es el proyecto BIOTIMP.

CHAPTER 1

Introduction

1.1 Motivation

Titanium is considered a key material for the actual biomaterial applications. Titanium is a strong, lightweight, silver-gray metal that is found commonly in igneous rocks and geological deposits. Titanium has the ability to bind with human bone in a process called biointegration or osseointegration. The mechanical properties of titanium are also similar to bone. Because of this, and the fact that the body does not reject it, titanium can be used as medical and dental implant. In general, titanium is known to be stable over long implantation times and resistant against corrosion, due to its surface oxide (passive) layer

(*1*). Other known properties of titanium are its capacity to adsorb osteogenic proteins and to induce differentiation of bone cells (*1–5*). Although numerous studies (*6–10*) have been addressed to the use of titanium for the replacement of body functions, there are still unsolved problems in the design of titanium devices. Nevertheless, titanium implants are successfully used in orthopedics, osteosynthesis and maxillofacial area (*2*). The current titanium surgical implants have a high success rate (90% to 95%), in healthy patients (*11*). In the case of dental implants, the improved healing response and early loading, i.e. an accelerated osseointegration, are still open issues (*2*).

Biomineralization is the natural process produced in human beings and animals resulting in the formation of bones and teeth. The mechanisms that lead the biomineralization are currently being discused (*12*). Bonelike coatings are often applied to metallic implants to enhance the clinical success (*3*). Various methods have been employed to deposite hydroxyapatite (HA) onto metal implant surfaces to improve and accelerate their integration with bone tissue (*13–15*). A key step in the HA coating process is the initial nucleation of calcium phosphate on the implant surface. Various methods (*16–18*) are used to design surfaces capable for nucleating apatite. The nucleation plays a decisive role in determining the crystal structure and size distribution (*19*). Therefore, understanding the fundamentals of nucleation is crucial. The deposition of significant amounts of calcium phosphate on titanium requires the incubation in Simulated Body Fluid (SBF) for several days or longer (*4*, *5*, *20*, *21*). However, the induction period of apatite nucleation is remarkably long for functionalized titanium surfaces. Therefore, there is an interest in decreasing the induction period or speeding up the nucleation process of bonelike apatite. During this time, ions and complexes from the SBF are adsorbed onto the titanium surface leading to the formation of an apatite layer. To our knowledge, only a few studies have been conducted on the use of self-assembly techniques to produce Ca/P layers on Ti in SBF. Certain surface functional groups are effective to nucleate calcium phosphate on titanium surfaces

(22). In this context, the chemical functionalization of commercially pure titanium using organophosphonates for a biomimetic purpose has not been exploited yet.

1.1.1 Glossary

This glossary collects a selection of technical words related to titanium and its modification with biomimetic purposes. The words are shown on a hierarchical order.

- Biomaterial. A synthetic material used to replace part of a living system or to function in intimate contact with living tissue.

- Apatite. A group of phosphate minerals, formed by calcium phosphate and usually referring to hydroxylapatite (or hydroxyapatite (HA)), fluoroapatite (or fluorapatite), and chloroapatite (or chlorapatite), as the presence of hydroxide (OH^-), fluoride (F^-), and chloride (Cl^-) ions, respectively. In particular, hydroxyapatite is the main constituent of tooth enamel, and a special form of apatite found in bone: bone-like apatite.

- Calcium phosphate (CaP). A family of minerals containing calcium ions (Ca^{2+}) together with orthophosphates (PO_4^{3-}), metaphosphates or pyrophosphates ($P_2O_7^{4-}$) and occasionally hydrogen or hydroxide ions. Calcium phosphate is formed when free calcium interacts with phosphate and its chemical formula is $Ca_3(PO_4)_2$.

- Nucleation. Series of atomic or molecular processes by which the atoms or molecules of a reactant phase rearrange into a cluster of the product phase large enough as to have the ability to grow irreversibly to a macroscopically larger size. Most nucleation processes are physical, rather than chemical.

- Crystal growth. Major stage of a crystallization process, and consists in the addition of new atoms, ions, or polymer strings into the characteristic arrangement of a crystalline Bravais lattice. The growth typically follows an initial stage of either homogeneous or heterogeneous nucleation.

- Induction time. Amount of time elapsed between the contact of a supersaturated solution with a surface and the observation of crystals on it. Factors such as ion concentration, temperature, agitation, presence of impurities, can affect the induction time.

- Cell attachment (or cell adhesion). Binding of a cell to a surface, such as an extracellular matrix, another cell or a biomaterial.

- Cell proliferation. Process where a cell grows or the cell number density increases.

- Cell differentiation. Process where a cell becomes more specialized. Differentiation dramatically changes as the cell size, shape, membrane potential, metabolic activity, and responsiveness to signals. Cells can have very different physical characteristics although they have the same genome.

- Bioactivity. The property of a biomaterial to directly bond with new forming bone. The biomaterial interacts with the natural environment of the body and determines a positive biological effect. For instance, the synthetic calcium phosphate (CaP) is able to induce biological integration to living soft and hard tissues.

- Biocompatibility. The behaviour of a biomaterial to produce little or no immune response into the body.

- Osteoconductivity. Ability of a biomaterial to serve as a scaffold or template to guide formation of newly forming bone along its surface. The biomaterial stimulates the migration of adjacent bone - forming cells to induce the growth of bone tissue.

- Osteointegration. The full process of obtaining a firm anchoring and incorporation of the biomaterial into living bone without fibrous tissue formation at the interface.

1.1.2 Titanium

Titanium (Ti) is the ninth most abundant element on Earth, with 0.8% in weight. Titanium is known since XVIII century. In 1795 Heinrich Klaproth rediscovered it althought he was not able to get the pure metal. Despite its large presence in the crust, in 1937 titanium began to be used in a large variety of applications thanks to the efficient separation of minerals (*23*).

Currently, titanium is obtained in large quantities classified as commercially pure titanium (different grades), titanium alloys or alloying titanium (*24*). Commercially pure titanium (cpTi) is classified into four grades depending on the amount of interstitial elements (Table 1.1). Preparation of commercially pure titanium is difficult while the preparation of its alloys is easier.

Pure titanium has the characteristic of being thermodynamically unstable and highly reactive in presence of oxygen (*23*). Titanium spontaneously forms titanium oxide. Due to this high reactivity, a clean titanium surface is rapidly polluted by adsorption of adventitious organic molecules (e.g. from the ambient atmosphere). This cannot be avoided under normal laboratory or industrial production conditions.

In metal titanium, the oxygen has a limited solubility. For this reason, the $O : Ti$ ratio is much lower in the bulk metal than on the surface. The oxide layer formed on the titanium surface usually has an average thickness of 3 - 7 nm (*23*), and it slowly increases over periods of time of months to years upon normal conditions. Depending on the oxidation state of metal titanium, different stochiometries are known (*25*): TiO_2 (+IV), Ti_2O_3 (+III), TiO

(+II) and *Ti* metal (0); being the most stable and common oxide the titanium dioxide. At room temperature, native oxide films are mostly amorphous, but at higher temperatures $\geq$ (500^{o}C), two crystalline phases are observed: rutile and anatase (*26*). In both cases, titanium atoms are coordinated to six oxygen anions, the preferred coordination in many titanium compounds (*23*). The existence of a stable, repassivating, chemically inert and corrosion-resistant oxide layer is the primary reason for the passive properties of titanium metal surfaces. However, the knowledge of the characteristics and properties of the oxide layer during each production step of an implant still remains incomplete.

The interaction between titanium oxide and biological fluids is important for understanding the biocompatibility of titanium. Its known that, after implantation in bone, titanium is tolerated by human tissues. A high affinity between titanium dioxide and calcium phosphates has been also reported (*2*). The biocompatibility may be explained by two parameters: a high surface density of hydroxides and a negative electrical charge at physiological pH. Both factors induce strong protein - surface interactions (*1*).

The high reactivity of titanium makes the obtention of pure metal very hard. Pure titanium is soft and ductile, and it is very easily damaged by mechanical twinning in sectioning and grinding. All refractory metals are indeed very difficult to section and have low grinding and polishing rates.

Table 1.1: ASTM classification for commercially pure titanium as the chemical composition in wt%. (*27*)

Grade	Fe max	O approx	N max	C max	H max
I	0.2	0.18	0.03	0.1	0.0125
II	0.3	0.25	0.03	0.1	0.0125
III	0.3	0.35	0.05	0.1	0.0125
IV	0.5	0.40	0.05	0.1	0.0125

1.1.3 Calcium phosphate

Calcium phosphate represents the most important and widely exploited class of bio-inorganic materials used to modify titanium surfaces for bone - bonding biomedical applications. Calcium orthophosphates are of special significance in the field of biomaterials because they compose the main mineral part of bones and teeth (*28*–*32*). For more than three decades, calcium orthophoshates ceramics have found clinical applications in orthophedic, spinal and maxillofacial surgery as bone substitutes (*33*–*36*). The synthetic bone - like apatite coatings are successfully used for filling bone defects in various clinical indications as they are considered bioactive and osteoconductive, guiding the bone healing process (*3*). The core mechanism of bioactivity is the partial dissolution and release of ionic products *in vivo*, elevating local concentrations of calcium and phosphate and precipitating a biological apatite on the biomaterial surface (*37*, *38*). This apatite layer formed *in vivo* is colonized by osteoblastic cells producing the bone extracellular matrix. All calcium ortophosphates consists of three major chemical elements: calcium (+II), phosphorus (+V) and oxygen (-II) (*39*). Calcium orthophosphates comprise a wide family of compounds having various chemical compositions, crystallographic structures, and solubility in water (Table 1.2).

1.2 Biomimetic strategies

Calcium phosphate coatings on metal implants show high biocompatibility and enhanced corrosion resistance but, on the other hand, exhibit poor adhesion properties due to their brittleness (*3*). The brittle nature of calcium phosphate is a serious drawback during surgical operation or after implantation, since it does not provide the necessary mechanical stability of the interface between the coating and the titanium substrate.

Table 1.2: Chemical compositions and Ca/P ratios, of some synthetic and biological calcium orthophosphates. (3) ⊔ represents a lacuna in the crystal lattice of hydroxyapatite.

Orthophosphate	Abbreviation	Chemical formula	Ca/P
Dicalcium phosphate dihydrate (brushite)	DCPD	$CaHPO_4$. $2H_2O$	1.0
Octacalcium phosphate	OCP	$Ca_8(HPO_4)_2(PO_4)_4$. $5H_2O$	1.33
Calcium-deficient apatite	CDA	$Ca_{10-x\sqcup x}(HPO_4)_x$ $(PO_4)_{6-x}(OH)_{2-x\sqcup x}$ (0 < x < 2)	Variable 1.33 - 1.66
Amorphous calcium phosphate	ACP	$Ca_x(HPO_4)_y(PO_4)_z$. nH_2O n = 3.0-4.5; 15-20 wt% H_2O	Variable 1.2-2.2
β-Tricalcium phosphate	β-TCP	β-$Ca_3(PO_4)_2$	1.50
α-Tricalcium phosphate	α-TCP	α-$Ca_3(PO_4)_2$	1.50
Hydroxyapatite	HA	$Ca_{10}(PO_4)_6(OH_2)$	1.67

The biomimetic coating process is defined as a method whereby a biologically active HA layer is formed on a substrate. Because of its similarity to the mineral phase of natural hard tissues, artificial HA is considered to be a bioactive material (40). It has been proved that thin HA layers formed on cpTi surfaces affect the cellular attachment and spreading (3). A thin HA layer appears to be more osteoconductive to cellular attachment rather than raw cpTi. For this reason, HA - coated implants develop a strong connection with the bone tissue in a short time (41).

Biologically active calcium phosphate ions are implanted into titanium surfaces to enhance the bioactivity and biocompatibility (42–47). Ion implantation improves the ability of titanium to induce the formation of natural calcium phosphate on the surfaces. The results reported in literature (48) show a higher ability to nucleate HA on the implanted surface compared to unmodified titanium surface. High dose of ion implantation into titanium alloys has also been shown to significantly enhance the MG - 63 cell adhesion and spreading (45). Nevertheless, ion implantation present problems as crystallographic damage, damage

recovery, amorphization, sputtering and ion channelling.

Various techniques have been developed for producing HA coatings on implant surfaces, such as plasma spraying (*49*), hot isostatic pressing (*50*), sol - gel technique and biomimetic precipitation(*51*). Unfortunately, subsequent heat treatment at high temperature results in cracking and poor bond strength between the HA coating and metal substrate. Besides, a HA coating desirable for optimal biocompatibility, could not be achieved through these methods.

The strategies of biomimetic precipitation, where calcium phosphate layers are formed on the biomaterial surface by immersion in SBF, is a low temperature process that offers the advantage of deposition on complex - shape and porous implants (*52*). In addition, the physiological conditions of the SBF allow incorporation (by codeposition) of osteogenic agents that are inactivated at high temperatures (*53*, *54*). Calcium phosphate precipitation is similar to biological mineralization. The SBF is an artificial supersaturated calcium phosphate solution with ion concentrations and pH value similar to those ones of human blood plasma. SBF has been frequently used to create biomimetic apatite coatings on different biomaterials (*55*). Nevertheless, the mechanical stability of the calcium phosphate coating typically requires a rough titanium surface to ensure the mechanical retention of the coating. In contrast to geologically generated apatites, crystals grown from a SBF or during *in vivo* biological processes, are of nanoscopic size, nonstoichiometric, and lacking long - range order (*56*).

1.3 Chemical functionalization with organophosphonates

Modifications of the roughness of titanium surfaces and its effect on the *in vitro* and *in vivo* biological responses have been extensively investigated (*57*, *58*). Techniques such

as machining, sand blasting, plasma spraying, chemical or acid etching have been used to produce topographical features distributed randomly over the surface. Instead, we have focused on smooth surfaces to achieve a controlled surface chemical modification. It is possible to form chemically controlled, structurally ordered films on different metal oxide substrates (*59*). This system involves the spontaneous adsorption of certain components from a solution in contact with the substrate (*60*). Phosphates and phosphonates are molecules with high affinity towards metal oxides (*61*).

The stability of organophosphonates on oxide - covered surfaces is based on their high interfacial bond strength due to the different bindings to the substrate and on the molecular van der Waals interactions of the alkyl chains (*62*). Alkyl phosphates and phosphonates constitute two further systems that have been shown to form Self Assembled Films (SAFs) on metal oxide surfaces. Liu. et al. (*53*) produced a range of alkyl - based SAFs on titanium foil, each containing differente end groups: $-OH$,$-COOH$, phosphate ($-PO_4H_2$), and vinyl ($-CH = CH_2$). Crystalline HA formation was succesfully obtained with $-PO_4H_2$ and $-COOH$.

The alkyl - phosphonate SAFs have been shown to have a better surface coverage and hydrolytic stability in alkaline conditions as compared to certain types of silane films (*63*, *64*). These properties make phosphonate platforms very promising candidates for real - life applications that require long - term stability of the deposited layer. Nevertheless, unlike SAMs on gold surfaces, it is not common in the literature to find an optimized procedure to produce SAFs on metal titanium. Adhesion and stability of phosphoponic acids on titanium oxides (specially TiO_2) are greatly enhanced by thermal annealing. Heating the deposited film results in covalent attachment of the alkylphosphonates to the substrate (*65*). Phosphonic acid based SAM formation has been reported on Al_2O_3, TiO_2, ZrO_2, planar mica, and SiO_2 substrates, although proof of monolayer films has only been provided

in a few cases (65).

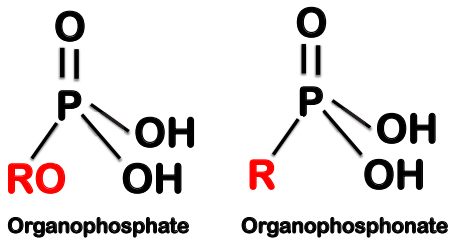

Figure 1.1: Phosphate and phosphonate molecules.

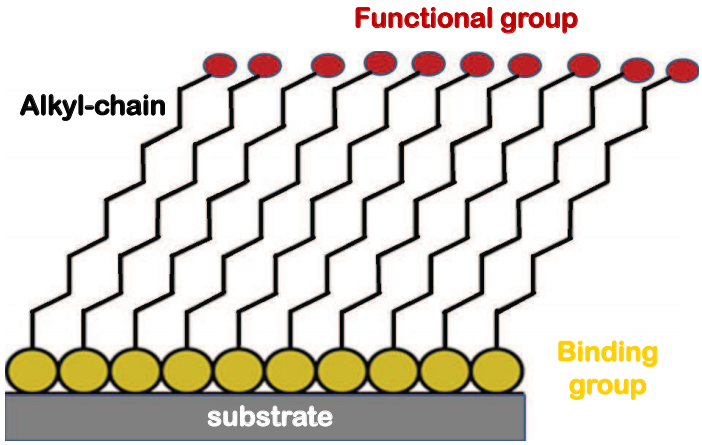

Figure 1.2: Scheme of an organophosphonate molecule: binding group, alkyl - chain and fuctional group.

Organophosphonates and organophosphates are structurally similar. The difference between phosphate and phosphonate is the absence of an oxygen atom between phosphorus and the first carbon atom of the alkyl chain in the molecule. An organophosphate has four oxygens with an alkyl group connected via a phosphoester bond. Phosphonates have three oxygens with a carbon attached directly to phosphorus (Fig. 1.1). Phosphonates have the advantage of being more chemically stable than the phosphates (66). Also, the lack of a hydrolyzable $P-O-C$ linkage makes phosphonate compounds more stable in aqueous solution and easier to make SAMs with than organophosphate compounds (67). A phosphonate is a salt or an ester of the family of phosphonic acids. Their use in a variety

of applications is well stablished and their importance in a range of fields is increasing (*68*). Organophosphonates are characterized by three main parts: the binding group, the alkyl - chain and the fuctional group (Fig. 1.2). In a dense well - packed molecular layer, only the terminal functional group is exposed to the environment, and this determines the physico - chemical properties of the modified surface (*69*). The binding group and the substrate form a covalent or ionic bond when the substrate is hydroxylated. This is due to the acidity of the phosphonic acids (pKa $\sim$ 2) that promotes the chemisorption to the oxide surfaces, such as carboxylic acids (*70*).

Generally, hydrophilic surfaces favor the HA formation more strongly than hydrophobic surfaces (*16*). Biocompatibility may be improved with the introduction of more hydrophilic groups and a decrease of hydrophobic groups on the biomaterial surface. Negatively charged surfaces are able to induce the HA formation rather than positively charged surfaces (*5*). The carboxyl group, is negative in aqueous solution because of the two oxygens, and can form hydrogen bonds becoming hydrophilic. Carboxyl end groups appeared to provide the optimal surface for nucleation and growth of biomimetic crystalline HA (*22*). The phosphonate functional groups are also potents nucleating calcium phosphate deposition on surgical titanium implants (*22*). Phosphonate head groups are a promising alternative since they are relatively robust and can be attached to a wide range of oxide surfaces.

The presence of $P-O-Ti$, $P=O$ or $P-OH$ in the SAF indicate that mono -, bi - and tri - dentate surface phosphonate units (see Fig. 1.3) can be present in these layers, respectively. The relative contribution of each form may vary according to the alkyl - chain (*71*).

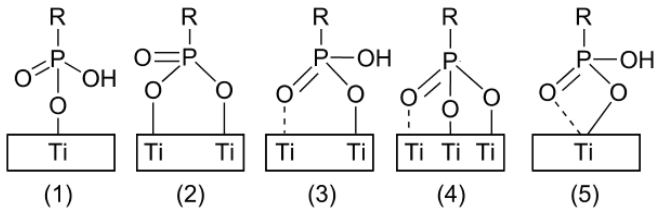

Figure 1.3: Scheme of the binding modes between phosphonic acid and titanium dioxide (*71*): (1) monodentate, (2) and (3) bridging bidentate, (4) tridentate and (5) chelating bidentate.

1.4 Nucleation and growth of bone - like apatite

The processes of calcium phosphate formation is important in our understanding of both bone and tooth formation (*72*). In bone and teeth, the formation of apatite crystals is preceded by an Amorphous Calcium Phosphate (ACP) precursor phase (*73*, *74*). The nucleation can be homogeneous, in absence of foreign particles or crystals in the solution, or heterogeneous, in presence of clusters or complexes in the solution. Both types of nucleation are collectively known as primary nucleation. The secondary nucleation takes place when nucleation is induced by the presence of crystals of the same substance (*75*). Homogeneous nucleation is rarely achieved since it is impossible to eliminate totally solid particles in the solution. Moreover, heterogeneous nucleation is energetically favored as compared to homogenous nucleation (*76*) even upon low supersaturation conditions. Secondary nucleation mechanism will be more favorable than both heterogeneous and homogeneous nucleations and thus produced at lower supersaturation conditions. Previous studies (*48*, *53*, *77*, *78*) on HA growth in *in vitro* models suggest that the precipitation is initiated by heterogeneous nucleation, process that is not affected by surface roughness (*48*). Three kinds of driving forces are thought to take place during the nucleation process in the solid - aqueous solution systems: electrostatic interaction, London van der Waals interaction and hydration interaction. The electrostatic interaction is considered as the main factor in inducing nucleation

of calcium phosphate. Yamashita et al. (*77*) demonstrated that heterogeneous nucleation of calcium phosphate happens on negatively charged surface. A negatively charged surface attracts positive calcium ions thereby increasing the local nucleation rate of apatite from the solution. One may also expect that the negative surface expels the phosphate anions. It is well known that SBF is supersaturated with HA, ACP and Octa Calcium Phosphate (OCP). This kind of solution is metastable and nucleation may take place if small changes occur in the solution. Nucleation occurs when an activation energy barrier is exceeded. This activation energy can be decreased by increasing the degree of super-saturation or by decreasing the interfacial energy. In fact, several studies have found that the calcium ions are rapidly adsorbed to the titanium surface (*5*, *79*). The least thermodynamically stable phase of calcium phosphate nucleates and grows on the surface, followed by nucleation and growth of more stable phases. The nucleation of OCP and ACP is energetically favored because the surface energy of HA is higher than that of OCP and ACP (*48*). The ACP formation is thought to proceed through prenucleation clusters: stable clusters that are present in solution already before nucleation. However, the role of such nanometer-sized clusters as building blocks for ACP has been debated for many years (*72*), and a number of differences between theoretical predictions and experimental results suggest that nucleation of solids from solution does not proceed via the classical pathway but follows more complex routes.

At the early stage of implantation, the fast dissolution of soluble coatings enhances bone formation, whereas non - soluble calcium phosphate leads to a better fixation between the implant and the hosting bone.

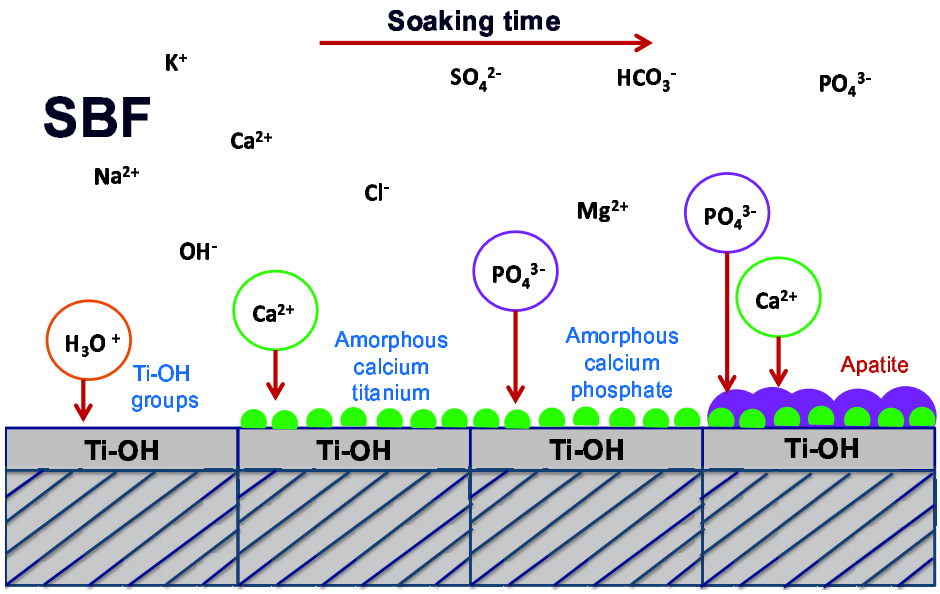

Figure 1.4: Layout of nucleation and growth of hydroxyapatite in time on a hydroxylated titanium surface inmersed in a SBF solution.

1.5 Aim and Challenges

The aim of this dissertation is to study the impact of the biomimetic properties of titanium surfaces on the *in vitro* biological events occurring during the early stages of osseointegration, in order to improve or accelerate it. We will focus on biomimetic titanium surfaces, namely cpTi coated by a osteoblastic precursor. This strategy of biologically inspired surfaces is based on the formation of a calcium phosphate layer on the biomaterial surfaces by immersion in a SBF. This route can be substantially improved if the cpTi surfaces are functionalized with self-assembled films of organophosphonates. Controlling chemical functionalization in soft matter enables the creation of novel biomaterials that positively interact with the host, in such a way that the biomimetic surface will guide cell growth and even, accelerate the foregoing biological events to bone healing. We expect that the final biomimetic coating is controlled by the properties of the underlying self - assembled film.

This dissertation is divided into six chapters, including the current chapter. The materials

and methods and the analytical techniques used for the characterization of the titanium surfaces and the coatings are detailed in Chapter 2. The protocol followed for the chemical functionalization of cpTi surfaces and the characterization of the modified cpTi surfaces are shown in Chapter 3. A preliminary study of the chemical functionalization of titanium surfaces with organophosphonates molecules and biomimetic coatings is described in Chapter 4. The effect of the phosphonate molecules in the nucleation and growth of HA and the subsequent cell behaviour is shown in Chapter 5. Finally, the effect of the immersion time in the SBF solution is described in Chapter 6.

The challenges found in this thesis work are listed below:

1) To obtain commercially pure titanium surfaces with a nanometer scale roughness.

2) To work with an evolving surface of titanium: oxidation state, stabilization of surface.

3) To design the chemical functionalization of commercially pure titanium surfaces.

4) Adaptation of cell culture protocols and other, cell assays on titanium samples with two different sides and with a very especific diameter.

5) To perform long-term SBF immersion from few days up to weeks.

6) Preparation of a large amount of samples (50 to 200 per study).

7) To measure the wettability of porous HA-covered surfaces.

CHAPTER 2

Materials and methods

2.1 Preparation of titanium surfaces

2.1.1 Ultrapolishing and cleaning

Pure titanium is soft and ductile due to this, titanium is very easily damaged by mechanical twinning in sectioning and grinding. All refractory metals are very difficult to section and have low grinding and polishing rates. However, we established a protocol for polishing cpTi surfaces with final roughness below micrometer scale ($R_q \geq 0.4$ nm, $R_a \geq 0.6$ nm over an area of 1 μm^2). Commercially pure titanium (cpTi) is most commonly used in

dental applications due to its high values of corrosion resistance and ductility.

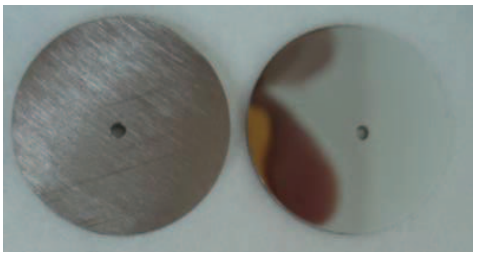

Figure 2.1: Images of a raw disc of cpTi (left) and an ultrapolished disc of cpTi (right).

We prepared titanium surfaces from ingots (16 mm - diameter) of cpTi grade II (Manfredi). The titanium ingots were cut into discs with a thickness of 1.6 mm. The titanium discs were finely polished (see Fig. 2.1) with a grinder (Beta Grinder/polisher, Buehler) using sandpapers of different degree and a wool with a suspension of diamond particles (9 μm) and next a colloidal silica solution (60 nm). After the polishing process, the titanium surfaces were subjected to a first cleaning process where the residues of the glue and polishing solutions were removed. This cleaning process consisted of ultrasonic rinses in acetone, soap solution, ethanol and finally Milli-Q water. Before the chemical functionalization, the samples were subjected to ultrasonic bath in acetone for 45 min and then they were dried with filtered argon gas (Linde UN 1006). Next, the samples were treated with radio frequency plasma (Emitech, KX1050 Plasma Asher) of argon to a power of 25 W for 15 min to remove organic impurities. Immediately after the plasma treatment, the oxidation state of the samples was stabilized in water for 24 h, and next they were dried with filtered argon gas. Finally, the samples were placed in an oven (DeLonghi EO420) at 140^{o} C for 15 min to remove traces of water and to hydroxylate the titanium surface (*59*, *80*, *81*).

Table 2.1: Molecules of the organophosphonate used in this work.

Organophosphonate	Abbreviation	alkyl-chain length (carbon units)	functional group
Octadecyl phosphonic acid	ODPA	18	methyl ($-CH_3$)
16-phosphono hexadecanoic acid	PHDA	16	carboxyl ($-COOH$)
12-Phosphonododecyl phosphonic acid	PDDPA	12	phosphonate ($-PO(OH)_2$)

2.1.2 Chemical functionalization

The chemical functionalization of the titanium sufaces was carried out with three different molecules of organophosphonate. The molecules selected are shown in Table 2.1 and Fig. 2.2. The alkylphosphonates have great affinity for metal oxide such as TiO_2. This affinity is due to the ability of the phosphonate group to displace the hydroxide ions that coordinate to the metallic specie exposed on the surface. This way, the alkylphosphonates form a permanent layer on TiO_2. Due to the amphoteric behavior of the surface titanol groups ($TiOH$), titanium reveals positive ($TiOH^+$) or negative (TiO^-) charge out its surface, depending on the pH. The isoelectric point (IEP) of the titanium is the pH value at which the zeta potential passes through zero (i.e. the substrate is electrically uncharged). As reported by Moraila - Martínez et. al. (*82*), the colloidal TiO_2 particles are positive in the pH range from 2 to 5 and the IEP is pH 5.5. Titanium surfaces contain abundant $TiOH$ groups onto their surface, which are acidic in alkaline conditions and basic in acidic conditions. It is also known that negative charge usually renders the surface more hydrophilic (*83*) (see Table 2.2). The presence of three oxygen atoms in the phosphonate molecule enables the covalent binding to the oxide surface in either monodentate, bidentate, or tridentate modes (see Fig. 1.3). Deposition of phosphonic or phosphate-anchored assembled layers from aqueous solution may not be appropriate for titanium surfaces. We suppose that

the immobilized organophosphonates molecules are not densely packed on oxide surface and as their molecules are collapsed, the expose of functional group of their molecule is significantly increased. Chemisorption via electrostatic interactions and/or hydrogen bonding can also occur. Alkylphosphonate molecules bind to the oxide surface following different mechanisms as the nature of the metal oxide. Binding of phosphonates to acidic metal oxide surfaces proceeds first via coordination of the phosphoryl oxygen to a acidic site on the surface, followed by heterocondensation with the surface hydroxyl groups (*84*–*86*). This heterocondensation is accelerated by the increased electrophilicity of the phosphorus atoms after the surface coordination of the phosphoryl group. Hydrogen bonding may take place instead of heterocondensation although this largely depends on the surface -OH content and the experimental conditions (*87*). The organophosphonic acid molecules as deposited film simply hydrogen - bonded are anchored to the substrate and perhaps also to the neighboring molecules. The molecule - molecule interactions (van der Waals and H-bonding) are apparently stronger than the substrate - molecule interactions in the deposited films.

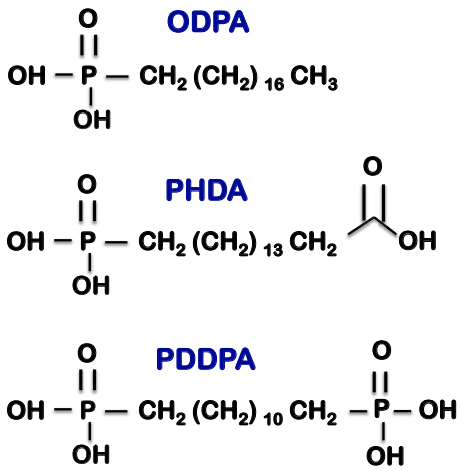

Figure 2.2: Chemical formula of the organophosphonates used in this work.

The rate of HA nucleation on surfaces modified with polar groups is faster than on

Table 2.2: Advancing and receding contact angles of cpTi surfaces reported by Moraila Martinez et. al. (*82*)

pH	θ_a (°)	θ_r (°)
9	66.5	24.2
5.5	76.2	37.5
2	79	43.5

methyl - terminated surfaces (*88*, *89*). The use of phosphonate and carboxyl groups as functional groups is very interesting to study the biomimetic synthesis of apatite because, $-PO(OH)_2$ and $-COOH$ groups are effective to nucleate HA from solutions similar to the body environment (*81*). The phosphonates are further increasingly used to treat disorders associated with bone formation and calcium metabolism. Each functional group may induce calcite nucleation following specific crystallographic planes and causes the growth in different crystallographic directions (*90*).

Phosphonates are highly water soluble while phosphonic acids are only sparingly soluble. The phosphonates are salts (M_2HPO_3) or esters ($OP(OR)_2R$) of phosphonic acids. Phosphonates are not volatile and are poorly soluble in organic solvents. Depending on the hydrophilic/hydrophobic nature of the alkyl chain terminated with $-PO(OH)_2$, $-COOH$, $-CH_3$ groups, the corresponding molecules can be readily soluble in aqueous or no polar media (*91*). The higher the dielectric constant of the solvents used from which the molecules are assembled, the lower the final surface density of molecules and, the greater the number of defects of the modified surface. Surfaces modified with molecules from polar solvents will produce poorly packed films because the solvent molecules decrease the intermolecular chain - chain interactions. Otherwise, nonpolar solvents do not influence the intermolecular interactions and the assembled films reveal a high quality (*92*). In this work, proof of the monolayer formation has been found only in a few cases. Due to this, we can assure the formation of Self - Assembled Films (SAFs) of organophosphonates rather than

SAMs.

The organophosphonate molecules (see Table 2.1) used were acquired from Sigma - Aldrich (97%). The PDDPA was dispersed in Milli - Q water and the PHDA and ODPA in TetraHydroFurane (THF, 99%, Sigma-Aldrich) at 1 mM. The incubation for the chemical functionalization was carried out after the clean titanium surfaces were taken from the oven and cooled at room temperature (15 min). The immersion in the organophosphonate solution (at 20^{o}C) was immediately carried out because of the extreme susceptibility of titanium surfaces to be polluted and hydroxylated (*69*). Next, the functionalized surfaces were dried with argon gas, then heated again in oven at 140^{o} C for 1 h and cooled at room temperature. The heat treatment enabled to enhance the extent of heterocondensation and to promote covalent bond formation via hydrogen bonding interactions (*87*). To remove any weakly bonded multilayer, the samples were sonicated in 0.5 M K_2CO_3 (2:1 ethanol/water) (99%, Sigma - Aldrich) for 5 min (*61*), followed by 10 min ultrasonic rinsing in Milli - Q water and finally dried with argon gas.

2.2 Simulated Body Fluid formulation

Simulated Body Fluid (SBF) solutions are able to induce apatitic calcium phosphate formation on metals, ceramics or polymers (with previous surface treatments) by immersion. In order to evaluate the biomimetic behaviour of materials, it has been proposed that the materials, which form a bonelike apatite on their surfaces in the simulated body fluid (SBF), can also form apatite in a living body and can bond to bone through the apatite layer. This means that the apatite - forming ability in the SBF is a measure of the in vivo bioactivity. SBF solutions, in close resemblance to the original Earles Balanced Salt Solution (EBSS) (*93*) and Hanks Balanced Salt Solution (HBSS) (*94*), were intended to mimic the

ion concentrations of human blood plasma. EBSS and HBSS solutions were developed by Ringer in 1882 (*95*) from the physiological saline. EBSS with 26 mM of HCO_3^- and a Ca/P molar ratio of 1.8, is relatively similar to the actual SBF solutions (*96*–*98*). Instead, HBSS solution has a Ca/P ratio of 1.62. It was recently reported (*52*) that HBSS solutions slowly induce apatite formation on titanium due to its low Ca/P ratio. For mimicking the ion concentrations of human blood plasma, SBF solutions have Ca^{2+} and HPO_4^{2-} concentrations of 2.5 mM and 1.0 mM, respectively (*99*). The pH value of SBF solutions is fixed to the physiological value of 7.4 using a buffer. The buffering agent TRIS (tris - hydroxymethyl - aminomethane)/HCl present in conventional SBF (c - SBF) formulations is able to form soluble complexes with several cations, including Ca^{2+}, which further reduces the concentration of free Ca^{2+} ions available for the calcium phosphate coating. c - SBF, developed by Tadashi Kokubo in 1990 (*51*, *96*–*98*), is indeed a TRIS/HCl - buffered variant of HBSS. HBSS and c - SBF solutions have identical carbonate ion concentration of 4.2 mM are not able to mimic the human blood plasma ($[HCO_3^-] = 27$ mM). Tas et al. (*55*, *100*) increased the carbonate ion concentration in a TRIS/HCl buffered SBF solution up to 27 mM (Tas-SBF). Dorozhkina et al. (*101*) highlighted the influence of HCO_3^- concentration in the SBF solution on the morphology and thickness of calcium phosphate coatings. Increasing the HCO_{3-} concentration in c-SBF from 4.2 to 27 mM led to the formation of homogeneous and much thicker carbonated HA layers. Other SBF formulations with decreasing amounts of initially dissolved carbonates are unstable. Besides, these recipes are not suitable for long - term use in biomimetic coating processes (*102*).

To accelerate the biomimetic coating processes, solutions with 1.5 times the ionic concentration of SBF are often used (*103*–*106*). Details of the SBF formulations are given in Table 2.3. Freshly prepared, c - SBF (*51*, *107*) and 1.5 $\times$ Tas - SBF (*52*) solutions were used in our experiments. Once the solutions were prepared, they were allowed to cool at room temperature and next, stored in a freezer at 5^{o}C. In this dissertation, we used both

SBF formulations. The first preliminary study was performed with c - SBF and the rest of the dissertation with 1.5 Tas - SBF.

Table 2.3: SBF formulations (pH 7.4 at $36.7^{o} - 37^{o}$ C, final volume 1 l).

Order	Reagent	c-SBF (g)	Tas-SBF 1.5 (g)
1	$NaCl$	7.996	9.8184
2	$NaHCO_3$	0.350	3.4023
3	KCl	0.224	0.5591
4	K_2HPO_4 * $3H_2O$	0.228	-
5	Na_2HPO_4	-	0.2129
6	$MgCl_2$ * $6H_2O$	0.305	0.4574
7	$1MHCl$	40 ml	15 ml
8	$CaCl_2$	0.278	-
9	$CaCl_2$ * $2H_2O$	-	0.5513
10	Na_2SO_4	0.071	0.1065
11	TRIS $(CH_2OH)_3CNH_2$	6.057	9.0855
12	$1MHCl$	$\sim$ 120 ml	$\sim$ 120 ml
13	Milli-Q water	up to 1000 ml	up to 1000 ml

2.3 Biomimetic precipitation

Although certain functional groups are effective to nucleate apatitic calcium phosphate on titanium surfaces, the subsequent deposition of significant amounts of bonelike apatite requires that the immersion in SBF is performed for several days or longer. The induction period of apatite nucleation is usually quite long. Thus, we intended to speed up the nucleation process of biomimetic apatite. It is known that HA mineral on the surface can provide potent nucleation sites because of the structural similarity with bonelike apatite (*53*). Moreover, the local calcium and phosphate concentration might increase with the HA dissolution (*108*, *109*). Therefore, if HA mineral is previously deposited on the surface, the nucleation and precipitation process of biomimetic apatite on this pre - deposited surface should be accelerated (*22*).

In this dissertation, we have developed a fast and direct route to deposit HA mineral on cpTi surfaces. To our knowledge, this is the first study devoted to form deposits of HA mineral on chemically functionalized cpTi surfaces. The calcium phosphate pre - deposit on the functionalized surfaces was performed with a fast precipitation method (*110*). The titanium samples were immersed in a 20 mM aqueous $CaCl_2$ (10 ml/sample) solution buffered at pH 7.4 with Tris-HCl buffer at 25^{o}C. Then, a 12 mM Na_2HPO_4 solution was slowly dropped under vigorous stirring up to 10 ml/sample. The resulting mixture was further stirred for 30 min and then washed with MilliQ water (10 ml/sample) under stirring (see Fig. 2.3). The overall process was repeated twice. Finally, the titanium samples coated by the pre - deposit were dried in still air.

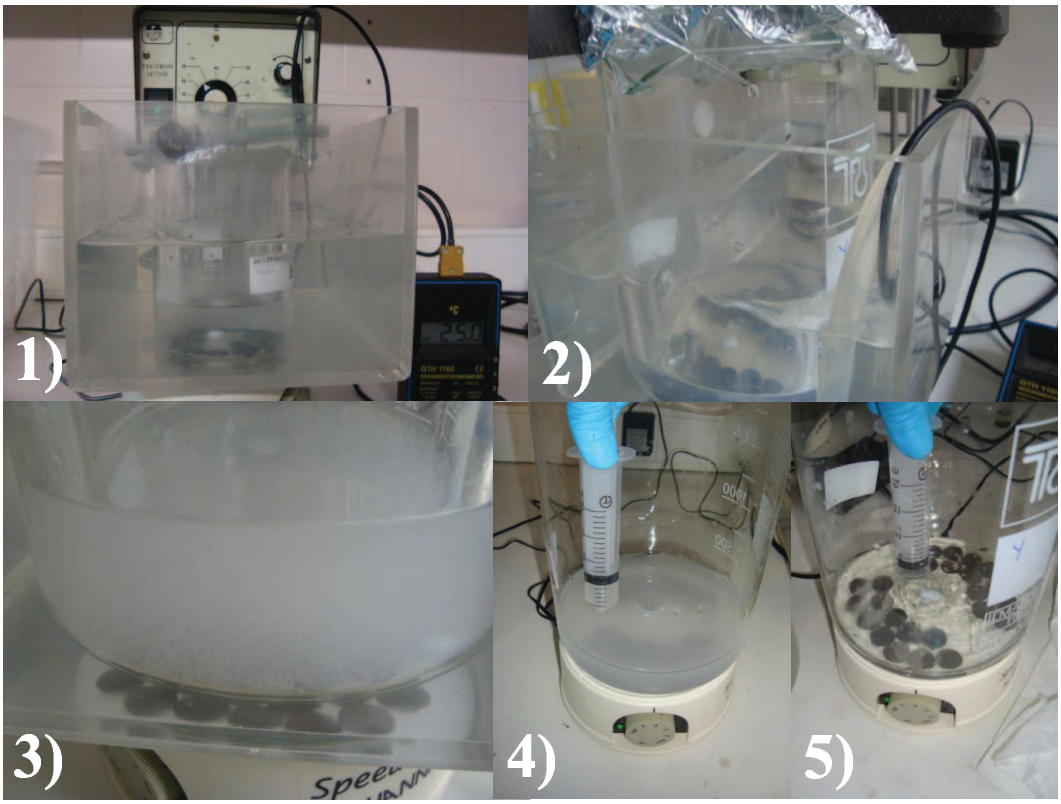

Figure 2.3: Pre - deposit process. 1) Titanium samples immersed in a 20 mM $CaCl_2$ solution at pH 7.4 (transparent). 2) Dropping of 12 mM Na_2HPO_4 solution (turbid). 3) Stirring for 30 min. 4) Removal of the remanent solution. 5) Addition of Milli - Q water under stirring.

The titanium samples were immersed (20 ml/sample) in 1.5 Tas - SBF for different times (12 h, 1, 2, 4, 8 and 16 days) in a glass beaker. The beaker was placed in an incubator (see Fig. 2.4 (a)) maintained at $36.7^{o} - 37^{o}$ C with a fan (Silver Crest, SHLF 2000 A1). The SBF solution was refreshed every 24 h to keep the optimal content. Finally, the samples were removed from the SBF solution, washed with Milli - Q water and dried at $36.7^{o} - 37^{o}$ C in still air.

The titanium samples immersed in SBF were placed horizontally, on the base of the incubation beaker and vertically using a support as in Fig. 2.4 (b). The HA deposition driven by gravity (ballistic - like process) on the horizontal samples could hinder possible differences between initial cpTi surfaces. The substrates were also supported vertically in the SBF solution to ensure that only crystals grown on the SAF would be actually bound to the surface (*52*). The vertical configuration of the titanium samples enabled to find significant differences in the biomimetic HA growth as the surface properties of each sample.

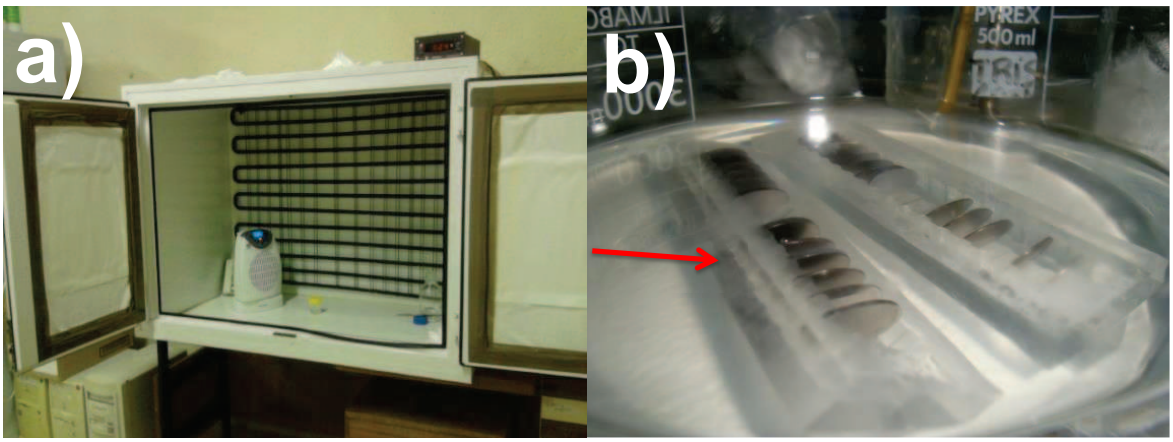

Figure 2.4: a) Incubator used for the biomimetic precipitation. The inner temperature was strictly controlled. b) Supports for vertically incubation of titanium samples.

2.4 Imaging Techniques

2.4.1 Atomic Force Microscopy

Atomic Force Microscopy (AFM) enables to scan the surface of a sample with a sharp tip. This tip has a few microns in length and less than 100 Angstroms in diameter. The tip is located at the end of a cantilever arm with a length of 100 to 200 μm. The force between the tip and the sample surface causes the bending of the cantilever. A detector measures this bending and thereby obtains a topographic map. In tapping mode the tip moves in intermittent contact with the surface. This mode was used for our analysis. The AFM models used in this work were: Nanoscope IV and Solver P47H (NT-MDT Co.) (see Fig. 2.5).

The AFM is placed on a vibration-isolated table. The scanning process is entirely controlled by a computer using the Nanoscope software (Digital Instruments) and NOVA software (NT-MDT), respectively. A CCD camera coupled to a microscope objective is placed vertically on the top of the AFM. This allows, through a monitor, look inside the measuring cell.

2.4.2 Confocal Microscopy

Confocal microscopy uses spatial filtering techniques to eliminate out-of-focus light or glare in samples with thickness exceeding the immediate plane of focus. This way three-dimensional structures are reconstructed from the obtained 2D images.

There are two types of confocal microscopy: White Light Confocal Microscope (WLCM) and the Confocal Laser Scanning Microscope (CLSM). WLCM allows to determine the profile and topography of microscopic three - dimensional object surfaces and multilayer

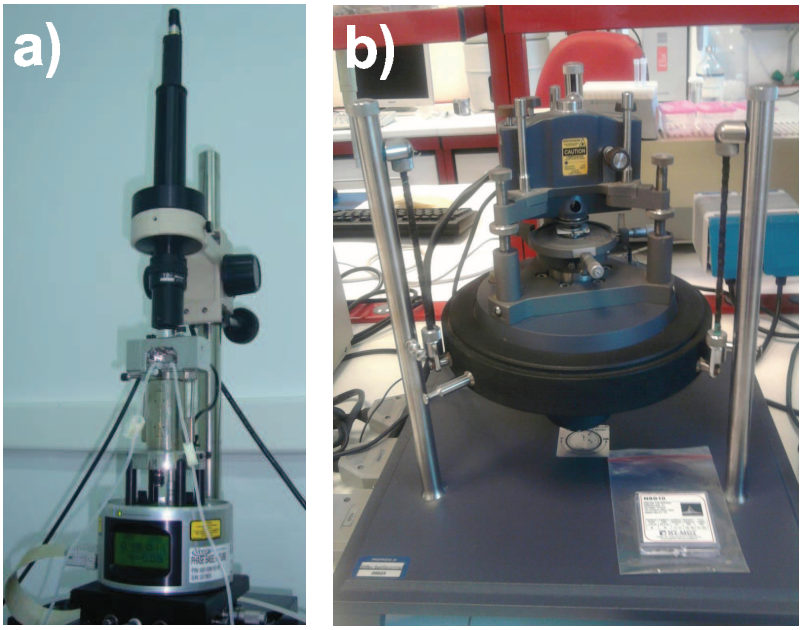

Figure 2.5: Atomic Force Microscopes used in this work. a) Nanoscope IV (Surfaces and interfaces laboratory, Department of Applied Physics, UGR) and b) Solver P4H7 (Nobil Bioricerche).

structures in a non - destructive way. It uses a single plane images "confocal" eliminating light from out of focus planes, so that areas that appear blurred when using conventional microscopes because out of focus points are totally absent from confocal images. The confocal microscope works with epilumination, that is reflected light from the samples. The WLCM used in this dissertation was the Nikon L150 (SENSOFAR) (Surfaces and interfaces laboratory, Department of Applied Physics, UGR).

The epi - fluorescence is the principle of CLSM. The coherent light emitted by the laser system (excitation source) passes through a pinhole aperture that is situated in a conjugate plane (confocal) with a scanning point on the specimen and a second pinhole aperture positioned in front of the detector (a photomultiplier tube). As the laser is reflected by a dichromatic mirror and scanned across the specimen in a defined focal plane, secondary fluorescence emitted from points on the specimen (in the same focal plane) pass

back through the dichromatic mirror and are focused as a confocal point at the detector pinhole aperture (*111*). The CLSM inverted Leica DMI6000 (CIC - UGR) and Confocal Fluorescence Microscope (CFM) Nikon A1 (CIC - UGR, campus health) were used for our cell fluorescense analysis.

2.4.3 Scanning Electron Microscopy

Scanning Electron Microscope (SEM) uses a focused beam of high - energy electrons to generate a variety of signals at the surface of solid specimens (*112*). The signals that derive from electron - sample interactions reveal information about the sample including external morphology (texture), chemical composition, and crystalline structure and orientation of materials making up the sample (*113*). In most applications, data are collected over a selected area of the sample surface, and a realistic image is generated.

The SEM is also widely used to identify phases based on qualitative chemical analysis and/or crystalline structure. Precise measurement of very small features and objects down to 50 nm in size is also accomplished using the SEM. Backscattered electron images (BSE) or Solid State Detector (SSD) can be used for rapid discrimination of phases in multiphase samples (*114*).

An electrically conductive (gold or carbono) coating is usually applied to the samples. The maximum size of the surface is in the order of 10 cm. Vertical dimensions are generally much more limited and rarely exceed 40 mm. The samples must be stable in high vacuum (10^{-5} - 10^{-6} torr). However, low vacuum SEM also exists.

The Environmental Scanning Electron Microscope (ESEM) allows to analyze specimens that are "wet" or uncoated in a gaseous environment. An ESEM employs a scanned electron beam and electromagnetic lenses to focus and direct the beam on the specimen surface in

an identical way as a conventional SEM. Nevertheless with its specialized electron detectors and its differential pumping systems, to allow for the transfer of the electron beam from the high vacuums in the gun area to the high pressures attainable in its specimen chamber, make it a complete and unique instrument designed for the purpose of imaging specimens in their natural state. The ESEM further decreases the measuring time because it allows to eliminate the sample preparation and high vacuum.

For this research, we employed the SEM (EVO MA10, ZEISS, Nobil Bioricerche) and ESEM (FEI, Quanta 400, CIC - UGR). SEM for the preliminary analysis (see Chapter 4) and ESEM for the rest of the work.

2.5 Surface chemistry and crystalline structure

2.5.1 X-ray Photoelectron Spectroscopy

X - ray Photoelectron Spectroscopy (XPS) is based on the photoelectric effect. The sample is irradiated with mono - energetic x - rays causing photoelectrons to be emitted from the sample surface (*115*). An electron energy analyzer determines the binding energy of the photoelectrons. From the binding energy and intensity of a photoelectron peak, the elemental identity, chemical state, and quantity of an element are determined. For XPS, Al Kα (1486.6eV) or Mg Kα (1253.6eV) are often the photon energies of choice.

The XPS technique is highly surface specific due to the short range of the photoelectrons that are excited from the solid. The energy of the photoelectrons leaving the sample are determined using a CHA (Concentric Hemispherical Analyser) and this gives a spectrum with a series of photoelectron peaks (*116*).

For each and every element, there will be a characteristic binding energy associated with each core atomic orbital. Each element will give rise to a characteristic set of peaks in the photoelectron spectrum at kinetic energies determined by the photon energy and the respective binding energies. The presence of peaks at particular energies therefore indicates the presence of a specific element in the sample under study, furthermore, the intensity of the peaks is related to the concentration of the element within the sampled region. The peak areas can be used (with appropriate sensitivity factors) to determine the composition of the materials surface. The shape of each peak and the binding energy can be slightly altered by the chemical state of the emitting atom. Hence XPS can provide chemical bonding information as well. XPS is not sensitive to hydrogen or helium, but can detect all other elements.

The peak - fitting process is affected by instrument design, instrument components, experimental settings, and sample variables. Most instrument parameters are constant while others depend on the choice of experimental settings. Variables that affect or define peak - fit results include chemical shifts, peakshapes, instrument design factors, experimental settings and sample factors.

The primary components of the XPS instrument are a vacuum system, the X - ray source, an electron energy analyzer and a data system. The central part is constituted by the main vacuum chamber in which the sample is analyzed. Conducting the experiment under vacuum conditions is due to the photoelectrons have to travel from the sample to the detector without colliding with any gas phase particle, some components such as X - ray source requires vacuum conditions to maintain the operation, and the composition of the sample surface has to remain unchanged during the experiment. Samples are introduced into a first chamber where the atmosphere comes to empty existing approach a vacuum at 10^{-6} Torr. Achieving ultra - high vacuum is a slow operation, lasting from several minutes

to hours. Placing the sample within the chamber is made by a bar attached to a holder. The sample analysis in a vacuum chamber, facilitates the transmission of the photoelectrons to the analyzer but more importantly minimizes the re-contamination rate of a freshly cleaned sample. This is crucial because XPS is very surface - sensitive, with a typical sampling depth of only a few nanometers (5 nm). Within the main chamber, the sample can be oriented in different positions and can choose the area of the working surface. X - radiation is monochromatized before reaching the sample by using a quartz crystal. This advantage allows the energy range in which the intensity of X - radiation is maximum (typically a width of 1 to 2 eV) avoid satellites peaks X - ray fluorescence, and prevent high energy electrons causing heat shock sample and degrade.

The XPS instruments used for our analysis are XPS PHI 5500 (ESCA SYSTEM, Perkin Elmer, property of *Nobil Bioricerche*) and XPS Kratos Axis Ultra-DLD (CIC - UGR), both with an Al Kα monochromator.

2.5.2 Energy Dispersive X - ray Spectroscopy

The SEM is also capable of performing analyses of selected point locations on a sample. This approach is especially useful in qualitatively or semi - quantitatively determining chemical compositions using Energy - Dispersive X - Ray Spectroscopy (EDX), crystalline structure, and crystal orientations using Electron Backscatter Diffraction (EBSD) (*117*). Interaction of an electron beam with a sample target produces a variety of emissions, including x-rays. An EDX detector is used to separate the characteristic x - rays of different elements into an energy spectrum, and EDX system software is used to analyze the energy spectrum in order to determine the abundance of specific elements. EDX can be used to find the chemical composition of materials down to a spot size of a few microns, and to create element composition maps over a much broader raster area. Together, these capabilities provide

fundamental compositional information for a wide variety of materials. EDX systems include a sensitive x - ray detector, a liquid nitrogen dewar for cooling, and software to collect and analyze energy spectra. The detector is mounted in the sample chamber of the main instrument at the end of a long arm, which is itself cooled by liquid nitrogen. The most common detectors are made of Si(Li) crystals that operate at low voltages to improve sensitivity. An EDX detector contains a crystal that absorbs the energy of incoming x - rays by ionization, yielding free electrons in the crystal that become conductive and produce an electrical charge bias. The x - ray absorption thus converts the energy of individual x-rays into electrical voltages of proportional size; the electrical pulses correspond to the characteristic x - rays of the element. EDX detectors on SEM cannot detect very light elements (H, He, and Li), and many instruments cannot detect elements with atomic numbers less than 11 (Na). Most SEMs use a solid state x - ray detector (EDX), and while these detectors are very fast and easy to utilize, they have relatively poor energy resolution and sensitivity to elements present in low abundances.

EDX microanalysis system used was EDAX Genesis detector Si (Li) SUTW (CIC - UGR).

2.5.3 X - Ray Diffraction

In the X - ray Diffraction (XRD) technique, the sample is illuminated with x - rays of a fixed wave - length and the intensity of the reflected radiation is recorded using a goniometer. This data is then analyzed for the reflection angle to calculate the inter - atomic spacing (d value in Angstrom units $\sim 10^{-8}$ cm). The interference of the scattered X - rays leads to the general phenomenon of diffraction.

The three - dimensional structure of nonamorphous materials, is defined by regular, repeating planes of atoms that form a crystal lattice. When a focused X - ray beam

interacts with these planes of atoms, part of the beam is transmitted, part is absorbed by the sample, part is refracted and scattered, and part is diffracted. X - rays are diffracted by each mineral differently, depending on what atoms make up the crystal lattice and how these atoms are arranged. A high voltage, typically 15 - 60 kV, is applied within the tube. This high voltage accelerates the electrons, which then hit a target, commonly made of copper. When these electrons hit the target, X - rays are produced. The wavelength of these X - rays is characteristic of that target. These X - rays are collimated and directed onto the sample, which has been ground to a fine powder (typically to produce particle sizes of less than 10 μm). The X - ray signal is detected and processed by a microprocessor or electronically, converting the signal to a count rate.

The XRD (XPert Philips, Ni filter) used for this research analysis was provided by the Department of Mineralogy and Petrology of the University of Granada.

2.6 Wettability

The hydrophobicity/hydrophilicity of a surface is usually expressed in terms of contact angle (see Fig. 2.6). Numerous methodologies have been developed and used for the measurement of contact angle (*118*).

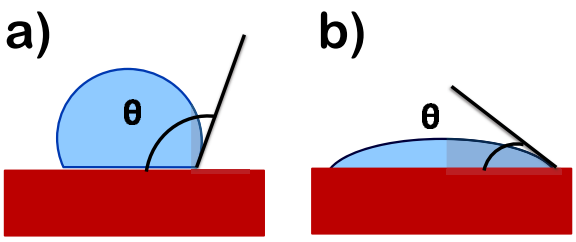

Figure 2.6: a) Water sessile drop placed on a hydrophobic surface. b) Water sessile drop placed on a hydrophilic surface.

There are two observable contact angles of great importance due to its reproducibility (*119*). The maximum angle is called *advancing contact angle* (ACA, θ_{AV}) and it is observed in situations where the liquid phase moves on the solid at the expense of the surrounding fluid phase. This angle can be observed at the downhill contact point of a sessile drop inclined at the moment it begins to slide (see Fig. 2.7). The minimum contact angle is known as *receding contact angle* (ACR, θ_{RE}) and it is observed in situations where the liquid phase moves back on the solid, and the wet area decreases in favor of the dry area. This situation is found at the uphill contact point of a sessile drop inclined at the moment it begins to slide. The difference between these two contact angles provides the amplitude of the contact angle hysteresis: H $= \theta_{AV}$ - θ_{RE}. On rough and chemically homogeneous surfaces, ACA is related to the maximum ascending slopes of the surface and RCA to the maximum descending slopes. On smooth and chemically heterogeneous surfaces, ACA is related to the low - energy chemical domains on the surface and RCA to the high - energy domains.

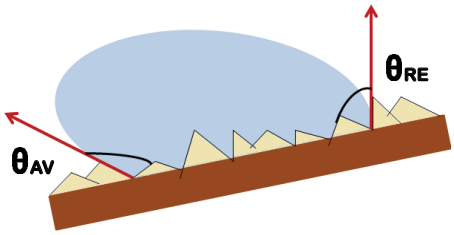

Figure 2.7: Observable contact angles on an inclined rough surface.

2.6.1 Tilted drop method

With the tilted drop method we were able to create sessile drops of controlled volume on an initially horizontal surface, which was then tilted. The inclination of the motor-driven platform, where the solid surface rested, was controlled by a computer. The optical system

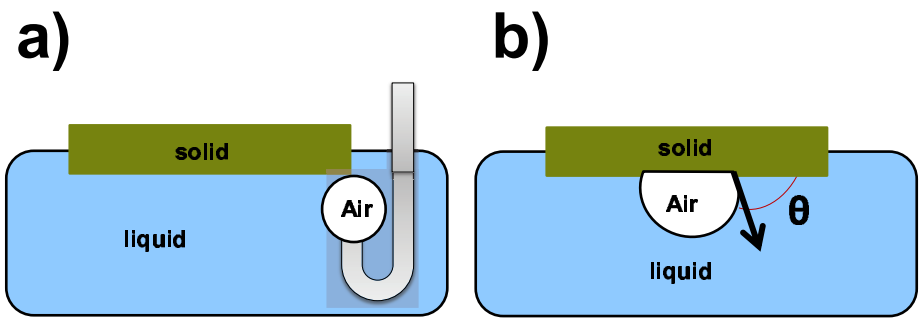

Figure 2.8: Scheme for static contact angle measurement with the captive bubble method.

was slaved to this platform. The tilted movement was continuous (5^{o}/seg) and the system acquired consecutive images. On each image, we just focused on the two contact line points where the highest and lowest contact angles were observed (*120*, *121*). We will refer to these points as the downhill and uphill points, respectively (see Fig. 2.7). We formed drops of 50 μl, once the drop was formed and before tilting the surface, we measured the initial contact angle, θ_0, using polynomial interpolation of the ends (uphill and downhill) of the drop profile. Images were analyzed by a program contrasted with the technique Axisymmetric Drop Shape Analysis-Profile (ADSA-P) (*119*) and an elliptic interpolation.

2.6.2 Captive bubble method

The captive bubble method was used to examine the titanium wettability in "underwater" conditions, which are more realistic for a biomaterial (*119*, *122*, *123*). In the captive bubble method, the surface is totally hydrated thus, a thin layer of water should exists between the solid and the bubble. Since the sample is immersed, this method further minimises the surface pollution. Moreover, the main difficulty found to measure contact angles on porous hydrophilic substrates, such as HA - covered titanium surfaces with sessile drops, is the inhibition that leads to non-reproducible and meaningless contact angle values (*118*).

In the captive bubble method, an air bubble is injected beneath the surface immersed in the liquid and is transported towards the solid surface due to the buoyant force (see Fig. 2.8). The observed contact angle is the supplementary angle of the corresponding contact angle of an inverted sessile drop. This way, the captive bubble and sessile drop methods are based on the same theoretical law. The contact angle reproduced with the captive bubble method is a static contact angle rather than an advancing or receding contact angle. We used fresh MilliQ water in all experiments at room temperature and by duplicate.

2.7 Cell response

Osteosarcomas are malignant bone tumors consisting of cells with abnormal cellular functions. Osteosarcoma-derived cells are commonly used as osteoblastic models. Osteosarcoma cell lines are available in unlimited number without the need for time consuming isolation or ethical approval, with the advantage of more reliable reproducibility. Two osteosarcoma-derived cell lines have been extensively used to investigate the biological events occurring on titanium surfaces: MG - 63 (*124*) and SaOS - 2 (*125*). Osteoblastic cells are responsible for the synthesis and mineralization of bone during both initial bone formation and later bone remodeling. Human osteosarcoma MG - 63 cells exhibit fundamental phenotypic characteristics of osteoblastic cells, thus they are cultured for the evaluation of cell response on the coatings. The cytokine and growth factor expression of SaOS - 2 cells have been reported to be similar to primary normal human osteoblast cells (*126*).

2.7.1 Cell culture

The cell line used for preliminary adhesion tests was SaOS - 2 (see Chapter 4) purchased from "Centro Substrati Cellulari dell'Istituto Zooprofilattico Sperimentale della Lombardia e dell'Emilia Romagna" (*127*). Cell adhesion tests have been conducted as the protocols listed in literature (*124*, *125*, *127*). A suspension of 1.05$\pm$0.13 x 10^5 SaOS - 2 cells (obtained by adding 2 ml of trypsin/EDTA solution inside a T75 Falcon flask) in 2.5 ml of McCoy's 5A medium, supplemented with 15$\%$ fetal calf serum, L - glutamine, penicillin, streptomycin and amphotericin B (all purchased from GIBCO, INVITROGEN Srl) was introduced into sterile 12 - well polystyrene culture plates (Cell Star, Greiner One). Cultures were kept at 37^{o}C in a humidified atmosphere of 95$\%$ air and 5$\%$ CO_2.

The MG - 63 cell line was mostly used in this dissertation. This line was purchased from American Type Cultures Collection (ATCC, Manassas, VA) and stored as described by Díaz - Rodríguez et. al. (*128*) in Dulbecco's Modified Eagle Medium (DMEM, Invitrogen Gibco Cell Culture Products, Carlsbad, CA) with 100 IU/ml penicillin (Lab Roger SA, Barcelona, Spain), 50 μg/ml gentamicin (Braum Medical SA, Jaen, Spain), 2.5 μg/ml amphotericin B (Sigma, St Louis, MO, USA), 1$\%$ glutamine (Sigma, St Louis, MO, USA), and 2$\%$ HEPES (2-[4-(2-hydroxyethyl)piperazin-1-yl]ethanesulfonic acid, Sigma), supplemented with 10$\%$ Fetal Bovine Serum (FBS) (Gibco, Paisley, UK). Cultures were kept at 37^{o}C in a humidified atmosphere of 95$\%$ air and 5$\%$ CO_2. Cells were detached from the culture flask with a solution of 0.05$\%$ trypsin and 0.02$\%$ Ethylene Diamine Tetra - Acetic acid (EDTA) (Sigma, St. Louis, MO, USA) and then washed and suspended in complete culture medium with 10$\%$ FBS. For the cell assays (except for Chapter 4), the titanium samples were sterilized by rinsing with ethanol synthesis grade and subjected to UV radiation for 30 min.

2.7.2 Cell adhesion

For the cell adhesion with the SaOS - 2, the titanium samples were placed in a 12 - well plate. The culture plates were then placed in an incubator at 37^{o}C, with 5% CO_2 and 98% relative humidity. The samples were removed from the multiwell after 72 h, gently washed with Dulbecco's Phosphate Buffered Saline (DPBS, Gibco, INVITROGEN Srl) to remove the non - adhered cells.

Cell adhesion was determined by the MTT (3-[4,5-dimethylthiazol-2-yl]-2,5 diphenyl tetrazolium bromide) method with the MG - 63 cell line. The osteoblasts were inoculated at 1 x 10^4 cell/ml in a 24 - well plate (Falcon, Becton Dickinson Labware, NJ, USA) in the ratio of 2 ml/well. The titanium samples were previously deposited in each well. The plate was kept at 37^{o}C in a humidified atmosphere of 95% air and 5% CO_2. The tests were performed at 24 and 48 h for each treatment. Next, the medium was replaced with Dulbecco's Modified Eagle Medium (DMEM) containing 0.5 mg/ml MTT (Sigma, St. Louis, MO, USA) and incubated again for 4 h. Cellular reduction of the MTT tetrazolium ring resulted in the formation of a dark - purple water - insoluble deposit of formazan crystals. After incubation, the medium was aspired and DiMethyl SulfOxide (DMSO) was added to dissolve the formazan crystals. The number of adhered cells on titanium surfaces was determined with a spectrophotometer (SunriseTM). The absorbance was measured at 570 nm wavelength. All measurements were conducted by triplicate.

2.7.3 Cell differentiation

To study the cell differentiation, Alkaline Phosphatase activity (ALP) of MG - 63 cells was measured. A concentration of 3 x 10^4 cells / ml was grown on titanium discs placed on a 24 - well plate for 24 h. After the incubation period, the supernatant was removed and

cells were lysed with Triton X - 100 (0.1%). After observing by microscopy that the cells were lysed, a buffer solution consisting of 10 mM Tris - HCl pH 7.8, 0.5 mM $MgCl_2$ was added, and Triton X - 100 at 0.1% to stop lysis. This cell extract was stored at -70^{o}C until processing.

For the ALP analysis, 50 μl of the extract of the lysed cells from each sample were used. The 50 μl of every sample were dispensed into 96 - well plates, and were added 50 μl of substrate (P - nitrophenol phosphate) (Sigma Chem Co. Comp., St . Louis, Mo, USA). This technique measures the formation of a yellow product (4 - nitrophenol) as a result of catalytic action of ALP on the substrate. Was incubated for 45 min at 37^{o}, then added 50 μl of 0.1 M $NaOH$ to stop the reaction. Finally the absorbance was measured with a wavelength of 405 nm.

Was determined the concentration of proteins contains in the lysed samples in order to express ALP activity in μM/min/mg of proteins. Since 1 μM/minuto equals 1 unit, finally ALP activity was expressed in U/mg of proteins.

2.7.4 Biomineralization

The mineralization was determined by assessing the formation of calcium nodules in the extracellular matrix as a result of culturing the cells in osteogenic medium, according to the methodology described by Bouvert - Gerbettaz et al. (*129*). The osteogenic medium was prepared from culture medium supplemented with 10% FBS, 5 mM β - glycerophosphate (Sigma - Aldrich Co. Chem Comp., St. Louis, Mo, USA) and 0.05 mM ascorbic acid (Sigma - Aldrich Co. Chem Comp., St. Louis, Mo, USA).

The test was performed by placing the titanium discs in a 24 - well plates. The MG - 63 cell line was suspended to a final concentration of $5x10^4$ cells/ml in osteogenic medium. A

volume of 2 ml obtained of cell suspensions in culture medium was placed on titanium discs, and were subsequently incubated at 37^{o}C under 5% CO_2 atmosphere. After four days, the culture medium was replaced with fresh medium of the same characteristics. From this time, the medium was replaced every three days.

The reading was performed by staining with Alizarin red obtained from the cells adhering to the culture flask, after being cultured in the conditions described above, for 7, 15 and 20 days. Elapsed the appropriate incubation times, the cells adhered to the discs were washed with 150 mM $NaCl$ and fixed with cold ethanol at 70% for 30 minutes. After being rinsed the samples three times with distilled water, the wells were incubated for 10 min with 1 ml Alizarin red 40 mM NaH_2P0_4 pH 4 at room temperature. Then the samples were washed 5 times with distilled water and incubated with PBS for 15 minutes at room temperature. The samples were observed under a microscope (URA TECHNIC, Navarra, Spain) valuing the number of nodules analyzed surface. These nodules have a crystalline red color correspond to the existence of precipitated calcium in the extracellular collagen matrix.

The quantitative reading of nodules formed in each sample was performed by spectrophotometry at a wavelength of 562nm. For this, the samples were incubated for 15 min in a solution of chloride cetilpiridinium 10% in sodium phosphate 10 mM (pH 7.0).

2.7.5 Cell fixation

Cell fixation for the SaOS - 2 cell line was performed for the observation by SEM and for the MG - 63 cell line for the observation by ESEM. The SaOS - 2 cells were fixed using 4% glutaraldehyde in DPBS for at least 48 h. After fixation, cells were dehydrated by immersion for approx. 48 h following ethahol - water series being the final step in absolute

ethanol (Fluka, Sigma-Aldrich Srl, Milan). The fixed and dehydrated samples were coated with a thin layer of gold (Agar Sputter Coater) for imaging with SEM.

Cell line MG - 63 were separated from the culture flask with a solution of 0.05% trypsin and 0.02% EDTA at 37°C for 10 min and then neutralized with culture medium supplemented with FBS 10%. Cells were collected and washed with Phosphate Buffered Saline (PBS) by centrifugation at 1200 rpm for 10 minutes. The sediment obtained was suspended in the appropriate culture medium supplemented with FBS 10%, adjusting to a final cell density of 2 x 10^4 cells/ml and then are cultured in sterile wells specific for microscopy (Nunc, Sigma Chemical Co., St. Louis , Missouri, United States). Previously were deposited the titanium discs. The samples were incubated at 37°C 5% CO_2 in a incubator for 24 h. After this time, cells were fixed with a cold acetone - methanol solution (v/v) for a period of 10 min at room temperature. Them, the cells were washed 3 times with PBS, locking - specific binding with FBS 10% in PBS for 30 min at room temperature. Subsequently, cells were labeled with two Abmos: anti - human fibronectin labeled with fluorescein isothiocyanate (FITC: green fluorescence) and anti - phycoerythrin labeled with human vimentin (PI: red fluorescence) at a concentration of 1:150 for 2 h at 37°C in darkness. Elapsed the 2 h, the cells were washed 2 times with PBS and nuclei were stained with DAPI (4 ',6-diamidino-2-phenylindole, Sigma Chemical Co., St. Louis, Missouri, USA) at a concentration of 10 μg/ml, for which was allowed to incubate for 15 min. After this time was again washed with PBS.

2.7.6 Cell stained

Cells were labeled with two proteins Abmos: human anti - fibronectin labeled with fluorescein isothiocyanate (FITC: green fluorescence) and human anti - vimentin labeled with phycoerythrin (PI: red fluorescence) at concentration of 1:100 for 2 h at 37°C in darkness.

Elapsed the 2 h, the cells were washed 2 times with PBS and nuclei were stained with DAPI (blue) (4, 6-diamidino-2-phenylindole, Sigma Chemical Co., St. Louis, Misuri, E.E.U.U.) to a concentration of 10 μg/ml incubating for 15 min. After the 15 min, the cells were washed again with PBS and visualized with CLSM.

CHAPTER 3

Chemical Functionalization of Commercially Pure Titanium Surfaces with Alkylphosphonates

The biological response to titanium implants is greatly mediated by the surface chemical composition and the ability of titanium oxides to adsorb molecules. Surface topography also plays a fundamental role in regulating cell shape, orientation and adhesion (*130*, *131*). Alkylphosphonates enable the formation of Self - Assembled Films (SAFs) on metal oxide surfaces. These SAFs of alkylphosphonates have a better surface coverage and hydrolytic

stability in alkaline conditions as compared to certain types of silane films (*63*, *64*). These properties make phosphonate platforms very promising for real - life applications that require long - term stability of the deposited layer. Unlike SAMs formed on gold surfaces, it is not common in the literature to find an optimized procedure to produce SAFs on metal titanium surfaces. The surface functional groups of SAF play important roles in determining the solid/ion cluster interfacial energies and therefore, different functional groups can have different nucleation abilities for calcium phosphate. Phosphonate and carboxyl groups are negatively charged at pH 7.4, and they will likely attract more positive calcium ions from SBF solution. This way, the interfacial energies of titanium/ion clusters are effectively decreased (*22*). For the chemical functionalization of cpTi surfaces, we used the so - called technique Tethering By Aggregation and Growth (T-BAG). This method (*61*) has been shown to be a simple and reliable way to assembly alkylphosphonates on metal oxide surfaces. We studied the three organophosphonates molecules ODPA ($-CH_3$), PHDA ($-COOH$) and PDDPA ($-PO(OH)_2$) with a chain length of $\sim$ 2.16, 1.92 and 1.44 nm respectively. The protocol for chemical functionalization was optimized with special attention to the cleaning and oxidation states of cpTi surfaces. We explored the thickness, quality (surface coverage, ordering), wettability and surface chemistry of each SAF.

3.1 Formation of Self - Assembled Films of alkylphosphonates

To determine the optimal route for the SAF formation on smooth cpTi surfaces with alkylphosphonates, four methods were compared. These methods are summarized in Table 3.1. Before the corresponding method of chemical functionalizaton all samples were sonicated in an acetone bath, dried in nitrogen gas and next treated in argon plasma (15 min,

25 W). The oxidation determines a key point in the functionalization since the alkylphosphonates have great affinity for metal oxide such as TiO_2. The oxidation state of the samples was stabilized in water for 24 h. To remove traces of water the samples were heated. The phosphonic acid molecules are very sensitive to the presence of water and contaminants, further the temperature strengthens the covalent bond with the surface oxide. The K_2CO_3 washing of samples is necessary to eliminate weakly anchored molecules. The main differences between the methods 1 and 2 are the time and process of incubation in the organophosphonate solution. In the method 1, the incubation was carried out sequentially followed by rinsing and heating steps. In the method 2, the incubation was continuous and rinsing and heating were conducted at the end. The method 3 was remarkablely different in comparison with the methods 1, 2 and 4, since the incubation was substituted by solvent evaporation. In the method 4, the surface oxidation previous to the chemical functionalization was performed by heating rather than in water. The optimal method was the second one, as the images obtained by AFM. In our preliminary study (see Chapter 4), we used the method 1. With both methods (1 and 2), we obtained very similar SAF structures although the method 2 was simpler and fast.

3.2 Ordering of Self - Assembled Films of alkylphosphonates

AFM images of the SAF surfaces are shown in Fig. 3.1. Topography differences between each method (see Table 3.1) are noticeable in all cases. With the method 1, every distributed morphologies are observed with the three molecules. With the methods 3 and 4, large clusters of alkylphosphonate and bare regions can be distinguished with the three molecules. Using the method 2 a nearly monolayer was formed with PHDA and PDDPA

(z $\sim$ 2 nm), while with ODPA the structure does not become a monolayer, it seems to be a multilayer film (z $\sim$ 6 nm). The morphology of the ODPA - SAF formed with the method 2 was very different to the rest of SAFs formed with the same method. Although the method 2 was the most suitable due to be a less time-consuming method in comparison with the method 1, not in all cases there was evidence of monolayer formation. A multilayer structure was mostly obtained, as explained in section 1.3. The chemical functionalization of the cpTi surfaces in the rest of this dissertation (except for Chapter 4) was performed with the method 2. This was the best route adapted to the T-BAG method.

Table 3.1: Different routes for the chemical functionalization of cpTi surfaces with organophosphonates.

Method	Description	Time
1	Oxidation in water (24 h), N_2 gas drying, heating at 140^o C (15 min), cooling at room temperature, incubation in solution of organophosphonate (48 h), heating at 140^o C (1 h), sonication in 0.5 M K_2CO_3 (2:1 ethanol/water) (5 min), sonication in Milli-Q water (10 min), N_2 gas drying, repetition from incubation twice.	6 days
2	Oxidation in water (24 h), N_2 gas drying, hetaing at 140^o C (15 min), cooling at room temperature, incubation in solution of organophosphonate (5 days), heating at 140^o C (1 h), sonication in 0.5 M K_2CO_3 (2:1 ethanol/water) (5 min), sonication in Milli-Q water (10 min), N_2 gas drying.	5 days
3	Placement of a drop of organophosphonate solution over an oxidated clean titanium sample, evaporation in oven at 120^o C (12 h), cooling at room temperature, sonication in 0.5 M K_2CO_3 (2:1 ethanol/water) (5 min), sonication in Milli-Q water (10 min), N_2 gas drying.	1/2 day
4	Oxidation of clean titanium sample at 230^o C (30 min), cooling at room temperature, incubation in organophosphonate solution (5 days), sonication in 0.5 M K_2CO_3 (2:1 ethanol/water) (5 min), sonication in Milli-Q water (10 min), N_2 gas drying.	5 days

Regarding the roughness of the cpTi surfaces modified with SAF, as illustrated in Table 3.2, the method 2 provided lower values of roughness and lower variability between Ra and Rq, together to the method 3. It is noticeable that when Ra $\sim$ Rq the SAF becomes more

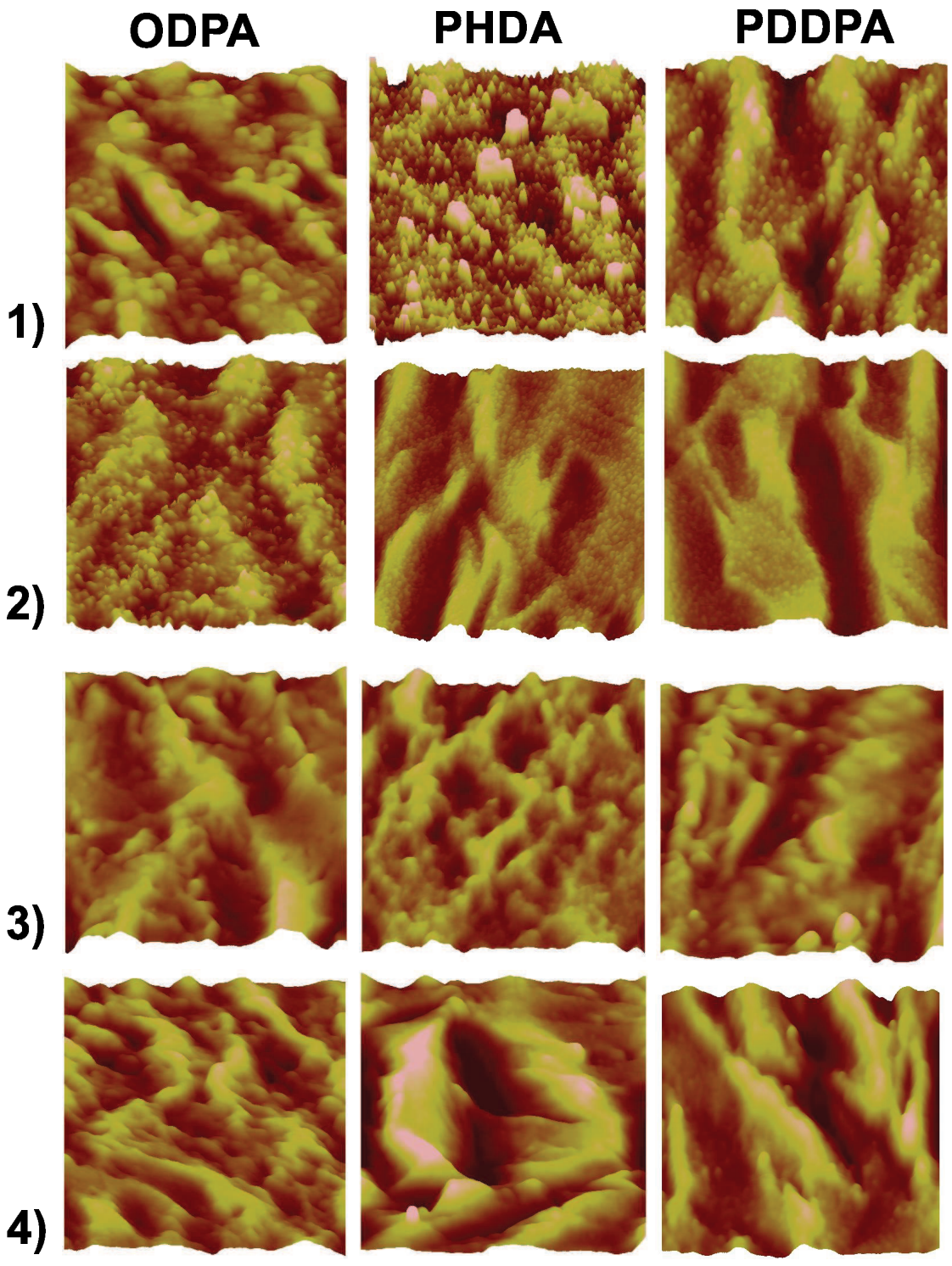

Figure 3.1: AFM images of the SAF surfaces obtained with the four methods listed in Table 3.1. The scan area is 1 μm^2 and z-scale = 10 nm.

uniform. This result postulates the uniform distribution of the phosphonate molecules over the cpTi surfaces. The method 3 produced SAFs with very similar values of Ra and Rq regardless of the phosphonate used. The SAF structures (Fig. 3.1) using the method 3 were also very similar although different to the SAFs produced with the method 2. The lowest roughness was obtained on the PDDPA - SAF with the method 2. On the other hand, the method 4 produced rougher surfaces followed closely by the method 1.

As explained before, the best method to functionalize the cpTi surfaces was the method 2 of Table 3.1 because the aim of the chemical functionalization was to form SAFs with high degrees of coverage. At a larger scale (50 μm^2), the SAFs formed with the method 2 are displayed in Fig. 3.2.

Table 3.2: Roughness values of the SAF surfaces obtained with the four methods listed in Table 3.1. The scan area is 1 μm^2.

Method	ODPA		PHDA		PDDPA	
	Rq (nm)	Ra (nm)	Rq (nm)	Ra (nm)	Rq (nm)	Ra (nm)
1	2.69	2.16	4.29	3	3.31	2.56
2	2.51	2	2.48	1.97	2	1.51
3	2.54	1.96	2.43	1.93	2.54	2
4	2.68	2.15	4.64	3.54	3.67	2.93

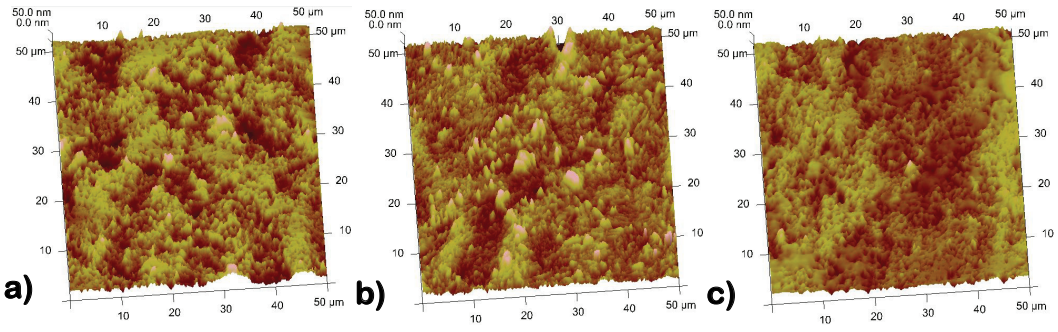

Figure 3.2: AFM images of the SAFs formed with the method 2 on cpTi surfaces: a)ODPA, b)PHDA and c)PDDPA. The scan area is 50 μm^2 and z-scale = 50 nm.

3.3 Thickness of Self - assembled Films of alkylphosphonates

Ellipsometry was used to measure the thickness of the TiO_2 layer in the ultra - polished cpTi surfaces and the rinse SAF after the chemical functionalization performed with the method 2 over hydroxilated cpTi surfaces. In Fig. 3.3 the structures used to model and fit the parameters of the models to the experimental data are shown, being valid the mixed layer model. In Fig. 3.4, the ellipsometric models employed are plotted. The good agreement between each model (continous line) and the experimental data (dotted line) is illustrated in Fig. 3.4. The thickness values obtained for each surface are shown in Table 3.3. The thickness of the TiO_2 layer formed on the ultra - polished cpTi surface is 6.7 nm, which is within the range reported in literature (see Section 1.1.2). The thickness for the SAF surfaces reveals that on the cpTi surface there was indeed a heterogeneous film formed by alkylphosphonate clusters rather than a well - ordered monolayer as observed in AFM images. The thickness error of Table 3.3 (4 - 5 nm) is of the order of the values of Ra and Rq of the SAF surfaces (Table 3.2).

Table 3.3: Values of thickness obtained by ellipsometry of the surface layer of the ultra - polished and chemically functionalized cpTi surfaces.

sample	thickness (nm)
ultra-polished	6.7 $\pm$ 1.1
ODPA	51 $\pm$ 5
PHDA	53 $\pm$ 4
PDDPA	43 $\pm$ 5

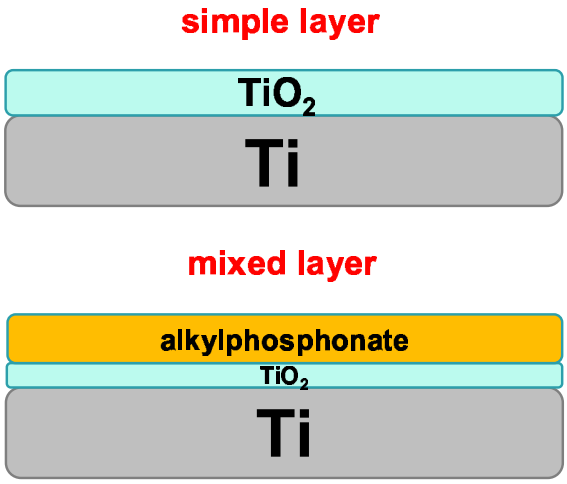

Figure 3.3: Ellipsometry models of surface layer used. For the ultra-polished cpTi surface, a simple oxide layer was assumed to form on the metal titanium bulk. For the SAF surfaces, the external layer is composed of oxide and orgonophosphonate molecule.

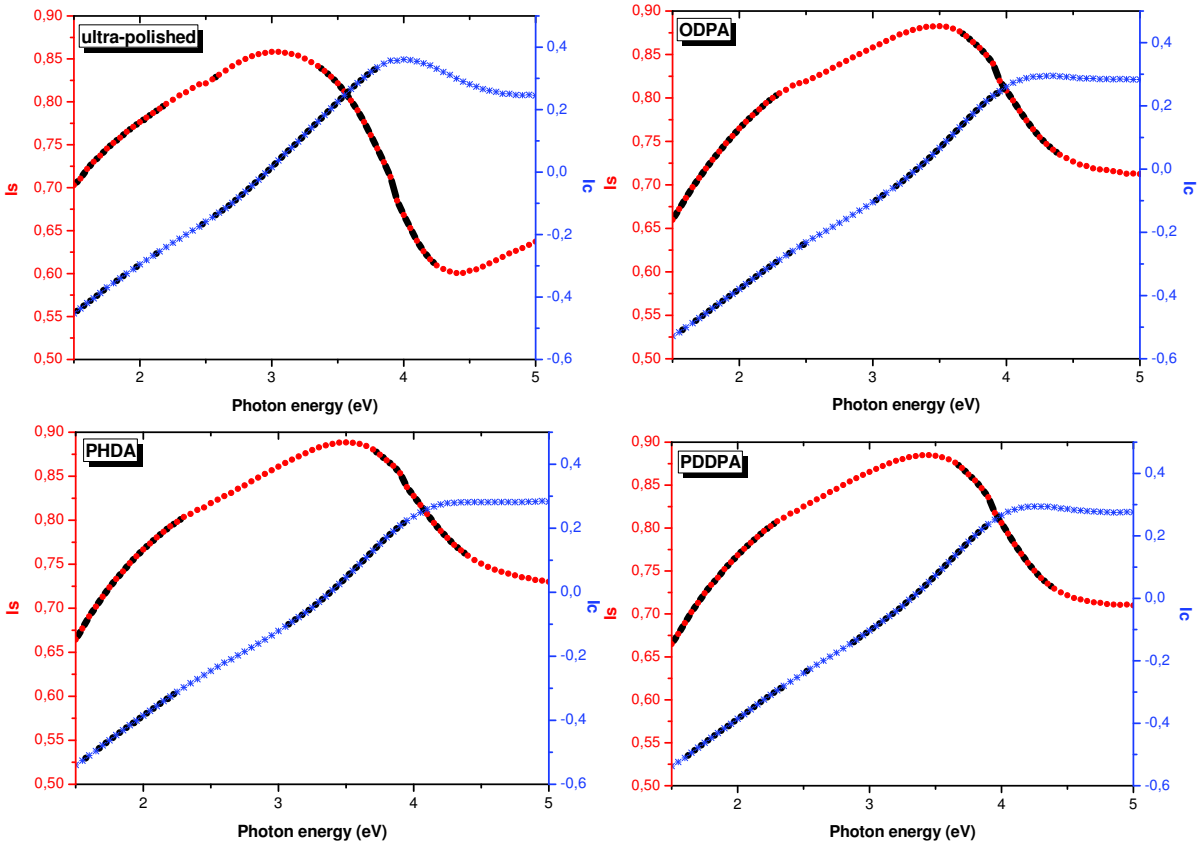

Figure 3.4: Ellipsometry data for the ultra - polished cpTi and SAFs surfaces. The first (Is) and the second (Ic) harmonics of the polarized light are plotted in function of the photon energy. Each graph shows the good agreement between each model (continous line) and the experimental data obtained (dotted line).

3.4 Chemical composition of Self - Assembled Films of alkylphosphonates

The XRD spectra of the cpTi surfaces before the chemical functionalization are plotted in Fig. 3.5. All spectra show the same crystallographic planes, corresponding to metallic titanium. It was also observed a very small amount of titanium hydride (TiH_2) over the ultra - polished cpTi surface and after being treated with argon plasma. This trace of TiH_2 was removed after immersion in water for 24 h. Poorly crystalline and amorphous titanium hydroxide was formed on the surface after 3 days (not shown). The titanium oxide significantly grew after this time in water. A weak peak of rutile was found in all samples. The XRD analysis was not conducted over the SAFs due to the limitations of depth resolution.

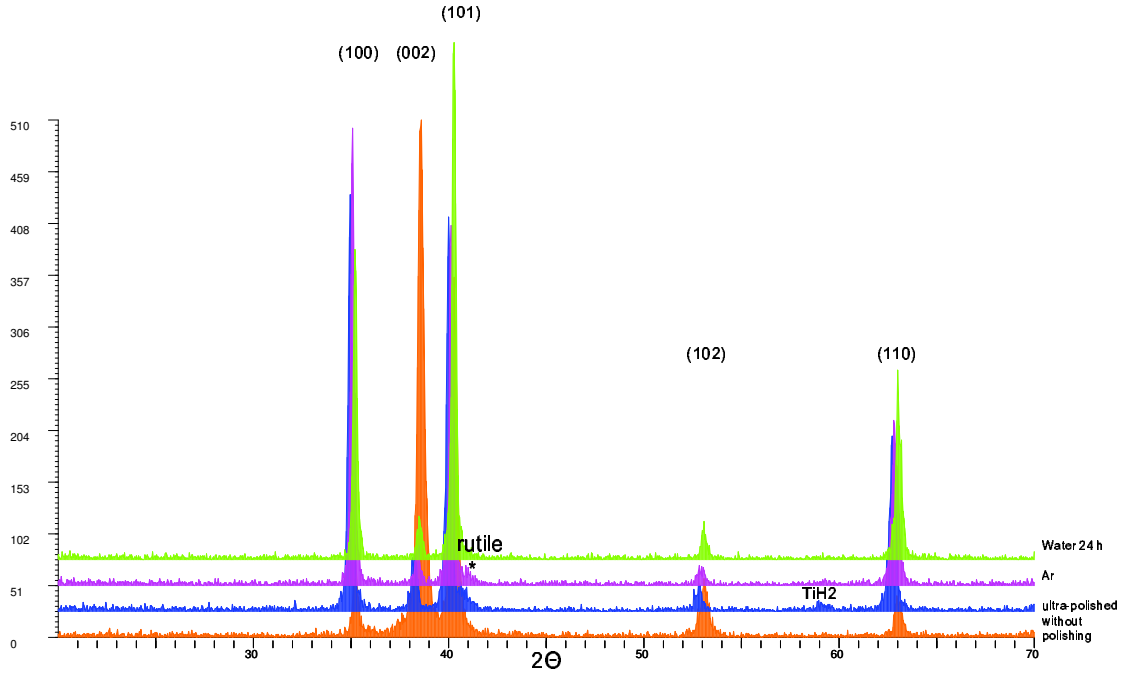

Figure 3.5: XRD spectra of the cpTi surfaces before the chemical functionalization.

The XPS spectra of the oxygen and titanium signals for the cpTi surfaces before the chemical functionalization and for the SAFs formed are plotted in Fig. 3.6. Three deconvolution peaks of oxygen were found as reported in the literature for alkylphosphonates (*132*–*135*). These peaks ($O1s$ (1), $O1s$ (2), and $O1s$ (3)) were observed in the ranges 530.2 - 530.6, 531.1 - 531.5, and 531.9 - 532.5 eV, respectively. The peak $O1s$ (1) was assigned to TiO_2 (rutile) (*136*, *137*), the peak $O1s$ (2) to $P-O-Ti$ and $P=O$ of the SAFs and to $Ti-OH$ of the cpTi surfaces before the chemical functionalization (*132*). Finally the peak $O1s$ (3) was assigned to $P-O-H$ of the SAFs and to $Ti-OH$ of the cpTi surfaces before the SAF formation (*132*). The presence of these bonds ($P-O-Ti$, $P=O$ and $P-O-H$) reveals mono-, bi- and tridentate orientation of the alkylphosphonate molecule over the cpTi surface. The signals of $P-O-Ti$ and $P=O$ bonds mostly indicate the presence of mono- and bridging bidentate modes (see Section 1.3). The $Ti2p$ spectrum is characterized by spin - orbit (3/2, 1/2) doublet components at 458.8 and 464.4 eV (*138*–*143*). The peaks of $Ti2p_{3/2}$ at 453.5 eV and $Ti2p_{1/2}$ at 459.5 eV are produced by the $Ti-Ti$ bond (*138*, *139*, *143*). Our cpTi samples (see Fig. 3.6) showed the $Ti2p_{3/2}$ and $Ti2p_{1/2}$ peaks between 458.8 and 459.1 eV and between 464.6 and 465 eV respectively. These peaks are associated to the $Ti-O$ bond (*144*). The titanium signal corresponds to the oxidation state Ti^{4+} and is assigned to rutile because the $Ti2p_{3/2}$ binding energy is associated to the $O1s$ (1) peak at binding energy of 530.5 eV (*136*). The carbon element can be identified with three contributions of different binding energy as shown in the $C1s$ spectra of Fig. 3.6. Three deconvolution peaks of carbon were found: $C1s$ (1), $C1s$ (2) and $C1s(3)$ (*145*). The main deconvolution peak ($C1s$ (1)) in the cpTi surfaces previous to the SAF formation, with a binding energy of 285 eV, corresponds to adventitious carbon ($-CH_2-$) (*116*). The $C1s$ (2) peak in the ultra-polished cpTi surfaces reveals the $C-N$ bond and in the hydroxylated cpTi surfaces the $C-O$ bond (*146*). The main $C1s$ (1) peak of the ODPA and PHDA surfaces are slightly shifted to the right respect to the

PDDPA surface. The $C1s$ (1) peak in the SAF surfaces, corresponds to the $C-C$ bond (*138*, *147*), with a binding energy of 285.5 eV for the ODPA and PHDA surfaces. In the case of ODPA, this peak also represents the $-CH_3$ terminal groups. The $C1s$ (1) peak for the PDDPA surface has an energy of 285 eV. Unlike the ODPA and PHDA surfaces, this peak reveals the formation of a monolayer rather than a multilayer (*65*). For the SAF surfaces, the $C1s$ (2) peak corresponds to the $C-O-P$ bond (*146*). The third peak ($C1s$ (3)) was weakly found in all the surfaces and it mainly represents the$C-OH$ bond that in the case of the PHDA surface it agrees with the $-COOH$ terminal group (*133*). For the phosphorus signal, we have two contributions at 133 (PDDPA) and 134 (ODPA, PHDA) eV and at 139 eV (see Fig. 3.6). The first peak between 133 and 134 eV corresponds to the PO_4^{3-} bond (*147*, *148*). The second phosphorus peak at 139 eV found in the three SAFs reveales a phosphorus with pentavalent-oxidation state (phosphorane) and apparently in the $P-O$ bond (*149*–*151*). The percentages of each signal are collected in Table 3.4. The percentage of titanium reaches approximately the same value in the surface pretreatments, although the oxygen and carbon signals fluctuate as the treatment. For the case of surface immersed in water, the oxygen percentage increases respect to the ultra - polished surface at the same time that the carbon percentage decreases. And after heating, the carbon signal increases and the oxygen signal decreases due to uncontrolled pollution. The carbon percentage increases in the PHDA and PDDPA surfaces due to the anchoring of alkylphosphonate molecules cases, so that the carbon chain is exposed. The high percentage of phosphorus in the PDDPA surface agrees with the double $-PO(OH)_2$ group.

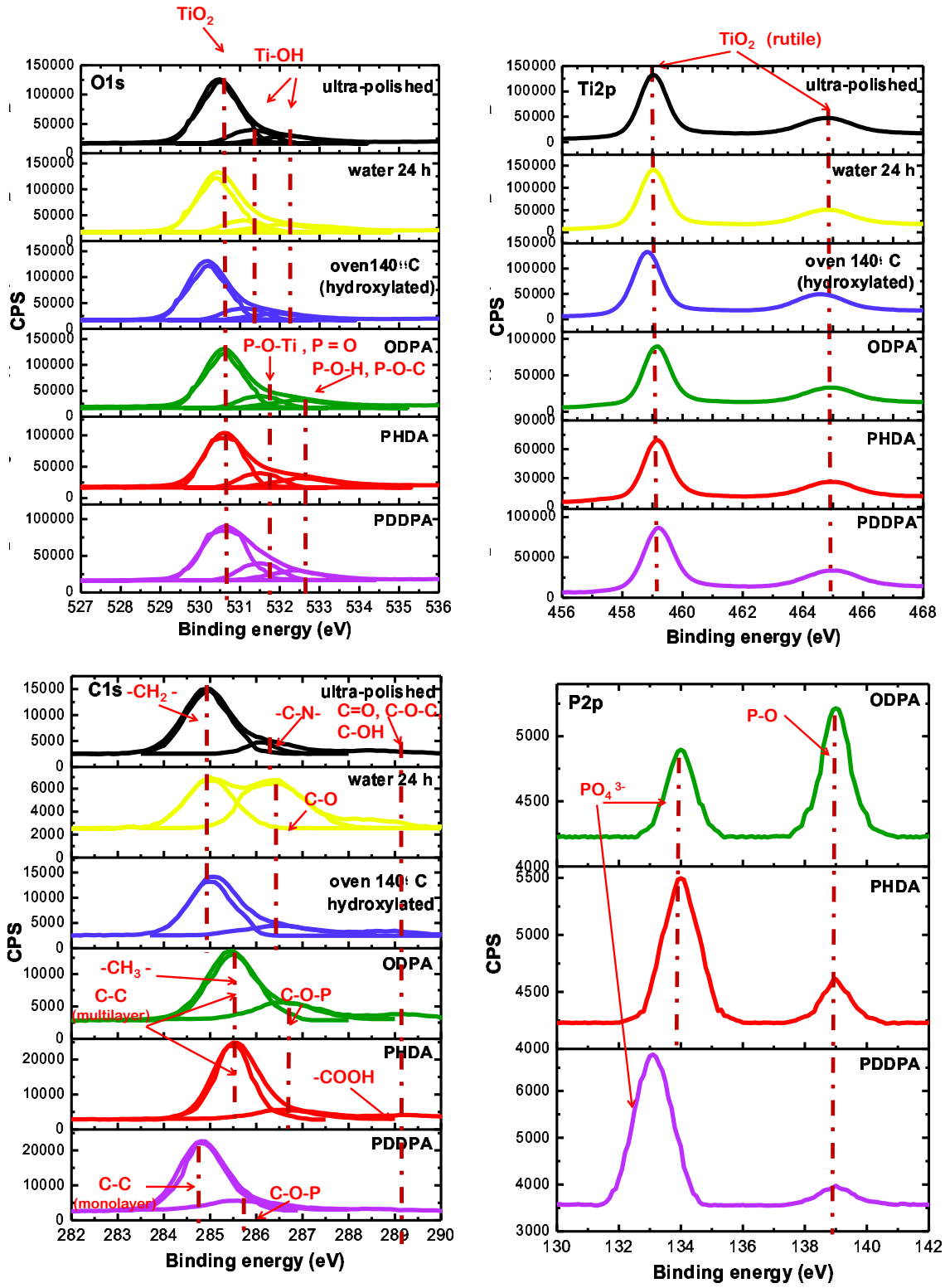

Figure 3.6: XPS spectra of O1s, Ti2p, C1s and P2p signals for cpTi surfaces and SAF surfaces.

Table 3.4: Percentages of the Ti, O, C and P signals shown in Fig. 3.6.

sample	% Ti	% O	% C	% P	O/Ti
ultra-polished	20.42	53.44	26.14	0	2.6
water 24 h	22.53	60.66	16.81	0	2.7
hydroxylated (heated)	20.58	55.08	24.34	0	2.7
ODPA	20.20	57.06	22.61	0.14	
PHDA	15.16	45.79	38.10	0.95	
PDDPA	13.68	45.32	37.35	3.65	

3.5 Wettability of Self - Assembled Films of alkylphosphonates

The water contact angles measured with the tilted drop method over the chemically functionalized cpTi surfaces are plotted in Fig. 3.7. The contact angles (advancing and receding) of control cpTi surface was $\leq 20^{o}$. The highest value of advancing contact angle corresponds to the PHDA - SAF $(84 \pm 0.4)^{o}$ and the lowest one to the PDDPA - SAF $(64 \pm 1.2)^{o}$. The ODPA - SAF revealed an intermediate value of $(78 \pm 1.4)^{o}$. This advancing contact angle is significantly lower than the contact angle value typically reported for a methyl - terminated surface ($\geq 100^{o}$) (*69*, *147*). This indicates that the surface density of ODPA molecules adsorbed on the cpTi surface was not maximum. The contact angle for the carboxyl - terminal group (PHDA) on titanium surface is reported to be between $50 - 70^{o}$ (*22*, *133*, *152*) and for the phosphonate - terminal group (PDDPA) 37^{o} (*153*). These values are below the advancing contact angle measured for our SAF surfaces. Contact angle hysteresis is a key to understand the arrangement of the molecules on the titanium surface. High values of contact angle hysteresis points out to disordered structures (*154*). The highest value of hysteresis corresponds to the PHDA surface $(49 \pm 1.4)^{o}$ followed by the PDDPA surface $(37 \pm 1)^{o}$, and finally the ODPA surface$(31 \pm 1)^{o}$. The head

group plays a critical role for the stability and packing order of the SAF. Head groups such as $-COOH$ and $-PO(OH)_2$ usually produce a decrease in the SAF order rather than $-CH_3$ (*67*, *155*). This reflects the mixed structures of the PHDA and PDDPA surfaces. The advancing contact angles of the PHDA and PDDPA surfaces are associated to the alkyl - chains exposed toward the water. The receding contact angles are affected by the presence of the corresponding hydrophilic terminal group although they are modulated by the existence of bare surface regions. Both advancing and receding contact angles for the ODPA surface decreased due to the existence of uncoated regions of the cpTi surfaces. The advancing angle of the PDDPA surface is lower than the PHDA one due to that the PHDA surface contains a greater number of alkyl - chains. Thus the PHDA and PDDPA surfaces have higher molecular density than the ODPA surface, which is a uncompleted SAF.

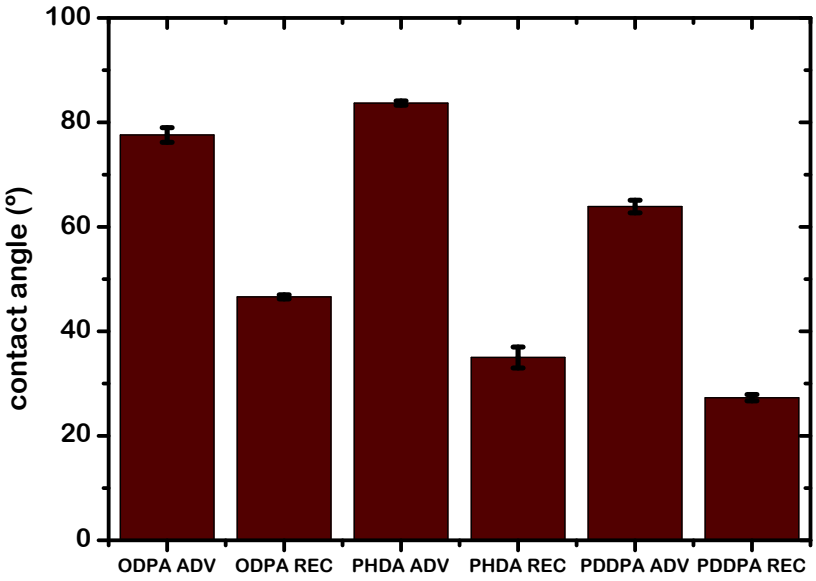

Figure 3.7: Advancing and receding contact angles for each SAF surface.

CHAPTER 4

Growth of Biomimetic Hydroxyapatite on Commercially Pure Titanium Surfaces Functionalized with Alkylphosphonates. A preliminary study

In this preliminary study we carried out experiments with cpTi surfaces modified with two phosphonates molecules: ODPA and PHDA, following the method 1 described in Chapter 3. The incubations in c - SBF were performed directly over the functionalized cpTi surfaces

for 72 h. The cell cultures were conducted with the pre - osteoblastic cell line SAOS - 2 at 24 and 72 h. The chemical functionalization and the biomimetic coatings were examined with AFM and XPS. The adhered cells were visualized with inverted optical microscope (Motic AE31) and SEM.

4.1 Morphology analysis

In Fig. 4.1 we illustrate the AFM topographies of the titanium surfaces over an area of 1 μm^2. The cpTi surfaces before the chemical functionalization (Fig. 4.1 (a) - (b)) were less rough than the modified cpTi surfaces (Fig. 4.1 (c) - (d)). Moreover, the morphology and amplitude of ODPA - SAF was different to the PHDA - SAF.

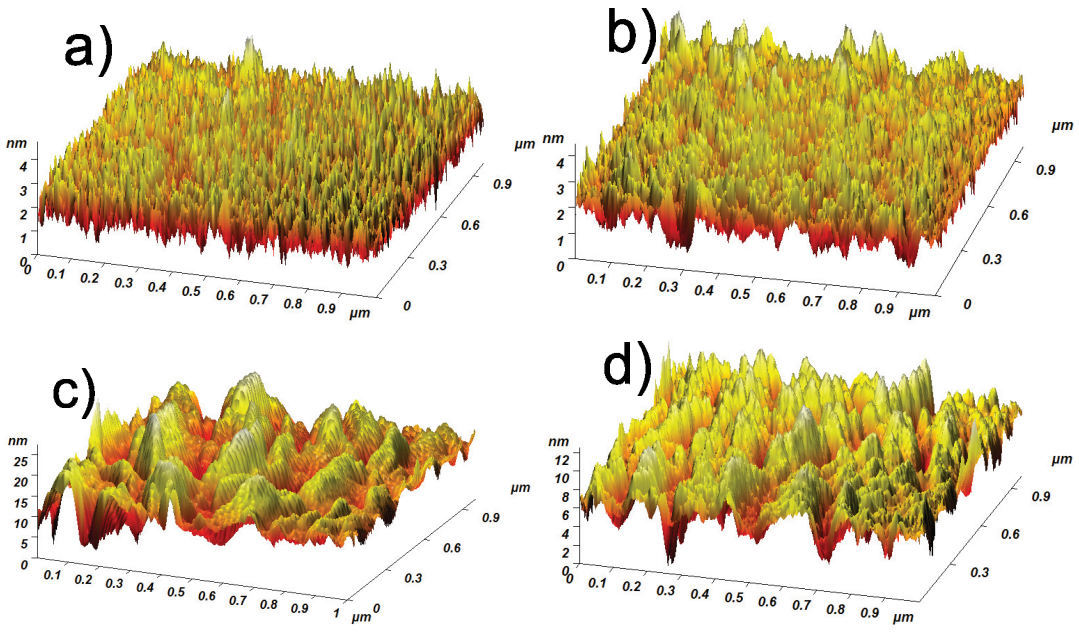

Figure 4.1: Height AFM images of titanium surfaces: a) clean ultra - polished , b) hydroxylated, c) ODPA - SAF and d) PHDA - SAF over a scan area of 1 μm^2.

The roughness values (R_a and R_q) of the ultra - polished cpTi surfaces after each treatment are shown in Fig. 4.2. The roughness of the clean cpTi surfaces remained below 1 nm.

The argon plasma treatment provided the minimum surface roughness.

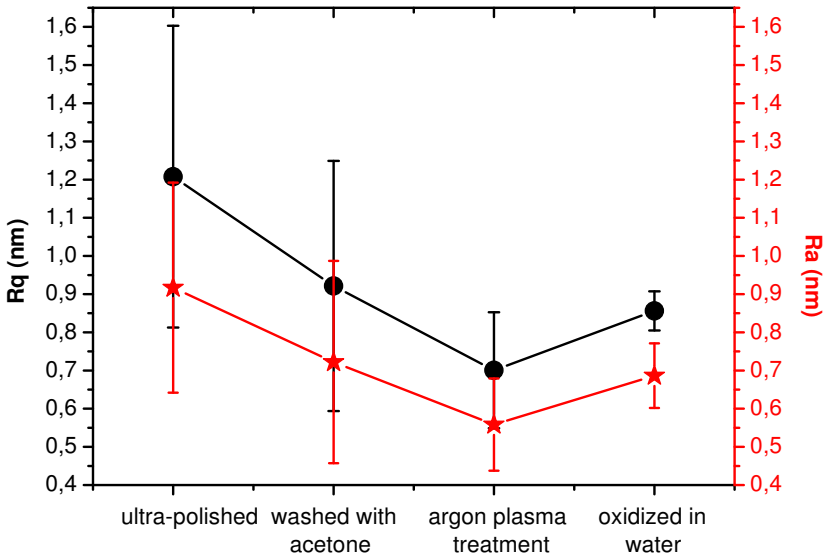

Figure 4.2: Roughness values of cpTi surfaces after polishing, cleaning and oxidation (scan area of 1 μm^2).

The SEM analysis of the SAFs and the biomimetic coatings formed after 72 h in c - SBF are shown in Fig. 4.3. It was not possible to appreciate the SAF over each cpTi surface (Fig. 4.3 (a) - (b)). However, there is a clear difference between the biomimetic HA coatings (Fig. 4.3(c) - (d)).

4.2 Surface chemistry analysis

In Fig. 4.4 we plot the XPS peaks of the $Ti2p$ and $C1s$ signals. The binding energies found for $Ti2p$ correspond to rutile (*136*, *137*). The strong $Ti2p$ signal indicates that the SAFs and biomimetic coatings are thin. We also found $C1s$ spectra carbon signal. The deconvolution peak for the ultra - polished titanium at 285.29 eV is assigned to adventitious carbon (-CH_2-) (*116*). For the ODPA and PHDA SAFs, the $C1s$ spectra provide deconvolution peaks at $\sim$ 285 eV ($C-H$) (*156*) and $\sim$ 286 eV ($C-O$), respectively. For the case of the

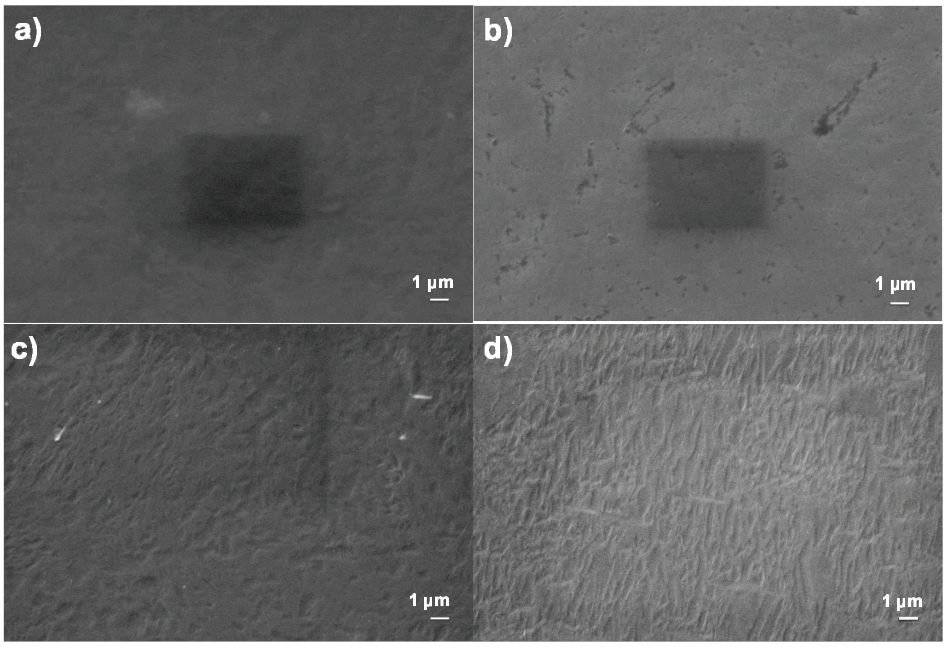

Figure 4.3: SEM micrographs of a) ODPA - SAF and b) PHDA - SAF and c) ODPA - SAF and d) PHDA - SAF after immersion in SBF. The dark square was produced by the incidence of the electron beam after reducing the scanning area.

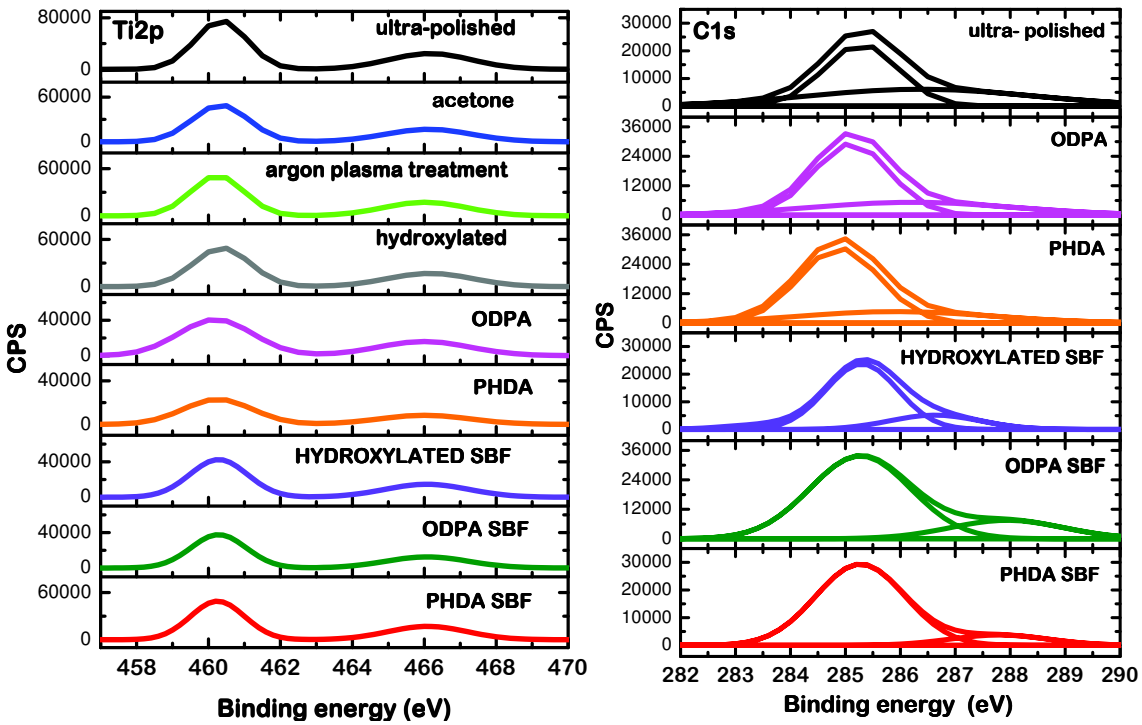

Figure 4.4: XPS spectra of $Ti2p$ and $C1s$ signals.

HA coatings, the $C1s$ spectra of the hydroxylated, ODPA - SAF and PHDA - SAF surfaces provide a deconvolution peak at 285.4 eV. The oxygen at this binding energy is bond to the hydroxyl groups (OH). The second deconvolution peak appears at 286.6 eV ($C-O$) in the hydroxylated sample and at 288 eV ($C=O$) (*157*) in the ODPA and PHDA samples.

In Fig. 4.5 the spectra of $P2p$ and $Ca2p$ signals are plotted. The observed deconvolution peak with the binding energy at $\sim$ 138 eV in the ODPA - SAF and PHDA - SAF surfaces corresponds at the oxidation state III of phosphorus also known as phosphine (*149*). The phosphine peak dissapears in the spectra of the coatings on the hydroxylated sample. This confirms that it is associated to the chemical functionalization based on the organophosphonate molecules. The main deconvolution peak at 133 eV corresponds to the $P2p_{3/2}$ signal (PO_4^{-3}) (*147*, *148*), as found in hydroxyapatite (*144*). In the phosphorus spectra of the HA coating formed on the PHDA - SAF, we found a third peak at the binding energy of 135 eV, corresponding to an oxygen ligand (*158*). In the calcium spectra, the main deconvolution peak is at 348.6 eV ($Ca2p_{3/2}$ calcium element) (*159*). The second deconvolution peak is found at 352 eV ($Ca2\ p_{1/2}$) and it is associated to the bond with hydroxyl groups (*160*). The Ca/P ratios obtained in the biomimetic coatings are shown in Table 4.1. The Ca/P ratio increases from the hydroxylated cpTi surface up to the PHDA - SAF. The maximum value is close to 1.67, the value reported in the literature for the stechiometric hydroxyapatite (*161*).

Table 4.1: Ca/P ratios for the obtained cpTi surfaces after 72 h in SBF.

sample	Ca/P
hydroxylated	1.357
ODPA - SAF	1.400
PHDA - SAF	1.538

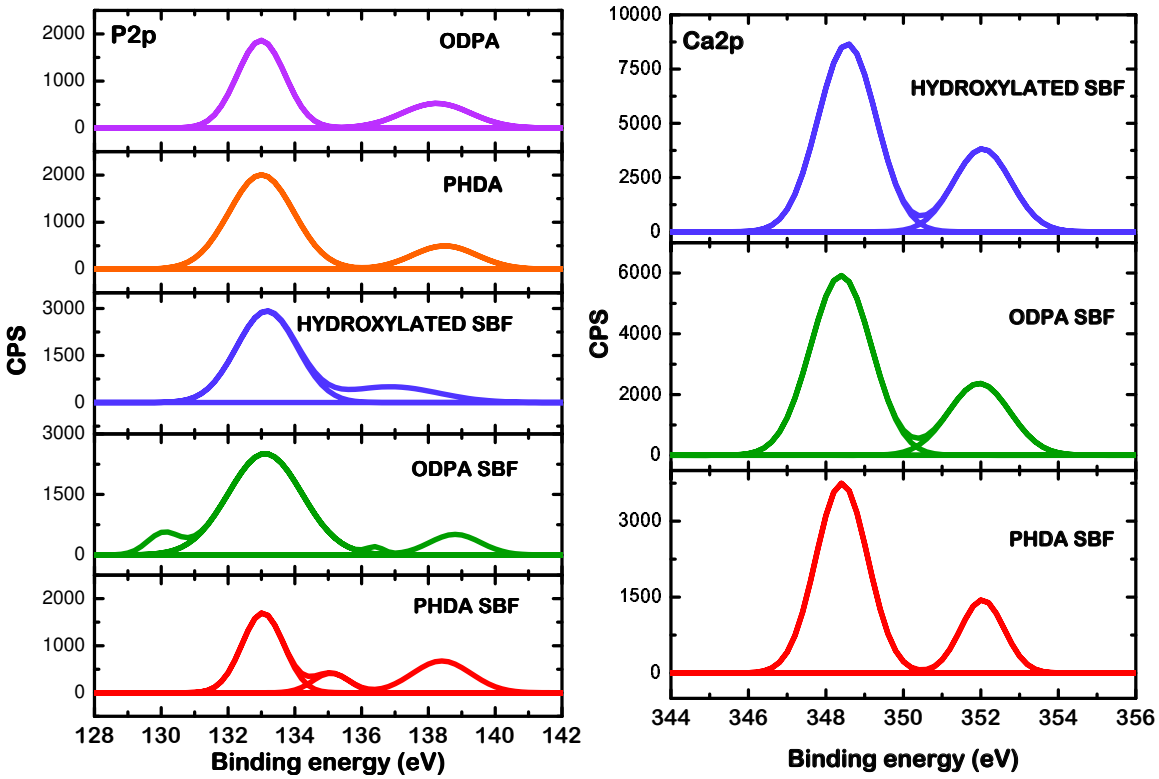

Figure 4.5: XPS spectra of $P2p$ and $Ca2p$ signals.

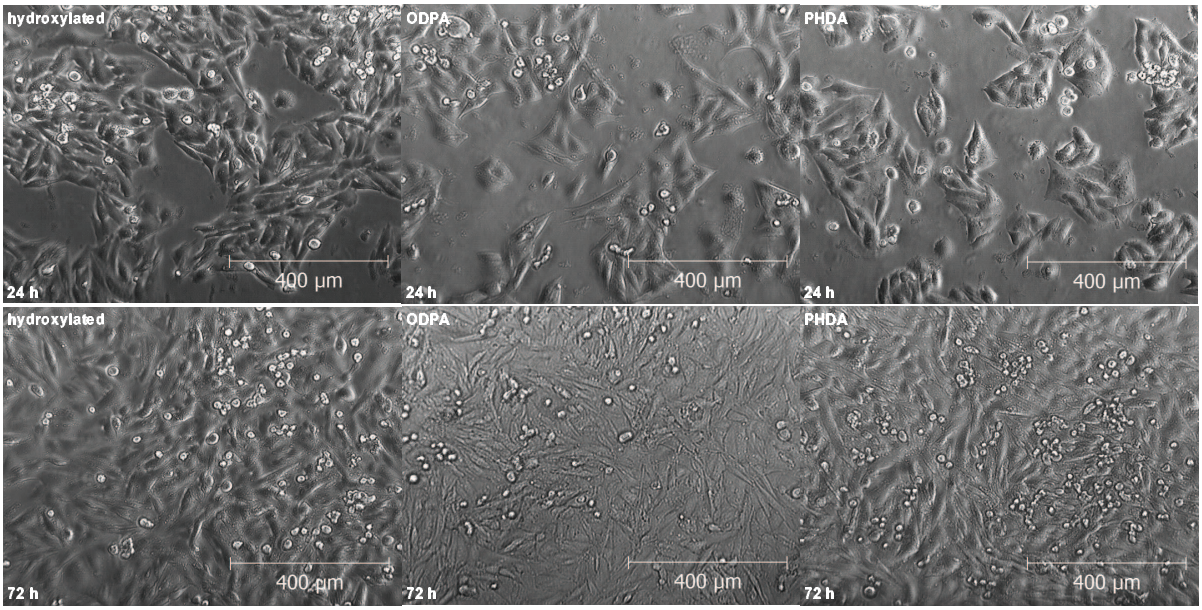

Figure 4.6: Optical images of SAOS-2 cells on the biomimetic HA coatings after 24 and 72 h.

4.3 Cell assays results

Finally, from the cell cultures, we found differences between 24 and 72 h (see Fig. 4.6). At 24 h, the cell spreading is very similar between the HA coatings formed on the hydroxylated, ODPA - SAF and PHDA - SAF surfaces. However, after 72 h, the differences are noticeable. The hydroxylated and ODPA - SAF samples revealed similar degree of cell coverage but the PHDA - SAF sample provided a full coverage surface. The adhered cells on the ODPA - SAF, PHDA - SAF and hydroxylated samples were observed by SEM (Fig. 4.7). It is validated the fact that after 72 h, the PHDA - HA coating produced a full cell coverage. Moreover, for 24 h a more cellular activity (cell shape) is observed on the PHDA - HA coating. Instead the cell appearance on the hydroxylated - HA coating was different: fibroblast-like flat cells. The biological activity on the PHDA - HA coatings postulates the bone formation.

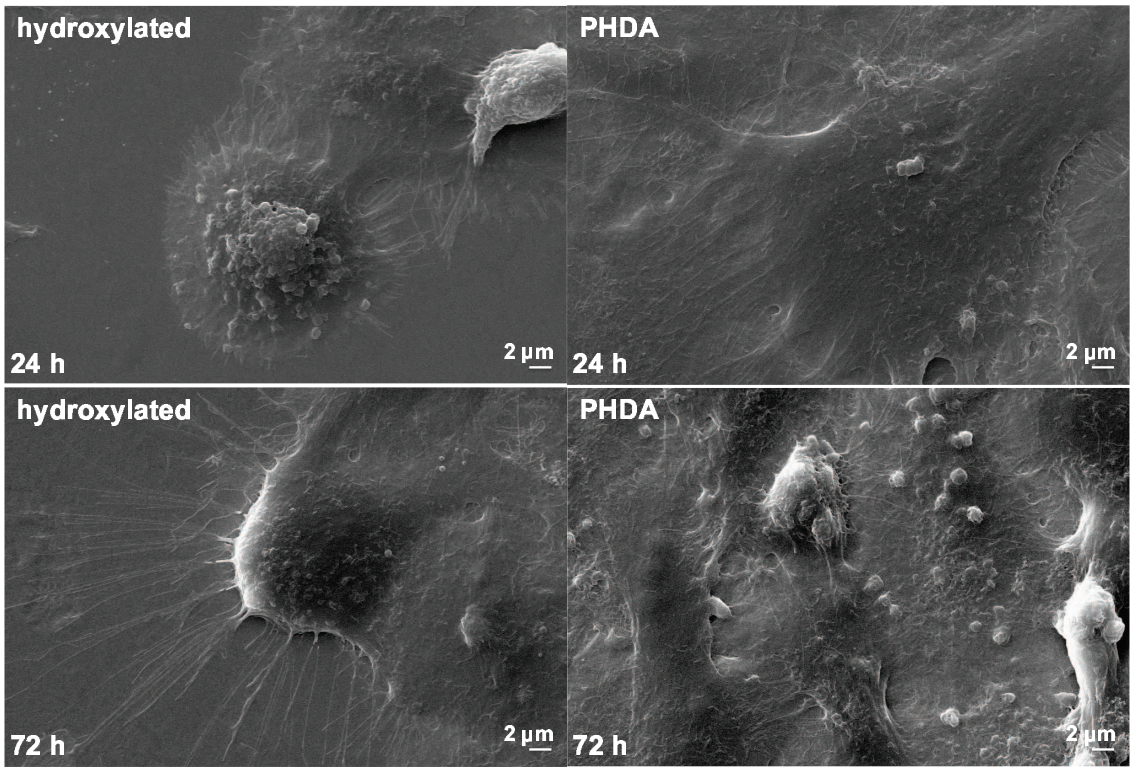

Figure 4.7: SEM micrographs of SAOS-2 cells on the biomimetic HA coatings formed on hydroxylated and carboxyl - terminated cpTi surfaces (PHDA - SAF).

CHAPTER 5

Growth of biomimetic hydroxyapatite on chemically - functionalized titanium surfaces. Effect of the alkylphosphonate film

In this chapter, we examined the role of the functional groups of the SAF formed on the cpTi surfaces in the HA nucleation and growth by biomimetic precipitation. We explored three alkylphosphonic acids with three different terminal end groups: methyl, carboxyl and phosphoryl. We studied the morphology, topography, surface chemistry and wettability of the HA coatings. The details of the chemical functionalization of cpTi surfaces described

in Chapters 2 and 3. The process of biomimetic precipitation was described in Section 2.3. Based on the results of biomimetic HA coatings described in Chapter 4, in the current chapter we conducted a previous nucleation of nascent calcium phosphate (*110*) to reduce the time of biomimetic HA growth. We further increased the concentration of ions in the SBF formulation up to 1.5 times the recipe of Kokubo (*51*, *96*, *97*). Biomimetic precipitation was performed with the samples oriented vertically and horizontally and at 2 days of immersion in SBF. However, in Appendix A, we show some results for longer times. Finally, we carried out *in vitro* experiments of cell adhesion with the osteoblastic linage MG - 63, which may provide more information about the osteointegration of the biomimetic HA coatings obtained. As mentioned in Chapter 2, the MG - 63 cell line exhibits fundamental phenotypic characteristics of osteoblastic cells. Osteoblastic cells are responsible for the synthesis and mineralization of bone during initial bone formation and bone remodeling. Several techniques are listed in the literature to assess adhesion but the results from one test cannot be directly compared with another. Qualitative comparison is possible with numerous tests such as scotch tape test, peel test, scratch tests, etc. Nano - indentation with an AFM or with a scanning probe microscope (SPM) is becoming popular due to its versatility with various films. However, the results of all the above tests are affected by stresses and defects in the films and hence it is difficult to determine the true adhesional force. For this purpose, contact angle measurements are performed to evaluate the accurate adhesion energy.

5.1 Morphology analysis

5.1.1 Calcium phosphate coatings previous to biomimetic precipitation

The nascent CaP layer was performed with a fast precipitation method as described in the Section 2.3. As observed in Fig. 5.1 a), c) and d) the topographical features are more visible and distributed over the entire surface. On the ODPA surface (Fig. 5.1 b)) the nascent CaP film reveals less and uneven topographical features. The roughness parameters of the CaP layers (Fig. 5.2) increased as compared to the values of the chemically modified cpTi surfaces (see Table 3.2). Except for the error bars of the roughness of the hydroxyl - terminated surface and the phosphoryl - terminated surface, the highest roughness value was obtained with the underlaying PHDA - SAF, and the lowest value with the ODPA - SAF. From here, all the biomimetic coatings were performed over surfaces covered with a CaP layer.

From the ESEM images (Fig. 5.3), we can appreciate how the CaP layer reveals different crystal phases. The crystal planes are clearly seen on the hydroxylated and ODPA surfaces (a) and b) Fig. 5.3), being more amorphous the crystalline forms of the hydroxylated surface and less amorphous the crystalline forms of the ODPA surface. As soon as crystal growth begins in a polar region, mass transport to the growing crystals depletes calcium and carbonate ions over the local methyl - terminated region to the point of undersaturation. We can appreciate the morphological similarity between the hydroxylated and ODPA surfaces, confirming the existence of $-CH_3 + TiO_2$ groups over the ODPA surface. Otherwise, the CaP layer on the PHDA and PDDPA surfaces look like globular structures. As expected, validated by XRD, the CaP layer of all surfaces is weakly crystallized due to the non -

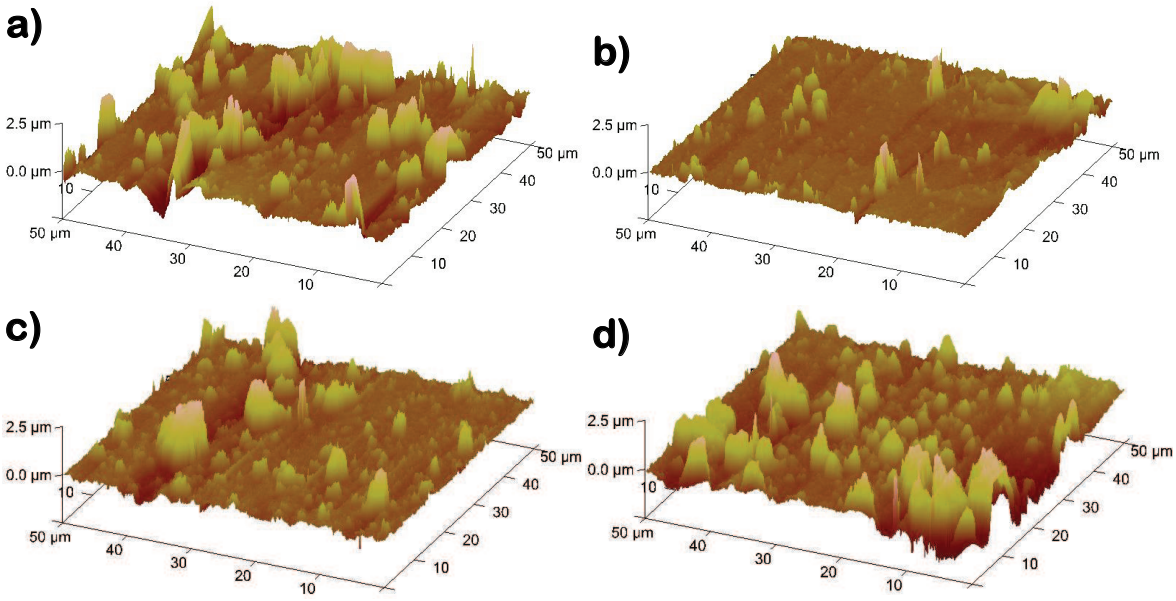

Figure 5.1: AFM images of the chemically - modified cpTi surfaces coated by the CaP layer previous to the biomimetic precipitation: a) hydroxylated, b) ODPA, c) PHDA and d) PDDPA. The scan area was 50 x 50 μm^2.

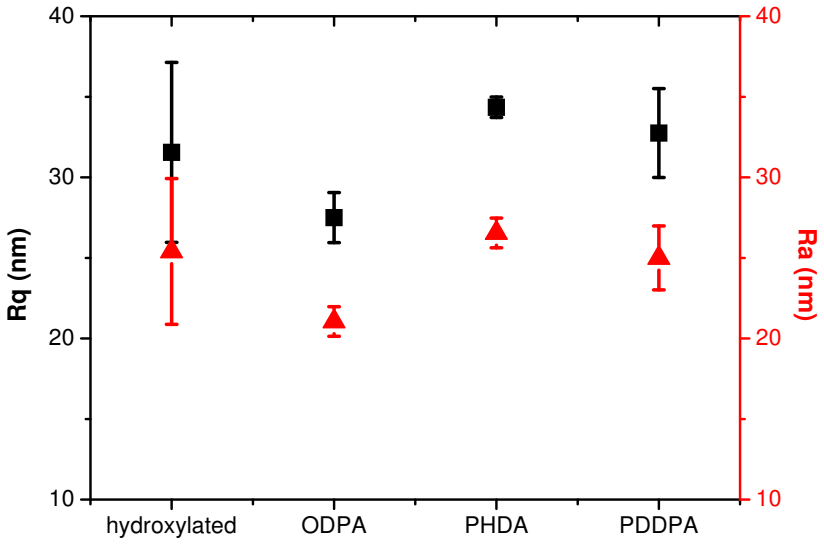

Figure 5.2: Roughness values of the CaP layer formed on the chemically - functionalized cpTi sufaces before the biomimetic precipitation. The scan area was 1 x 1 μm^2. The values were averaged over two different AFM images.

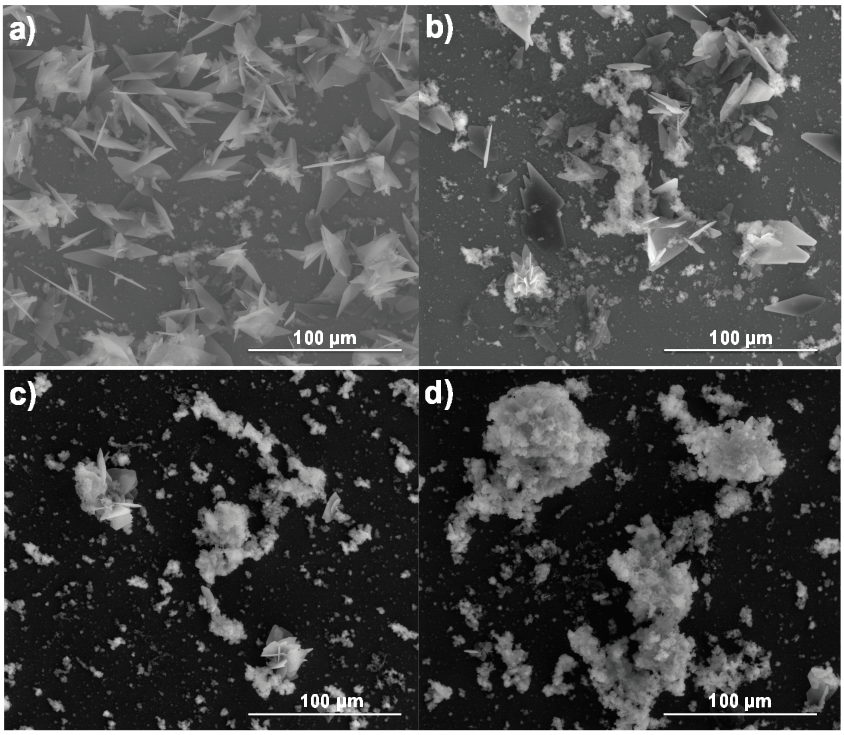

Figure 5.3: ESEM micrographs of the chemically - modified cpTi surfaces coated by the CaP layer previous to the biomimetic precipitation: a) hydroxylated, b) ODPA, c) PHDA and d) PDDPA.

physiological conditions used in its deposition.

5.1.2 Hydroxyapatite coatings

In Fig 5.4 we observe clear differences between the HA coatings formed on the cpTi surfaces modified with functional groups and with different sample orientation during the SBF immersion. Regarding the sample orientation during immersion in SBF, the HA coatings produced mostly in the vertical orientation showed higher globular features and surface coverage degree. The PHDA - SAF produced the greatest uniformity in the HA coating and the best definition of globular shape. It is worthing to notice that the aspect of the HA coatings is significantly different to the nascent CaP layers formed previously to the

biomimetic precipitation (Fig. 5.1).

A grape bunch - like morphology is mostly identified in the ESEM images (Fig. 5.5). Some cracks can be appreciated due to the dehydration of the HA coating. However, a new precursor crystalline phase of apatite can be observed on the vertically - subjected surfaces. Moreover, the vertical orientation mostly leads to biomimetic coatings with greater coverage degree on the titanium surfaces.

The roughness values of the HA coatings produced by biomimetic precipitation after 2 days are plotted in Fig. 5.6. There is a noticeable effect of the sample orientation (vertical or horizontal) for the hydroxylated and ODPA surfaces during the precipitation. The HA coatings were rougher on the vertically - subjected samples.

The thickness values of the HA coatings were estimated by WLCM (see Table 5.1). Two profiles are plotted in Fig. 5.7. The thickness values for the CaP layer formed before the HA coating varied between 0.7 and 1 μm. However, the thickness of the HA coatings reached a constant value of 1 μm except for the PHDA surface, where the value increased up to 2 μm. These values were validated with the ESEM images of cross-sectioned samples (Fig. 5.8).

Table 5.1: Thickness values of the coatings obtained after the pre - deposit of calcium phosphate and after the biomimetic precipitation (2 days SBF immersion, vertically subjected samples).

SAF	CaP layer (μm)	HA coating (μm)
hydroxylated surface	0.7	1
ODPA	0.8	1
PHDA	0.8	2
PDDPA	1	1

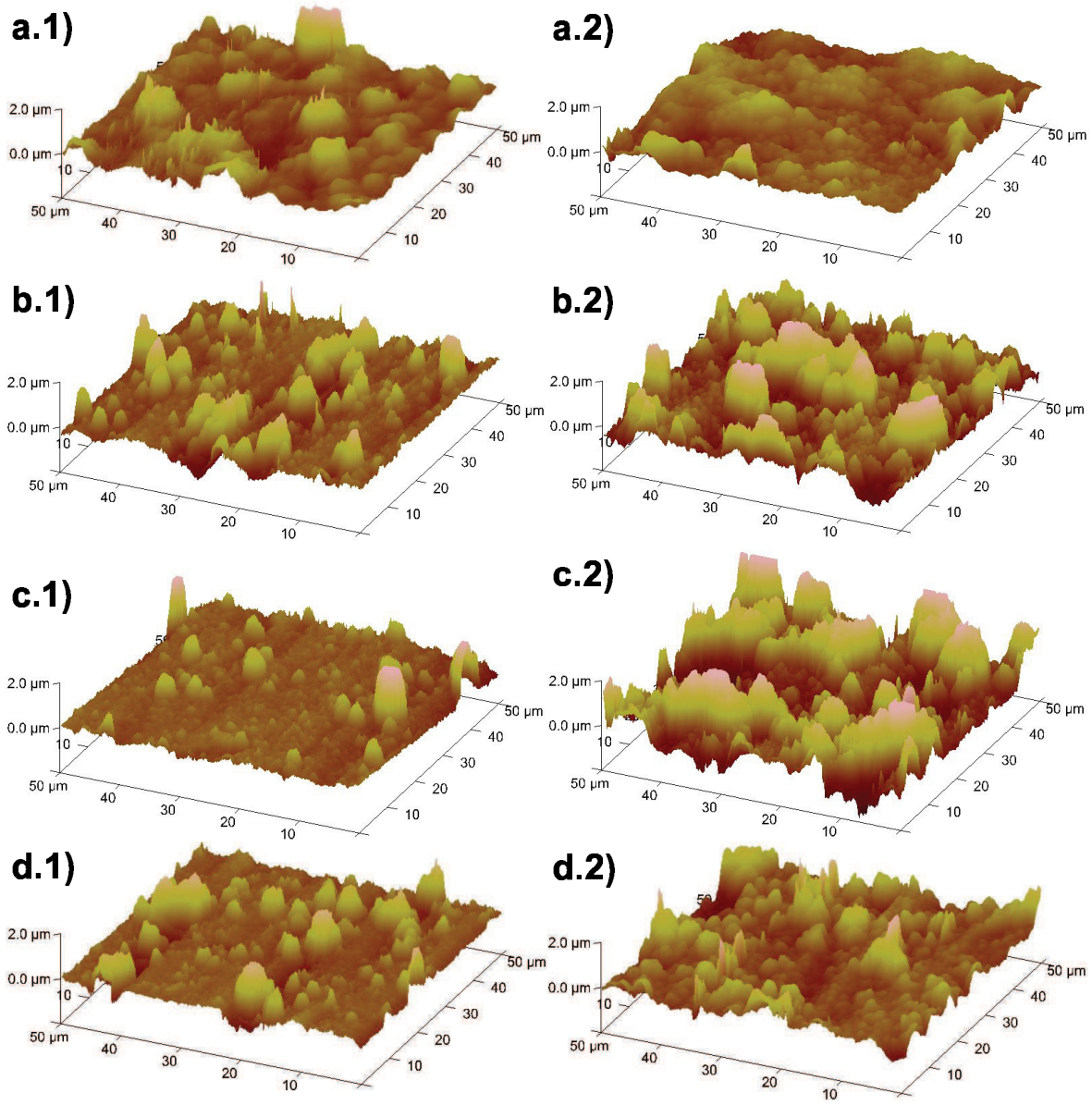

Figure 5.4: AFM images of the HA coatings formed at 2 days on the surfaces modified with different SAF: 1) horizontally - subjected and 2) vertically - subjected, a) hydroxylated, b) ODPA, c) PHDA and d) PDDPA. The scan area was 50 x 50 μm^2.

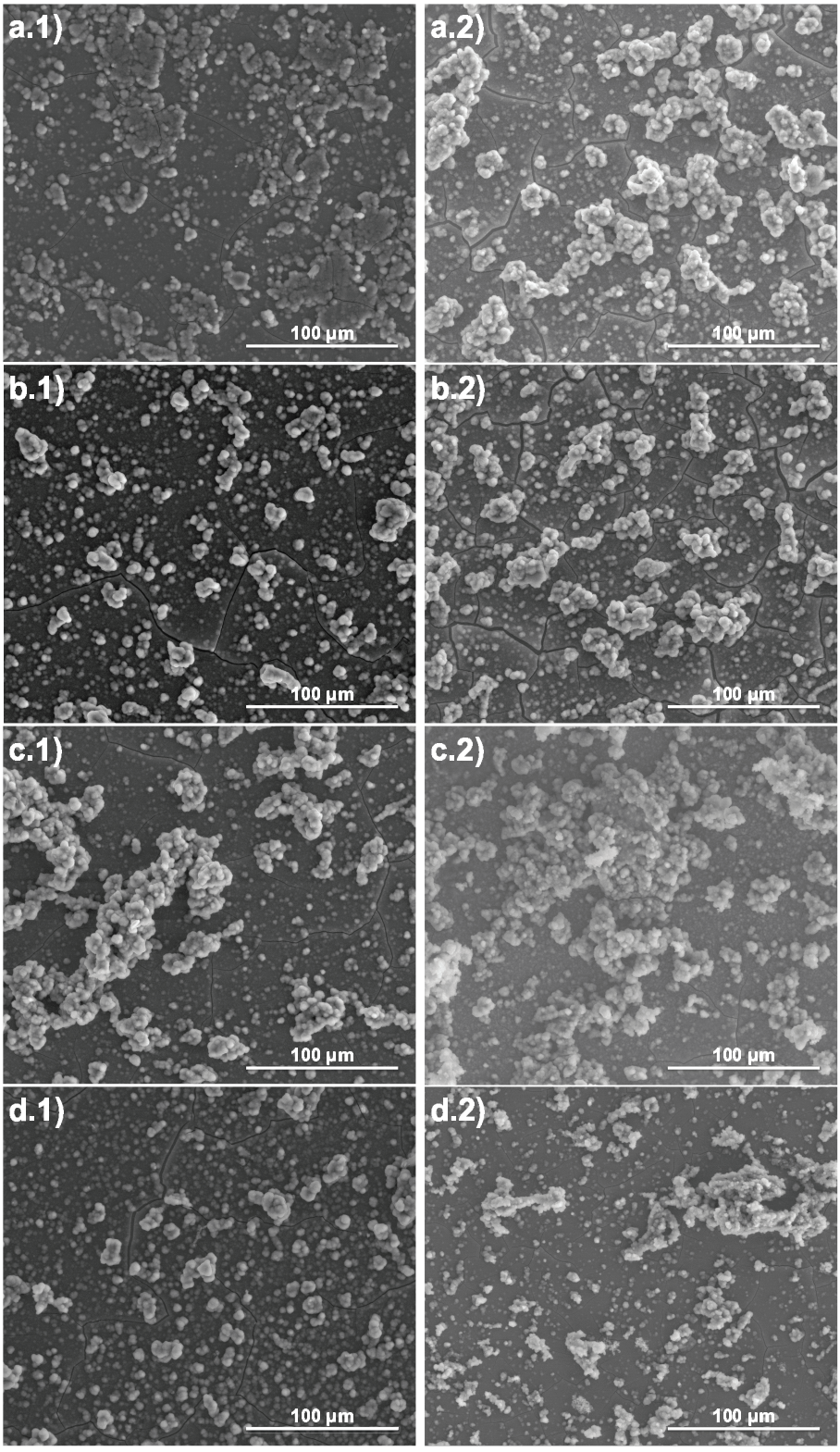

Figure 5.5: ESEM images of the HA coatings formed at 2 days on the surfaces modified with different SAF: 1) horizontally - subjected and 2) vertically - subjected, a) hydroxylated, b) ODPA, c) PHDA and d) PDDPA.

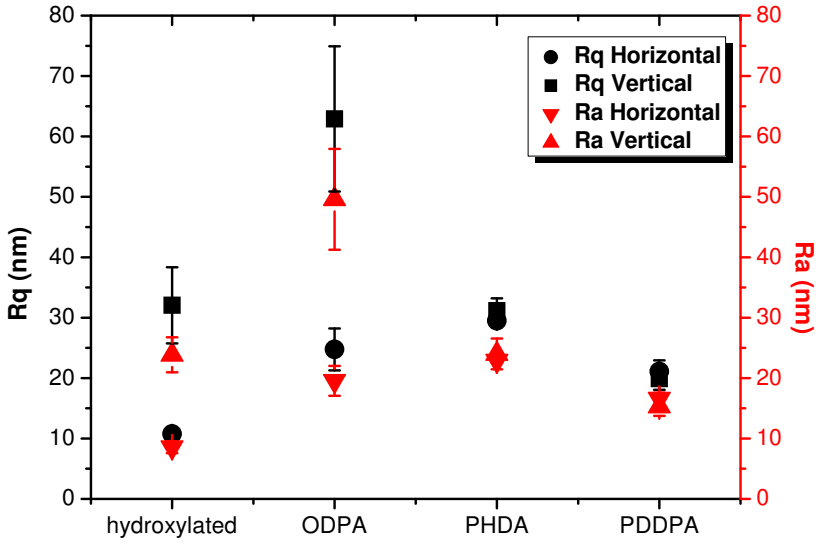

Figure 5.6: Roughness values of the HA coatings formed after 2 days in SBF with horizontal and vertical orientation. The scan area was 1 x 1 μm^2. The values were averaged over two different AFM images.

5.2 Surface chemistry analysis

Based on the observed differences in the AFM and ESEM images, as in the roughness values, we focused mainly in the HA coatings produced with the vertical incubation in SBF. In Fig. 5.9 we plot the XPS spectra for the phosphorus and calcium found on the nascent CaP layers and the HA coatings after biomimetic precipitation at 2 days with the horizontal and vertical orientations of sample. The $Ca2p_{3/2}$ peak at 346.9 eV and the $Ca2p_{1/2}$ peak at 350.4 eV correspond to the binding energies for the orthophosphate phase close to HA (*162*). The $P2p$ peak at 133 eV agrees with the data reported for HA (*144*). The $Ca2p_{3/2}$, $Ca2p_{1/2}$ and $P2p$ signals corresponding to the nascent CaP layer were slightly shifted respect to the HA peaks. This shift reveals the amorphous nature of the CaP layer previous to the HA coating. The Ca/P ratios for each surface are shown in Table 5.2. The Ca/P ratio value for the nascent CaP layer corresponds to Amorphous Calcium Phosphate (ACP) phase. Instead, the Ca/P ratio values for the HA coatings correspond to Calcium

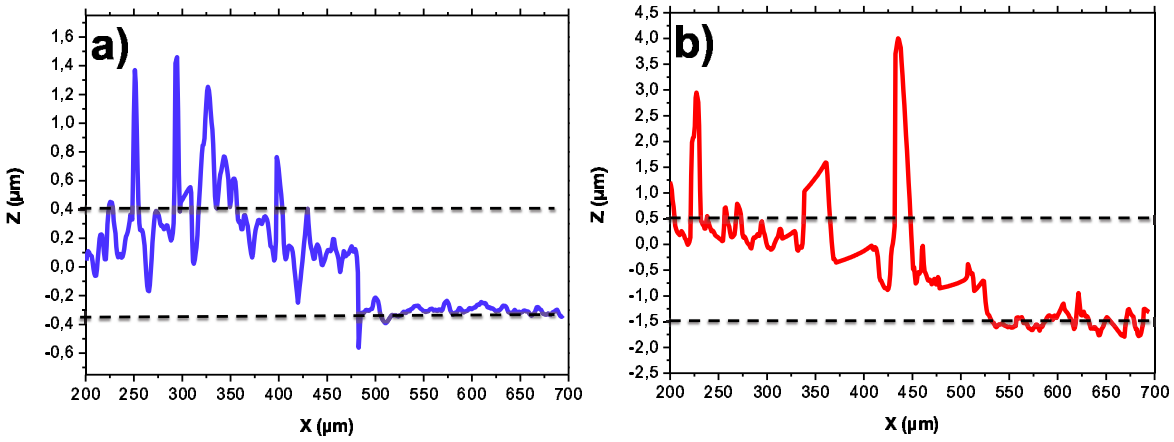

Figure 5.7: Examples of the profiles obtained by WLCM: a) Hydroxylated surface with CaP layer and b)PHDA surface with HA coating formed at 2 days in SBF (vertically-subjected sample). The dashed lines were used to estimate the thickness of each layer.

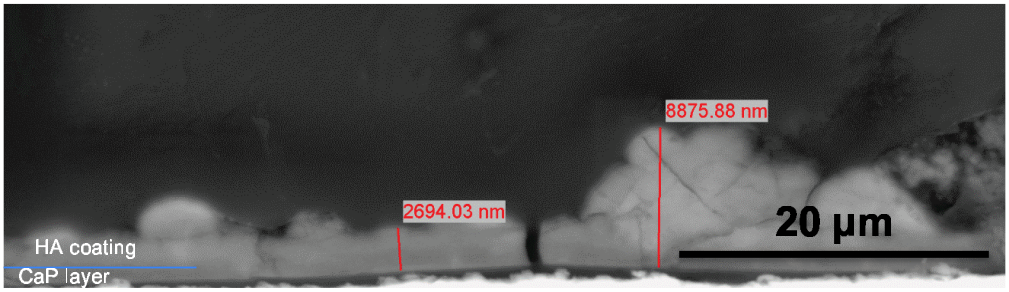

Figure 5.8: ESEM image of a cross-sectioned sample of HA coating formed on the PHDA surface.

Deficient Hydroxyapatite (CDHA). Regarding to the XRD analysis, in Fig. 5.10 and 5.11, we plot the spectra for the CaP layers and the HA coatings respectively. For the early CaP deposit, we found the peaks corresponding to titanium and the amorphous phases of CaP. The XRD peaks of CaP correspond to brushite and ACP (*163*, *164*). This result is consistent with the crystals observed in the ESEM images of the CaP layers (Fig. 5.3). Regarding the spectra of HA coatings, we found the titanium signal peaks and the rest of peaks correspond to apatite as referenced in literature (*48*, *99*, *106*, *165*, *166*).

Table 5.2: Ca/P ratios of the CaP layer before the biomimetic precipitation and the HA coatings produced with the horizontal and vertical orientations.

SAF	CaP layer	HA coating (horizontal)	HA coating (vertical)
Hydroxylated surface	1.136	1.326	1.434
ODPA	1.17	1.355	1.440
PHDA	1.149	1.349	1.380
PDDPA	1.146	1.374	1.406

5.3 Wettability analysis

The static values of water contact angle of the HA coatings formed on the four modified surfaces (hydroxylated, ODPA, PHDA and PDDPA), and of the uncoated cpTi surface (control) are plotted in Fig. 5.12. The measurements were performed by the captive bubble method, as described in Chapter 2. The contact angle values were in the range of 10^{o} to 25^{o}, namely, all the surfaces were significantly hydrophilic surfaces. The water contact angle value of the nascent CaP layers formed on the four modified surfaces previously to the biomimetic precipitation was $\approx 19^{o}$. A hydrophilic coating usually favours the protein adsorption, and increases the cell adhesion (*167*). However, there was no significant difference between hydroxylated, ODPA and PHDA surfaces ($\approx 20^{o}$). The HA coating formed on the PDDPA surface was the most hydrophilic coating ($\approx 16^{o}$).

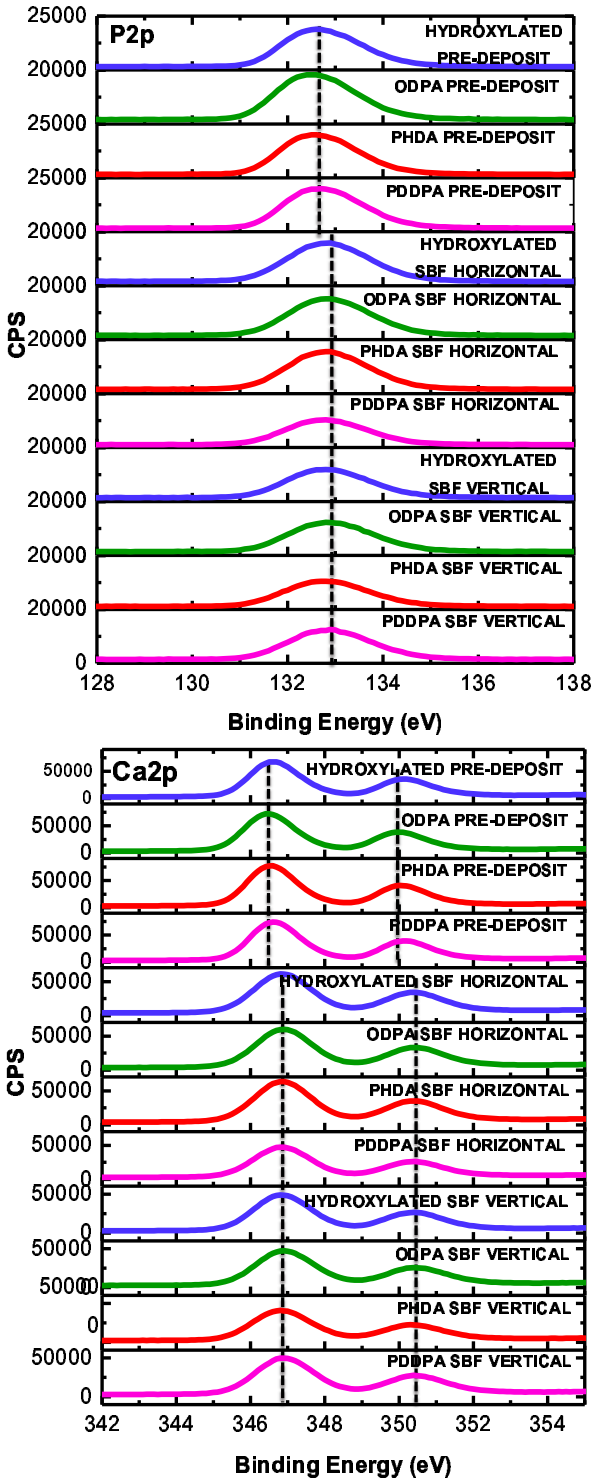

Figure 5.9: $P2p$ and $Ca2p$ XPS spectra for the nascent CaP layers before the biomimetic precipitation and the subsequent HA coatings with the horizontal and vertical orientations.

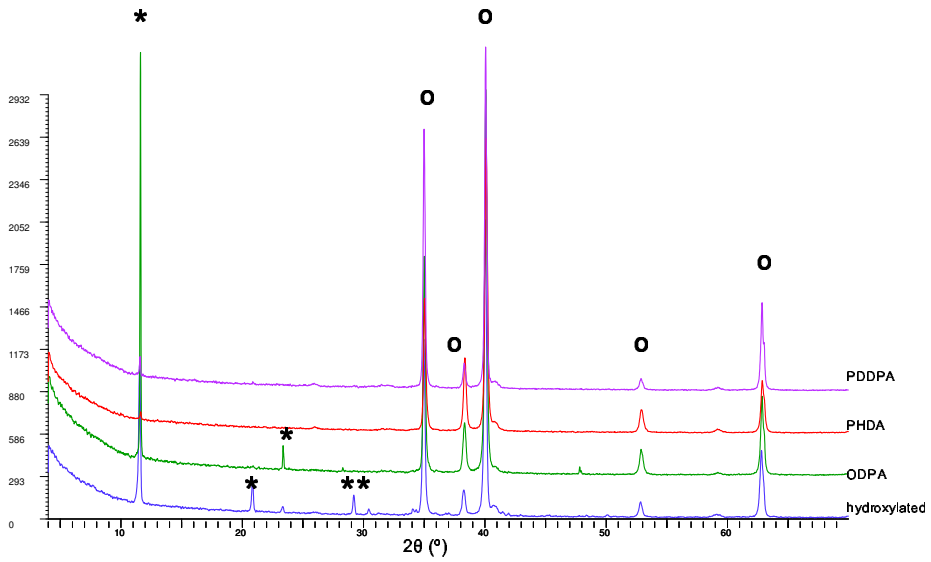

Figure 5.10: XRD spectra of the CaP layers obtained after pre - deposition. The "*" symbol corresponds to the peaks of brushite and the "o" symbol corresponds to titanium peaks.

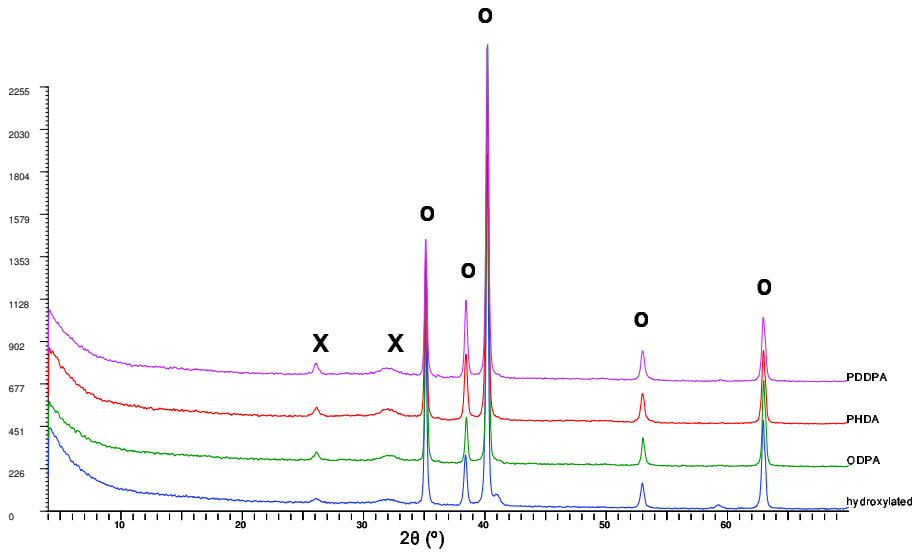

Figure 5.11: XRD spectra of the HA coatings obtained after biomimetic precipitation (2 days - SBF immersion vertically subjected samples). The "x" symbol corresponds to the peaks of apatite and the "o" symbol corresponds to titanium peaks.

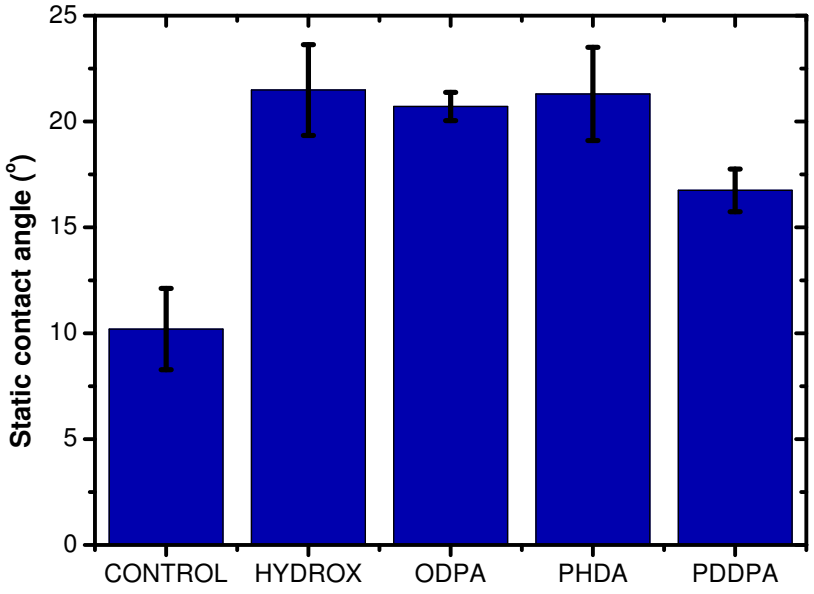

Figure 5.12: Static water contact angles of the HA coatings and the uncoated cpTi surface (control).

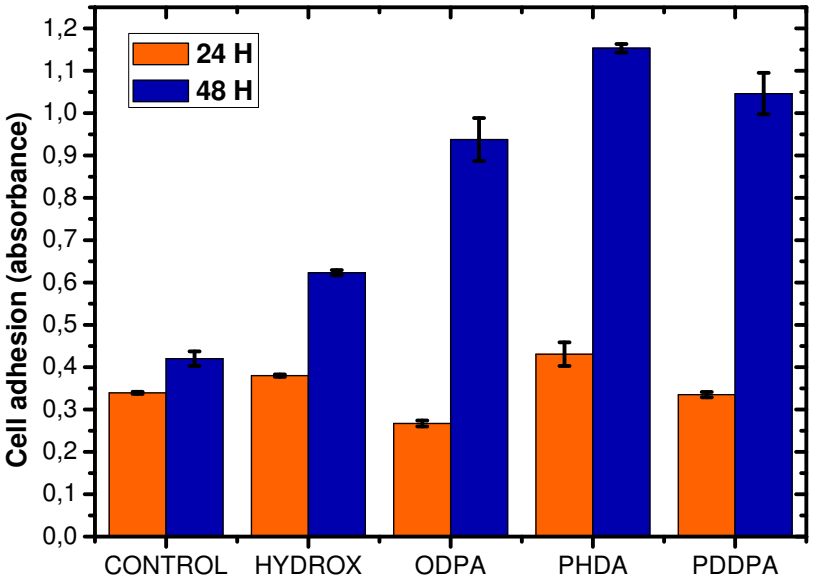

Figure 5.13: Cell adhesion results for the HA coatings formed on the modified surfaces (2 days SBF immersion) and the uncoated titanium surface (control).

5.4 Cell assays results

We plot the cell adhesion results on the HA coatings in Fig. 5.13. For 24 h, the ODPA surface showed the lowest adhesion, even below the control sample and the PHDA surface the highest value. For 48 h, the cell adhesion increased significantly. Although, the greater variations were found for the chemically - modified cpTi surfaces. The PHDA surface produced the most osteoconductive coating and next, the PDDPA surface. Surprisingly, the ODPA surface provided better results of cell adhesion that the HA coatings formed on the hydroxylated surface. This is justified by the surface heterogeneity in the SAF composed of bare regions, methyl - terminated regions and hydrocarbon - coated regions, as mentioned in Section 2.1.2, based on the preferential crystal growth of HA on polar sites (bare titanium regions) rather than on the nonpolar sites of the ODPA surface (unresolved monolayers, mesostructures, clusters, multilayers). This is confirmed by the morphological similarity observed in previous sections of this chapter, between the hydroxylated and ODPA surfaces confirming the existence of $-CH_3 + TiO_2$ groups over the ODPA surface.

CHAPTER 6

Growth of Biomimetic Hydroxyapatite on Chemically - Functionalized Commercially Pure Titanium Surfaces. Effect of immersion time in Simulated Body Fluid

In this chapter, the biomimetic properies of cpTi surfaces modified with SAFs of organophosphonates are explored in terms of the time of immersion in SBF. We compared the cpTi surfaces modified with different SAFs with bare cpTi surfaces subjected to five times of

biomimetic precipitation (1, 2, 4, 8 and 16 days). In addition to the surface characterization of the final apatite coatings, this chapter collects the results of cell adhesion, proliferation and biomineralization on those coatings. We used the three SAFs of alkylphosphonates described in previous chapters. The varying topographical features found in the AFM images of the biomimetic coatings produced under the same conditions and even on different surface regions of the same coating are due to polymorphism. The ability of a compound to exist in more than one crystal structure is known as polymorphism (*168*).

6.1 Microscopy analysis

In this section, the final coatings formed on the hydroxylated cpTi surface and the three SAFs (ODPA, PHDA and PDDPA) after 1, 2, 4, 8 and 16 days of SBF immersion were visualized with AFM and ESEM. It is important to remark that AFM provides the most superficial layer of coating. The inherent variability in nucleation may produce different results with small variations of local and global conditions.

6.1.1 AFM

The hydroxylated cpTi surface (Fig. 6.1) at 2 and 8 days looks topographically homogeneous and with very small globular formations. Instead, after 1, 4 and 16 days, the surfaces show large globular formations. For the ODPA - SAF (Fig. 6.2), the height amplitude increase up to the 4th day of incubation in SBF. After 8 days, the coating becomes more smooth but at 16 days, small globular formations are found again. On the PHDA - SAF (Fig. 6.3), after 2 days the apatite layer is noticeable and reveals larger globular structures. Finally, on the PDDPA - SAF (Fig. 6.4), at 1 and 8 days the topographic irregularities are

clear, while at 2 and 4 days the coating looks more homogeneous. Finally at 16 days, well - defined globular formations are observed. The roughness values obtained for every surface are shown in Fig. 6.5. The highest roughness values were obtained at 4 days of immersion with the hydroxylated cpTi surface and ODPA - SAF, at 16 days with the PHDA - SAF and at 1 day with the PDDPA - SAF. A second nucleation seems to begin at 2 days for the hydroxylated surface, at 8 days for the ODPA - SAF and at 4 days for the PDDPA - SAF. This second nucleation produces noticeable topographical changes on the surfaces as observed in the AFM images. The PHDA - SAF reveals an increasing roughness after 8 days of immersion in SBF. From the comparison of roughness values of the biomimetic coatings obtained for 2 and 16 days of immersion in SBF (Fig. 6.6), the PHDA - SAF mostly shows higher values of roughness and surface area than with the hydroxylated surface, ODPA and PDDPA - SAFs. Generally, the behavior is oscillatory pointing out to a process of nucleation, growth, nucleation and growth, which is also observed from the values of percolation and in the ESEM images shown later. Also we observed that at 16 days the area is similar for the four cases, this points out to a existence of overhangs and a porous structure. From the AFM images we obtained the Minkowski Functionals (MFs) (*169*) are connected to physically useful parameters like the threshold of percolation (*170*). Percolation (Pc) in disordered surfaces (2-D connected media) of implants affects the circulation of extracellular material, nutrient diffusion, cell adhesion and the ingrowth of bone tissue (*169*). This way, a high percolation threshold points out to better fluid retention properties because the fluid will not be able to move freely below this threshold due to the formation of air channels. The percolation threshold values obtained for all samples studied are collected in Table 6.1. The biomimetic coatings formed on the hydroxylated cpTi at 1 - 4 days reveal the highest percolation threshold. This points out to that this structure is not suitable to accelerate the cell response. At 8 days, the hydroxylated and ODPA - SAF produced biomimetic coatings with properties of increased fluid retention. Otherwise, at

this time (8 days) the coatings on the PHDA and PDDPA - SAFs reveal the best conditions for the cell response in terms of percolation. Finally, at 16 days the biomimetic coating on the ODPA - SAF is the least suitable followed closely for the PDDPA - SAF, and further for the hydroxylated surface. The lowest Pc values were found for the PHDA - SAF, except for 8 days of immersion in SBF, thus we conclude that the PHDA - SAF produces the coating with less fluid retention.

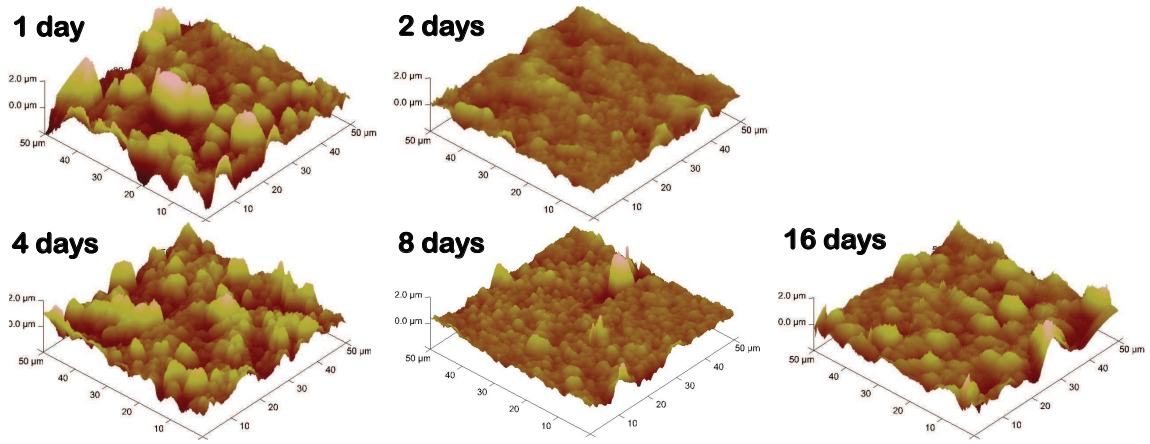

Figure 6.1: AFM images for the hydroxylated cpTi surface immersed in SBF for different times (scan area of 50 x 50 μm^2 and z - scale $=$ 2 μm).

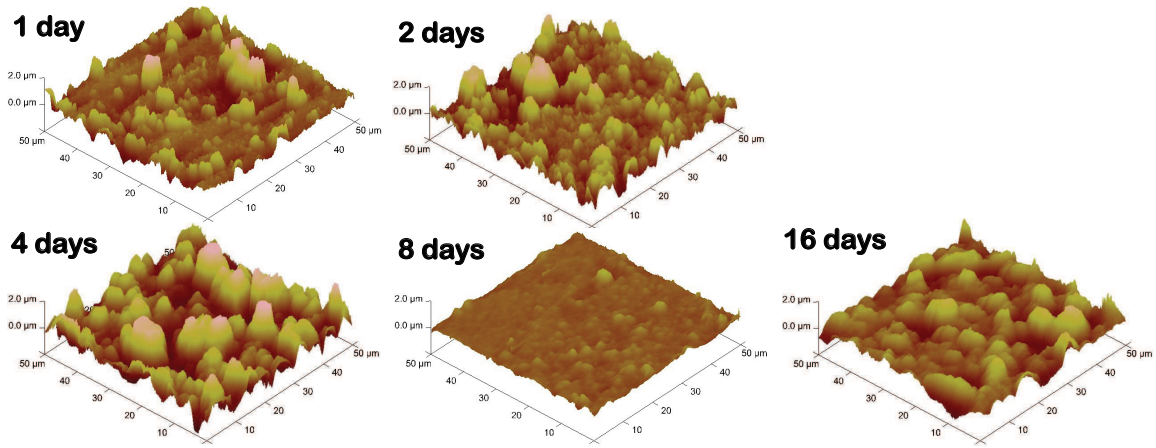

Figure 6.2: AFM images for the ODPA - SAF surface immersed in SBF for different times (scan area of 50 x 50 μm^2 and z - scale $=$ 2 μm).

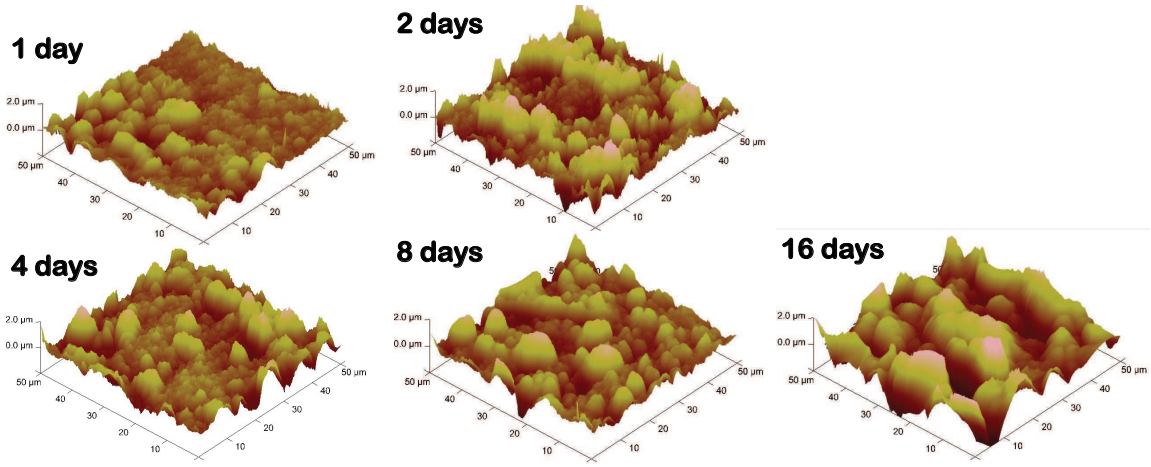

Figure 6.3: AFM images for the PHDA - SAF surface immersed in SBF for different times (scan area of 50 x 50 μm^2 and z - scale $=$ 2 μm).

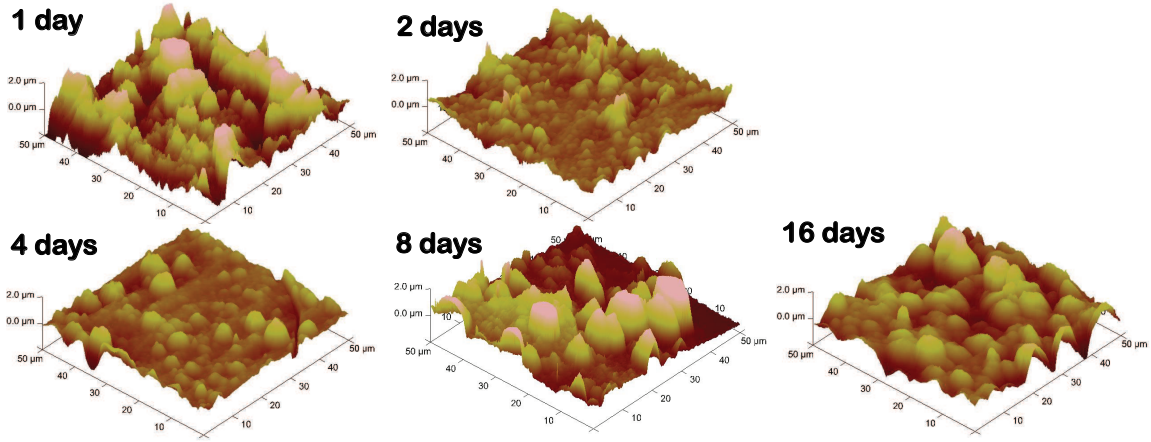

Figure 6.4: AFM images for the PDDPA - SAF surface immersed in SBF for different times (scan area of 50 x 50 μm^2 and z - scale $=$ 2 μm).

Table 6.1: Percolation threshold values for the hydroxylated cpTi surfaces and SAFs immersed in SBF for several days (data extracted over a scan area of 50 x 50 μm^2).

Surface	1 day	2 days	4 days	8 days	16 days
Hydroxylated	0.421	0.414	0.368	0.439	0.321
ODPA	0.382	0.382	0.329	0.446	0.464
PHDA	0.220	0.357	0.254	0.357	0.282
PDDPA	0.350	0.427	0.328	0.336	0.435

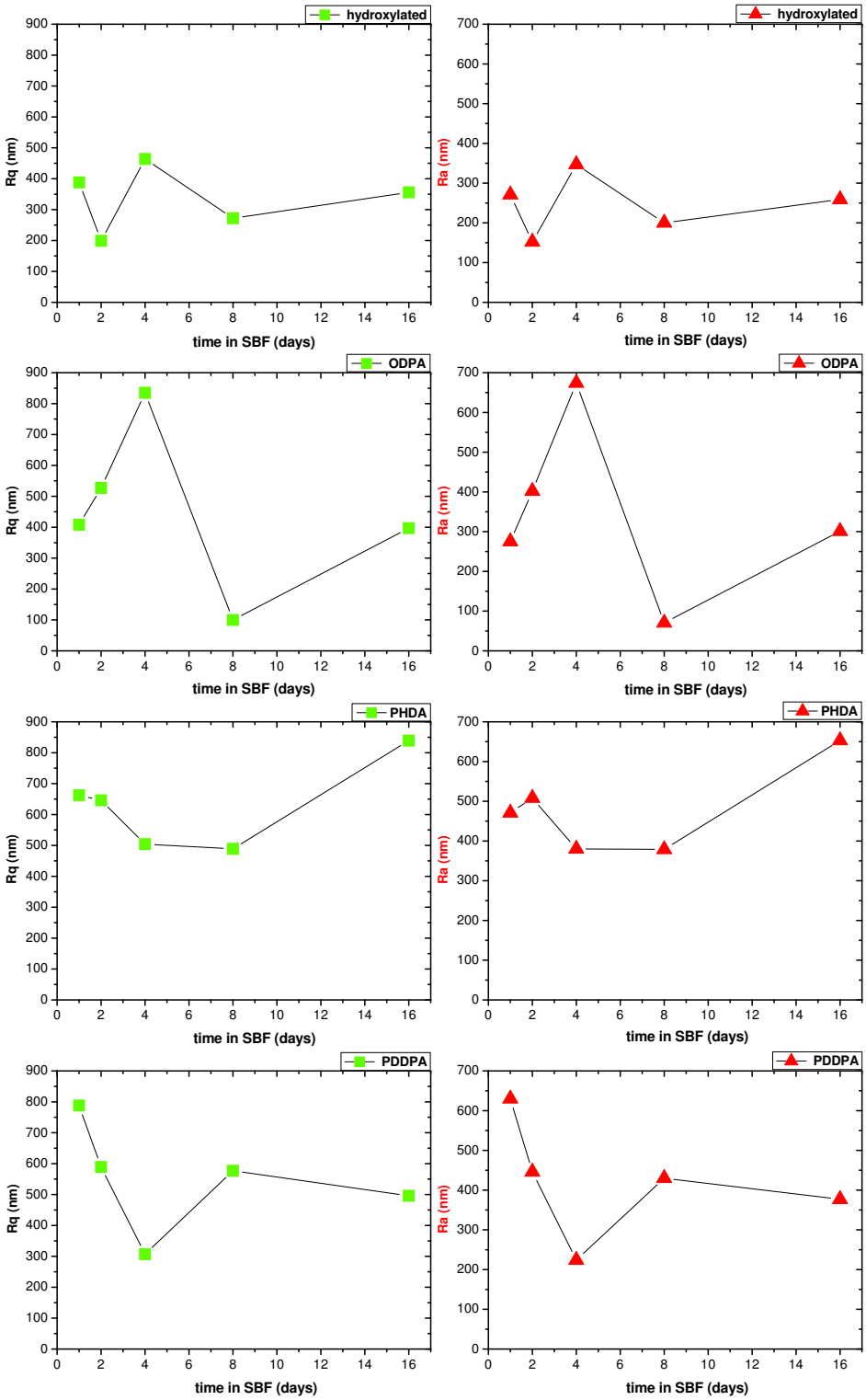

Figure 6.5: Roughness parameter values for the hydroxylated cpTi surface and SAFs immersed in SBF for several days (data extracted over a scan area of 50 x 50 μm^2).

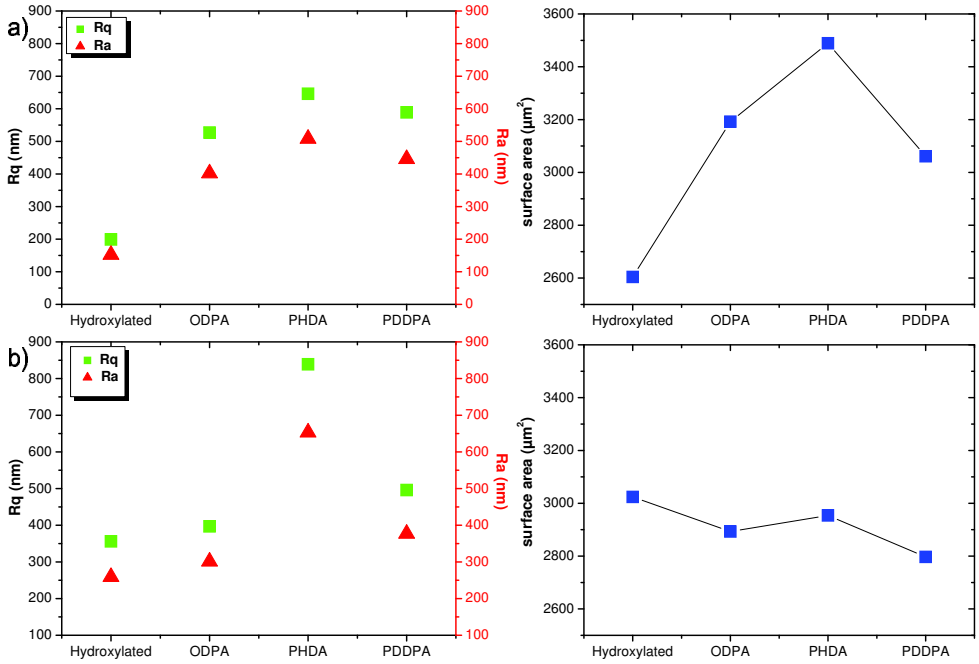

Figure 6.6: Roughness parameters and surface area for the hydroxylated cpTi surfaces and SAFs immersed in SBF for (a) 2 days and (b) 16 days (data extracted over a scan area of 50 x 50 μm^2).

6.1.2 ESEM

From the ESEM images, we can observe a larger-scale view of the morphology presented by every sample. In the case of the hydroxylated cpTi surface (Fig. 6.7), we can appreciate a homogeneous layer for 2 and 8 days in comparison with 1, 4 and 16 days. The morphology at 1 day is very different from the rest of coatings due to a more primitive stage of calcium phosphate layer. From the 2nd day, an rigid layer is formed (cracked by dehydratation) and then calcium phosphate globules are found on it. These globules cover entirely the surface from the 4th day, but after the 8th day the undercoat layer morphology is again revealed. Finally after 16 days in SBF, a grape bunch - like morphology is shown like for 2 days, although more developed and better defined. For the ODPA - SAF (Fig. 6.8), unlike the hydroxylated surface, a few isolated globular structures were found at 1 day. However, alike with the hydroxylated surface, the undercoat - like layer formed from the 2nd day is

observed with small globular structures that increase and cover the surface from the 4th day. But from the 8th day the undercoat layer morphology is found with large globular structures. After 16 days, the final grape bunch - like morphology is revealed. For the PHDA - SAF (Fig. 6.9) at the 1st day, we observe a unresolved stage of calcium phosphate layer and from the 2nd day, the underlying rigid layer appears with globular structures like in the hydroxylated surface and ODPA - SAF. However, the morphology of the coating continuously evolves from the 1st up to 16th day in comparison with the hydroxylated surface and ODPA - SAF. The final bunch - like morphology is observed after the 16th day of SBF incubation. Finally, for the PDDPA - SAF (Fig. 6.10) we also found a morphology evolution but from the 2nd to 16th day like with the PHDA - SAF.

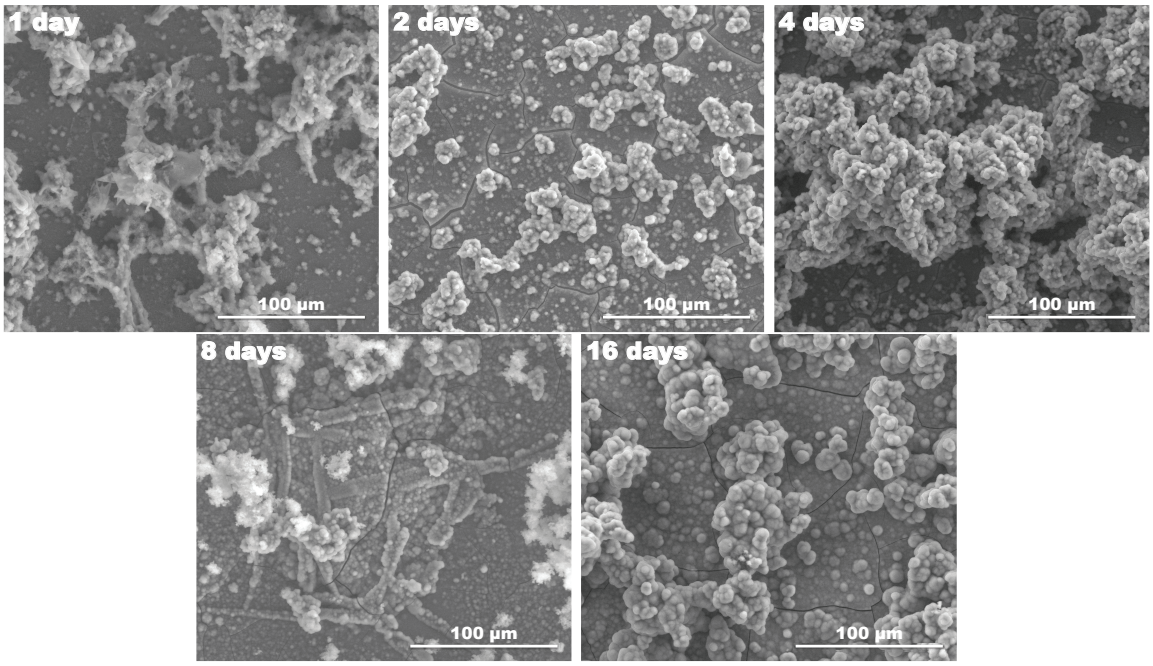

Figure 6.7: ESEM images for the hydroxylated cpTi surface immersed in SBF for different times.

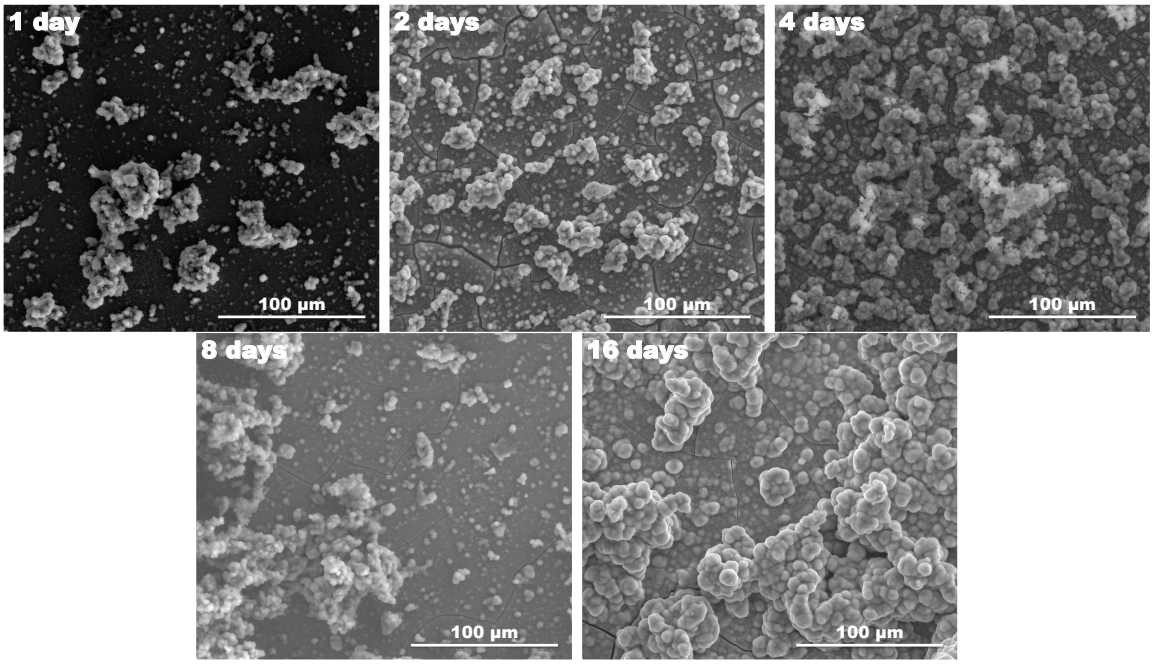

Figure 6.8: ESEM images for the ODPA SAF immersed in SBF for different times.

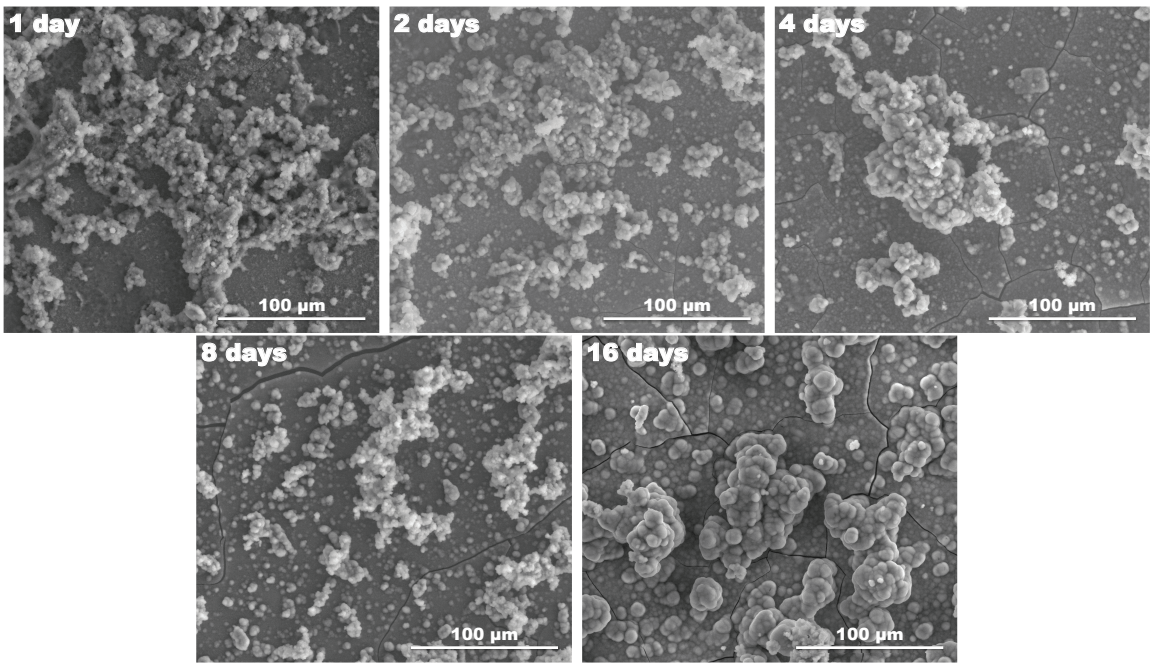

Figure 6.9: ESEM images for the PHDA SAF immersed in SBF for different times.

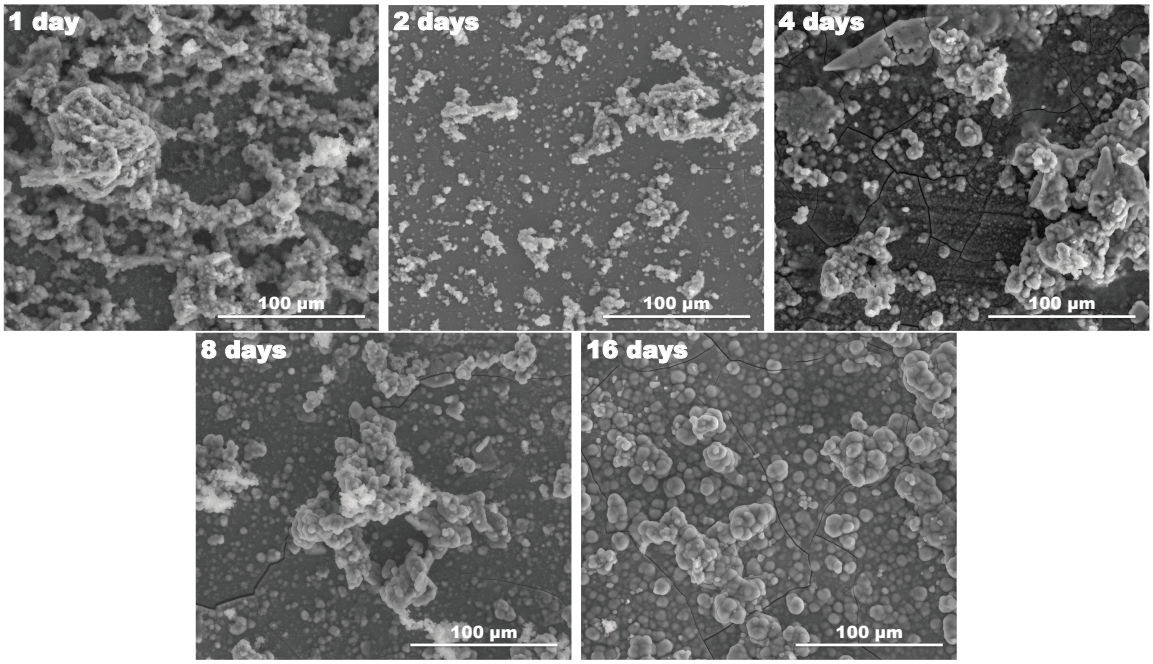

Figure 6.10: ESEM images for the PDDPA SAF immersed in SBF for different times.

6.2 Chemical analysis

Using EDX, we analyzed roughly the chemical composition of the final apatite coatings at 1 and 16 days of immersion in SBF. The EDX spectra are plotted in Fig. 6.11 for the hydroxylated cpTi surface and the ODPA - SAF and for the PHDA and PDDPA - SAFs in Fig. 6.12. The spectra reveal the presence of oxygen, calcium, phosphate and titanium. At 1 day, in all spectra the signal of titanium is significant in comparison with the weak titanium peak found at 16 days. For the hydroxylated surface and the PHDA and PDDPA - SAFs, the signals of calcium and phosphate at 16 days are greater than the titanium signal. Otherwise, with the ODPA - SAF, the calcium and phosphate signals are significant from the 1st day in SBF. These findings point out to the increase of thickness of the apatite layer formed on each cpTi surface from 1 to 16 days of incubation in SBF.

In Fig. 6.13, we plot the corresponding XRD spectra. All the spectra show the peaks

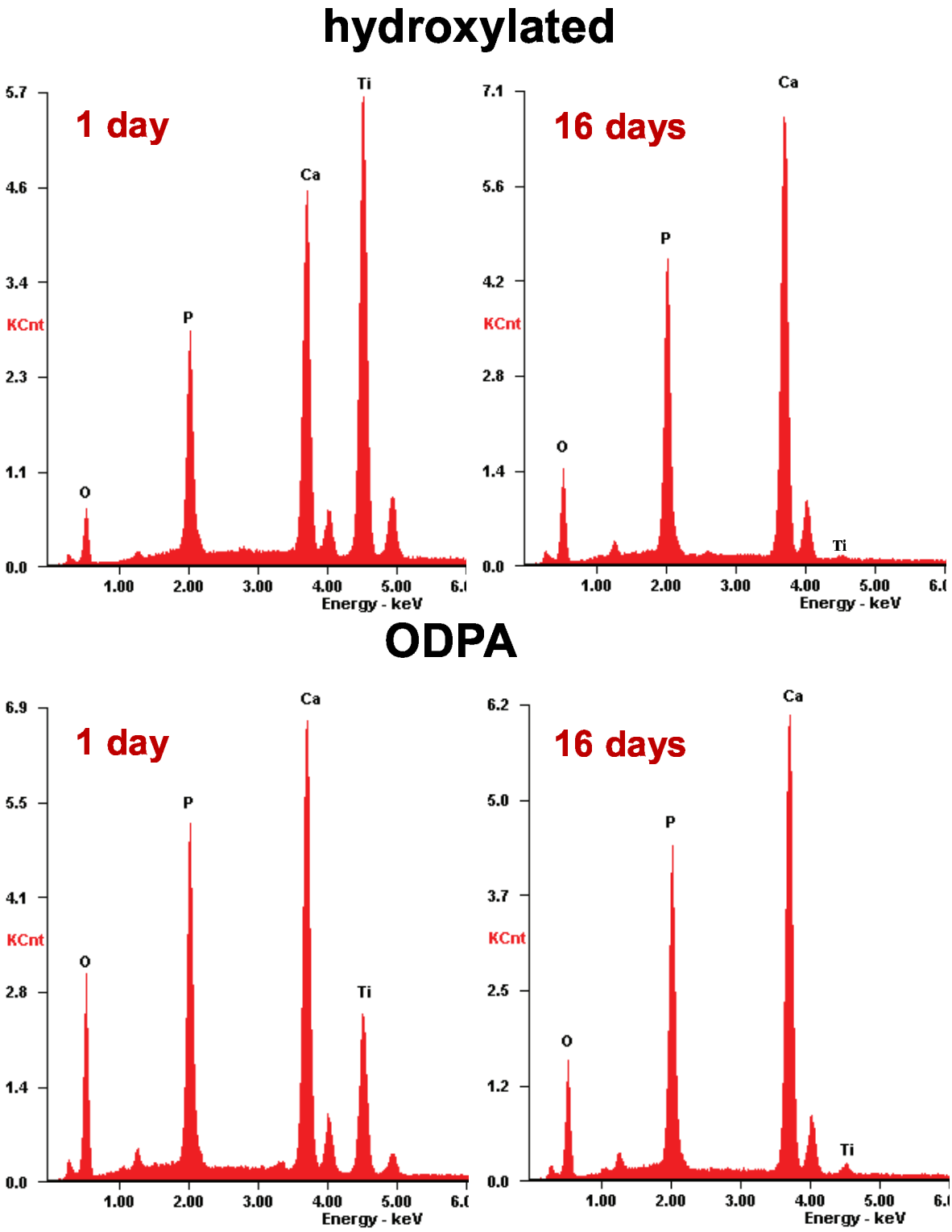

Figure 6.11: EDX spectra of coatings formed at 1 and 16 days of immersion in SBF for the hydroxylated cpTi surface and the ODPA - SAF.

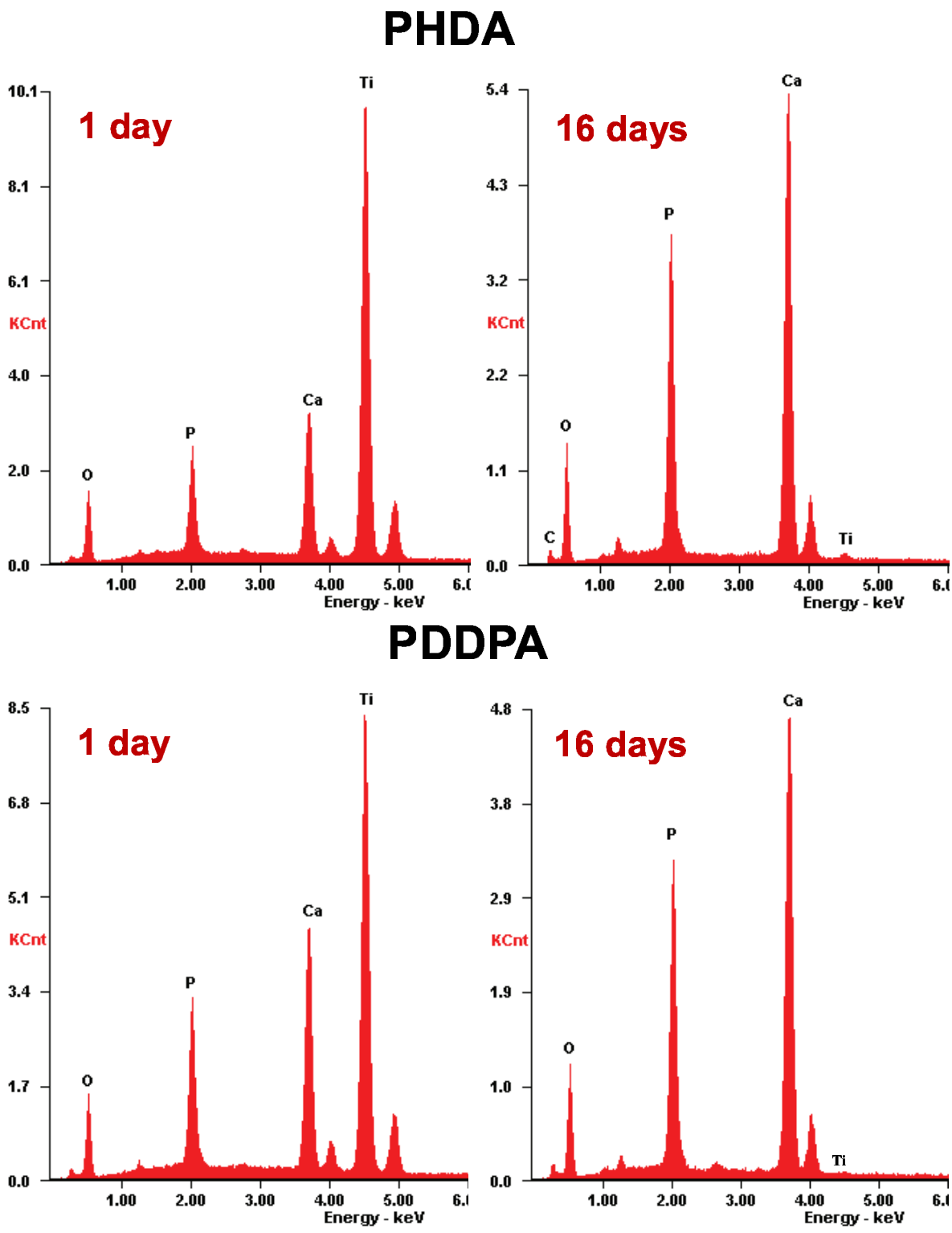

Figure 6.12: EDX spectra of coatings formed at 1 and 16 days of immersion in SBF for the PHDA and PDDPA - SAFs.

corresponding to hydroxyapatite (HA) as described in Chapter 5. The HA signal increases as the number of days of immersion in SBF. This points out to that the quality of apatite layer becomes significant from the first day of immersion in SBF.

For a more detailed analysis of surface chemistry, in the XPS spectra (Figs. 6.14 - 6.15) we found the $Ca2p_{3/2}$ peak at 347.2 eV and the $Ca2p_{1/2}$ peak at 350.7 eV, which both are associated to hydroxyapatite (*162*). Each $Ca2p$ peak displays a doublet band, which is typical for calcium oxide (*171*). The signal of $P2p$ reveals the formation of CaP films. The phosphorus peak has a different binding energy as the number of days of immersion in SBF. For 1 day and 2 days, the binding energies of the $P2p$ peaks are at 133.1 eV and 133.2 eV respectively, that associated with the binding energies of calcium and oxygen (530 - 531 eV) reveal an OCP phase. Instead, from 4 to 16 days, the phosphorus binding energy (133.5 eV) associated with calcium and oxygen corresponds to the HA phase (*144*, *162*). In Table 6.2 the Ca/P ratio values for each sample are collected. For 1 day, the Ca/P values agree with the theoretical OCP ratio (1.33) (*144*, *162*). The Ca/P ratio value from 2 to 16 days agrees with the values reported in literature for the Calcium Deficient Hydroxyapatite (CDHA)(1.4 - 1.5) (*162*). Particularly with the PHDA - SAF at 16 days, the biomimetic coating is very close to pure HA (1.67). The PHDA and PDDPA - SAFs showed a cyclical pattern in the Ca/P ratio value probably due to the dissolution of coating.

Table 6.2: Ca/P ratios for hydroxylated cpTi surface and SAFs immersed in SBF at different times (days).

Sample	1 day	2 days	4 days	8 days	16 days
hydroxylated	1.338	1.414	1.426	1.453	1.500
ODPA	1.353	1.407	1.412	1.421	1.521
PHDA	1.324	1.387	1.438	1.393	1.598
PDDPA	1.326	1.461	1.450	1.399	1.515

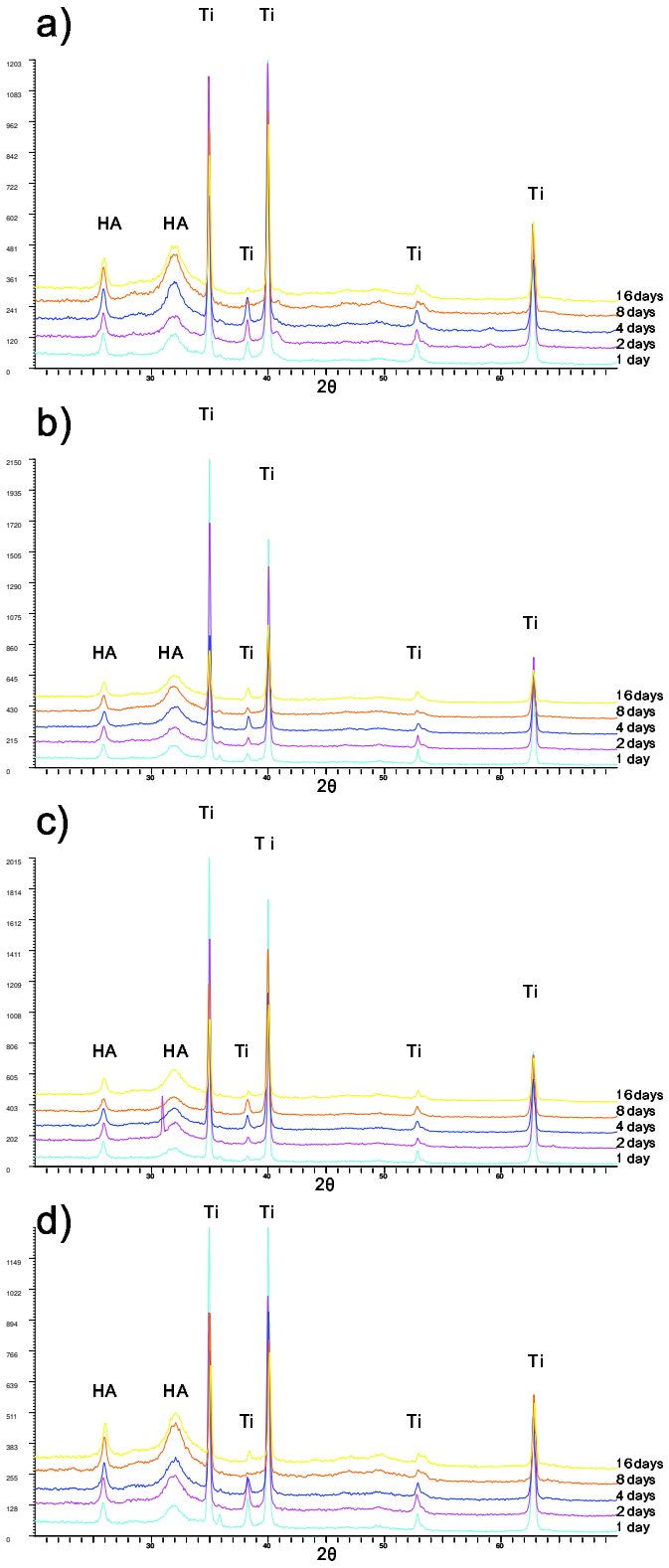

Figure 6.13: XRD spectra for the surfaces immersed in SBF at different times: a) hydroxylated cpTi surface, b) ODPA - SAF, C) PHDA - SAF, d) PDDPA -SAF.

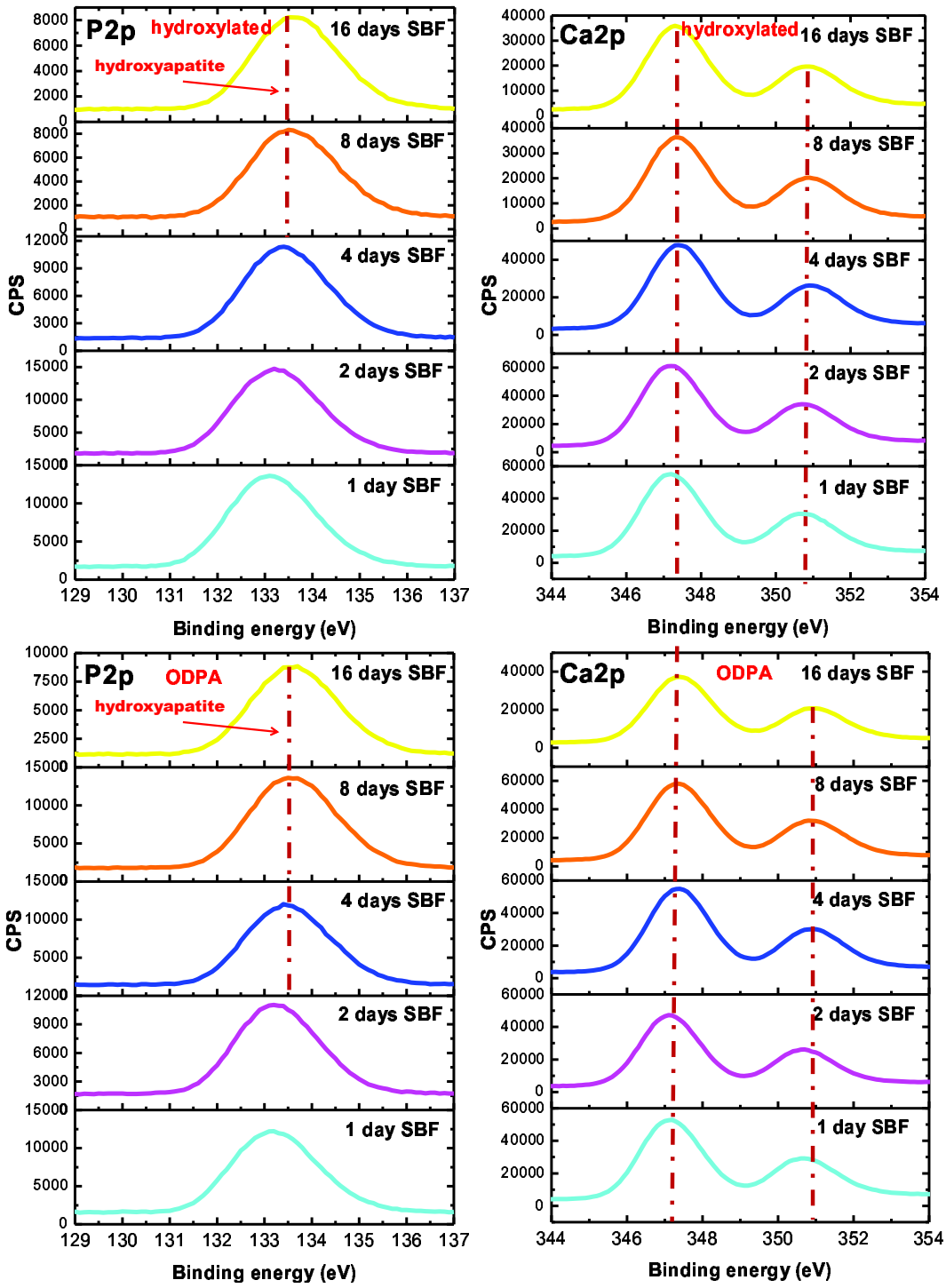

Figure 6.14: XPS spectra of the $P2p$ and $Ca2p$ signals for the hydroxylated cpTi surface and ODPA - SAF immersed in SBF at different times.

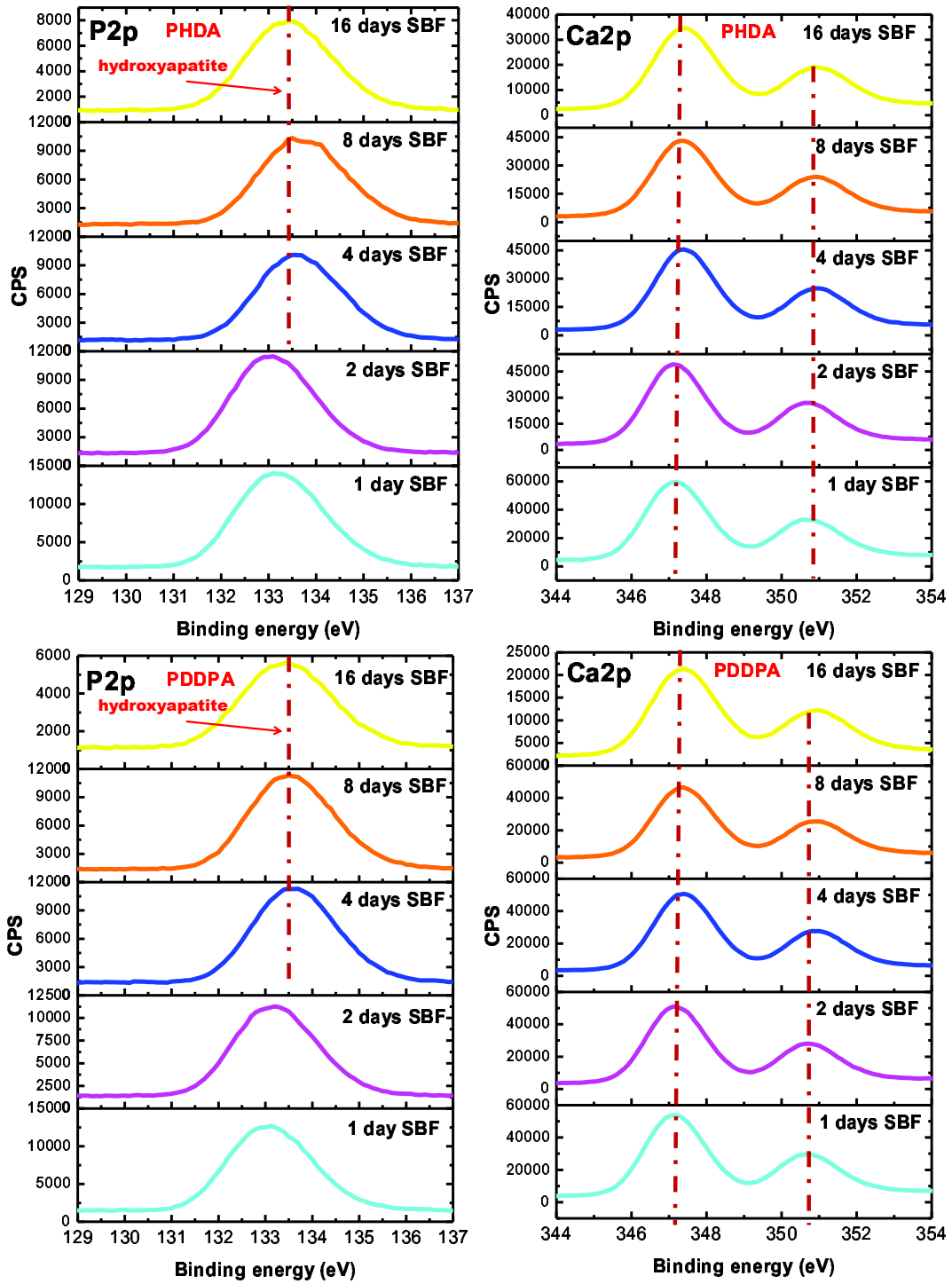

Figure 6.15: XPS spectra of the $P2p$ and $Ca2p$ signals for the PHDA and PDDPA - SAFs immersed in SBF at different times.

6.3 Biomimetic response

The results of cell adhesion, proliferation and biomineralization are shown in Fig. 6.16. For this study we focused on the hydroxylated cpTi surface and PHDA - SAF. This SAF produced the greater cell adhesion (see Chapter 5). We selected the first four times of incubation in SBF (1, 2, 4 and 8 days) because we were interested in those biomimetic precipitations with less time - consuming. As observed in the adhesion assays at 24 h, the best results were obtained for the apatite layer formed on the PHDA - SAF for the four times of immersion in SBF. The relative rate of increase of cell adhesion on the apatite layer formed on the PHDA - SAF regarding the hydroxylated cpTi surface was greater than 35%, with a maximum at 4 days in SBF.

For the proliferation experiments at 24 h, the cells grown on the coating formed on the PHDA - SAF (up to 4 days) showed a greater activity rather than the cells grown on the coating formed on the hydroxylated cpTi surface ($P < 0.001$). However, this difference disapears after 8 days in SBF because no significant change with respect to hydroxylated cpTi surface ($P = 0.75$) was observed. In general, after 48 h the proliferation increases compared with 24 h. After 48 h of cell proliferation, at 1 day in SBF, there was a noticeable increase in the cell growth on the PHDA - SAF respect to the hydroxylated cpTi surface. For the rest of times (2, 4 and 8 days in SBF), the differences were not significant.

In the biomineralization assays, after 15 days, the PHDA - SAF showed less early bone formation than the hydroxylated cpTi surfaces. The mineralization on the coating formed on the hydroxylated cpTi surfaces decreased as the time of immersion in SBF. However, for the PHDA - SAF at 2, 4 and 8 days in SBF the mineralization remained constant. We observed an increase of mineralization after 22 days relative to the results obtained after 15 days. However, regarding the hydroxylated cpTi surface, we found again a significant

decrease of biomineralization on the PHDA - SAF. The biomineralization at 22 days on the hydroxylated cpTi surface remained constant except for 1 day of SBF immersion. Instead, on the PHDA - SAF, the mineralization at 22 days remained constant from 1 up to 4 days in SBF and for 8 days in SBF, the calcium formation decreased. The greater osteogenic response (15 and 22 days of assay) of the biomimetic coatings formed on the bare cpTi surfaces may be related with the observation of the dissolution of the coatings formed on the PHDA - SAF in biologically - active medium, so the bonding strength of the coatings was unstable for the carboxyl surfaces and decreases with longer immersion time in SBF.

By CLSM we obtained images (Fig. 6.17) of cells on the coatings formed on these images are illustratives and do not enable to quantify the number of nuclei (blue) or cell bodies adhered. The cells were labeled with two Abmos (green and red) observed in the cytoskeleton. This staining indicates the cell vitality and development of the cytoskeleton. Hence, we conclude that on the biomimetic coating formed on the PHDA - SAF the cell vitality was greater although a greater cell density was further observed.

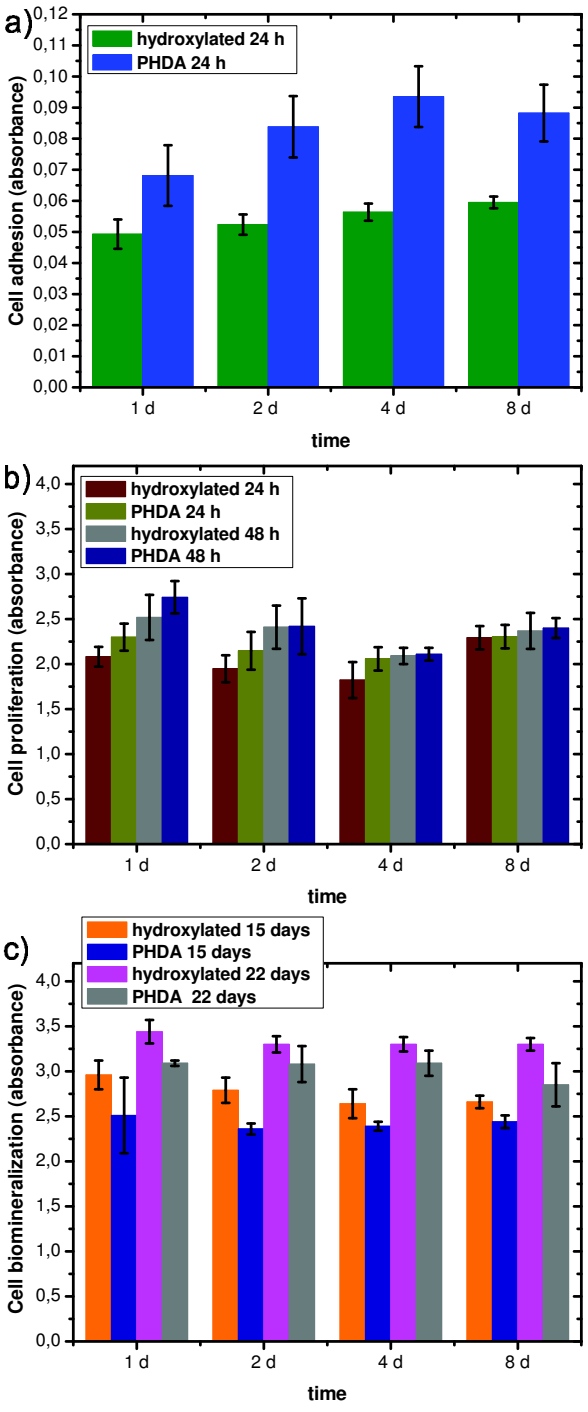

Figure 6.16: (a) Cell adhesion, (b) proliferation and (c) biomineralization for the hydroxylated cpTi surface and the ODPA, PHDA, PDDPA - SAFs immersed in SBF at different times.

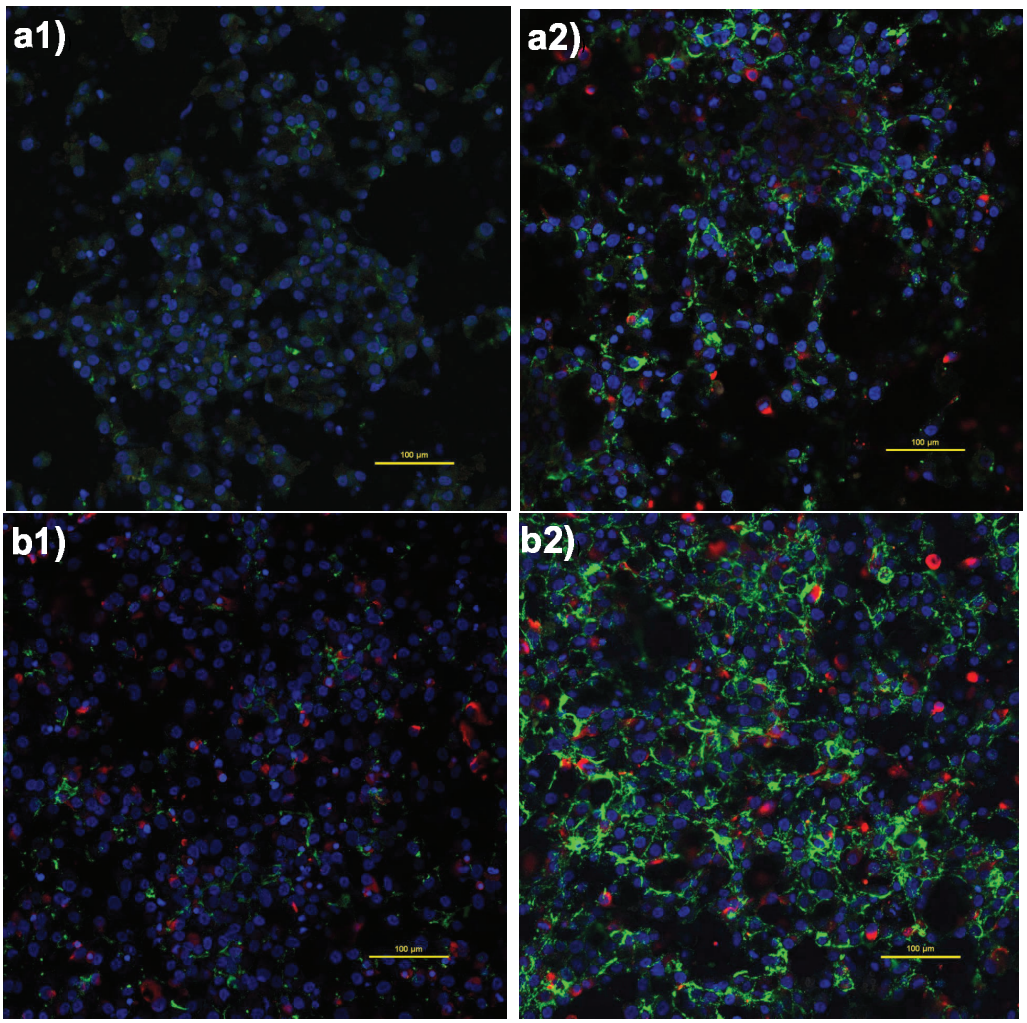

Figure 6.17: CLSM images of osteoblast - like cell on biomimetic coatings formed on: a) hydroxylated cpTi surface and b) PHDA - SAF. 1) 1 day in SBF, 2) 8 days in SBF. Blue color corresponds to cell nuclei, red and green to cytoskeleton of cells.

CHAPTER 7

Conclusions

Titanium is the standard material used for dental implants due to its mechanical properties similar to bone, resistant against corrosion and an excellent biocompatibility. The actual dental implants have a success rate up to 98 % in healthy patients. However, there are still certain unsolved problems in the design of titanium implants: the early loading after implantation and patients with severe bone loss. For this purpose, our focus was to induce a rapid osseointegration. Bioinspired coatings enable to accelerate the bone formation during the initial stages of osseointegration. The chemical tailoring of titanium surfaces with self - assembled films (SAFs) of organophosphonates provide an optimal range of biofunctions for a biomaterial. It is known that physiologically stable and interfacially adherent bone

- like apatite coatings may be formed from biomimetic precipitation on titanium surfaces modified with alkylphosphonate molecules. Certain terminal groups of these molecules are favourables for inducing apatite formation on titanium surfaces. To the best of our knowledge, a few works have been devoted to the formation of SAFs of phosphonates on cpTi surfacesand the subsequent nucleation and growth of hydroxyapatite (HA) coatings. The least thermodynamically stable phase nucleates and grows, followed for more stable phases. The nucleation is thought to proceed through prenucleation clusters present in the SBF already before nucleation, however, such nanometer - sized clusters as building blocks has been debated for many years.

This dissertation collects the results of a systematic study of the final biomimetic coatings formed on cpTi surfaces modified with different molecules of organophosphonate and at different times of immersion in Simulated Body Fluid. The number of explored parameters, the different techniques used to characterize the SAFs and biomimetic coatings and the *in-vitro* cell studies required to prepare a huge amount of samples and a time - consuming research with special attention to the cpTi surface quality. We studied two organophosphonate molecules with potent terminal groups for apatite nucleation: $-COOH$ and PO_3^4. The biomimetic precipitation is considered to be a low - cost and simple methodology although time consuming. To accelerate the biomimetic precipitation, a precursor calcium phosphate (CaP) layer was deposited with a previous fast precipitation under no physiological conditions on the modified cpTi surfaces. The aim of this precursor CaP layer was to accelerate the nucleation and growth of the final biomimetic coating under physiological conditions. Moreover, we used a concentrated recipe of SBF to enhance the nucleation process and the samples were vertically placed during incubation in SBF. The surface chemistry of all samples was examined by contact angle (CA), XPS, XRD and EDX. The topography and morphology were monitored by AFM, WLCM and ESEM. The *in-vitro* biological response on the biomimetic coatings was analyzed with cell adhesion, cell differentiation,

cell biomineralization, and cell vitality, observed by CLSM.

We were able to form Self Assembled Films (SAFs) rather than SAMs over the ultra - polished cpTi surfaces, as revealed by the layer thickness measured by ellipsometry ($\sim$ 43-53 nm), the advancing and receding CA values and the AFM images. The XPS signals of the $P-O-Ti$ and $P=O$ bonds mostly revealed the presence of mono - and bridging bidentate modes of alkylphosphonate molecules anchored to the cpTi surfaces. These films revealed mixed structures (clusters/multilayers, unresolved monolayers, bare regions) following the heterogeneity degree ODPA $<$ PHDA $\sim$ PDDPA. The lower contact angle hysteresis found with the ODPA - SAF points out to a less heterogeneous film because the surface energies of both the methyl terminal group and the alkylchains are very similar. However, there is a noticeable fraction of bare surface regions (hydrophilic defects, $Ti-OH$) over the carbon-based background. From the receding contact angles, we conclude that the PDDPA - SAF have a small fraction of bare surface regions although greater than the PHDA - SAF. From the advancing contact angles, the density of disordered layers (hydrophobic domains) was also small but different between PHDA and PDDPA - SAFs.

As expected, we found that the HA nucleation and growth on the cpTi surfaces were dependent on the underlaying SAF. The mechanisms of nucleation were different with polar ($Ti-OH$, $-COOH$ and $-PO(OH)_2$) and apolar ($-CH_3$) terminal groups of the SAF. The negatively charged surface attracts the positive calcium ions and this increases the local nucleation rate of apatite from the SBF solution. Due to the dissociation of hydroxyl groups, the bare cpTi surfaces were negatively charged but at different degree. However the $COO^- - Ca^{2+}$ bond was more favorable. For the methyl terminated - SAF, the apatite nucleation happened due to the bare titanium domains over the alkylchains/methyl background although the quality of the final coating was defficient.

Due to the own stochastic nature of nucleation, polymorphism was usually observed

over the HA coating for same molecule in a different sample. However, noticeable differences were found as the underlaying SAF. The results showed that the PHDA - SAF (carboxyl terminated) produced biomimetic coatings with greater values of roughness, thickness and Ca/P ratio (1.598), which was closer to the stoichiometric value of HA (1.67). All biomimetic coatings ("smooth" mineral surfaces at drop scale) were very hydrophilic ($< 25^{o}$) and their morphology evolved as the immersion time in SBF towards a final globular and cracked structure, with several nucleation - growth cycles. The calcium ortophosphates identified by XPS revealed the amorphous nature (ACP) of the CaP layer previous to the biomimetic precipitation, and the Ca/P ratio values for the coatings produced on the hydroxylated, ODPA - and PDDPA - SAFs corresponded to Calcium Deficient Hydroxyapatite (CDHA), as happens in natural bone and teeth previous to the formation of apatite crystals. Otherwise, the biomimetic coating formed on the PHDA - SAF was more cristallyne.

The biomimetic coating formed over the PHDA - SAF revealed the lowest liquid retention through its tortuous but interconnected structure, while for the remaining three cases (hydroxylated, ODPA - and PDDPA - SAFs) the liquid retention was greater and fluctuating depending on the days of immersion in SBF. This suggests that the time of SBF incubation is not unique, and it depends on each SAF. An optimal time should enable to reach a significant and stable level of roughness, low liquid retention and a balance between amorphism and crystallinity degree.

The biomimetic coating generated on the PHDA - SAF at a short incubation time (2 days) showed increased cell adhesion followed by the PDDPA - SAF, ODPA - SAF, the hydroxylated cpTi surface and finally the control sample with no treatment. The coating formed on the methyl - terminated cpTi surface showed better cell adhesion than the hydroxylated one, because the formation of apatite layer by heterogeneous nucleation on the disordered SAF with a few privileged sites over an apolar background was favoured rather

than the hydroxylated cpTi surface with a great density of $Ti - OH$ group. However, the biomineralization was better on the coating formed on the hydroxylated cpTi surface than for the PHDA - SAF. This could be due to that amorphous and metastable compounds as obtained are more soluble than the crystalline HA. Cell vitality on the HA coating formed on the PHDA - SAF was better. But, it is known that the bonding strength of the biomimetic coatings decreases with longer immersion times in SBF.

A crystalline coating is not optimal for rapid healing, but it favors the long - term stability of biomaterial. Based on this and our results, we postulate as the best option to the diphosphonate molecule (PDDPA) that showed a behavior between the hydroxylated surface and the carboxyl molecule (PHDA).

Further work should be addressed to explore the role of mixed and patterned SAFs. This would enable the positive and selective interaction with the host, to guide the cell growth and even to accelerate the integration into bone for healing.

CONCLUSIONES

El titanio es el material estándar utilizado para los implantes dentales debido a sus propiedades mecánicas similares al hueso, su resistencia contra la corrosión y por tener una excelente biocompatibilidad. Los implantes dentales en realidad tíenen una tasa de éxito de hasta 98 $\%$ en pacientes sanos. Sin embargo, todavía quedan algunos problemas sin resolver relacionados con el diseño de los implantes de titanio: la carga temprana después de la implantación y los pacientes con pérdida ósea severa. Debido a esto, nuestro enfoque fué inducir una osteointegración rápida. Los recubrimientos bioinspirados permiten acelerar la formación de hueso durante las etapas iniciales de la osteointegración. La adaptación química de superficies de titanio con películas auto - ensambladas (SAFs) de organofosfonatos proporciona una gama óptima de biofunciones para un biomaterial. Se sabe que a partir de la precipitación biomimética en superficies de titanio modificadas con moléculas de alquilfosfonatos, se puede formar un recubrimiento de apatita parecida a la del hueso que sea fisiológicamente estable e interfacialmente adherente. Ciertos grupos terminales de estas moléculas son favorables para inducir la formación de apatita en superficies de titanio. Dentro de nuestro conocimiento, pocos trabajos se han dedicado a la formación de SAFs de fosfonatos en superficies de cpTi, así como la posterior nucleación y crecimiento de recubrimientos de hidroxiapatita (HA). La fase de apatita termodinamicamente menos estable nuclea y crece, seguida por fases más estables. La nucleación se cree que se lleva a cabo a través de "clusters" presentes en el SBF ya antes de la nucleación, sin embargo estos "clusters", de tamaño nanométrico, como bloques de construcción han sido objeto de debate durante muchos años.

Esta tesis recoge los resultados de un estudio sistemático de los recubrimientos biomiméticos finales formados en superficies de cpTi modificados con diferentes moléculas de organofosfonato y a diversos tiempos de inmersión en Fluido Corporal Simulado (SBF). El número

de parámetros explorados, las diferentes técnicas utilizadas para caracterizar las SAFs y los recubrimientos biomiméticos y los estudios *in vitro* de células, requirió preparar una gran cantidad de muestras y una investigación de larga consumición de tiempo, con especial atención a la calidad de la superficie cpTi. Se estudiaron dos moléculas de organofosfonato con grupos terminales potentes para la nucleación de apatita : $-COOH$ y PO_3^4. La precipitación biomimética es considerada como una metodología de bajo coste y simple, aunque consume mucho tiempo. Para acelerar la precipitación biomimética, se depositó una capa precursora de fosfato de calcio (CaP) mediante una precipitación rápida bajo condiciones no fisiológicas en las superficies de cpTi químicamente modificadas. El objetivo de esta capa precursora de CaP fué acelerar la nucleación y el crecimiento del recubrimiento biomimético final bajo condiciones fisiológicas. Por otra parte, hemos utilizado una receta concentrada de SBF para mejorar el proceso de nucleación y las muestras se colocaron verticalmente durante la incubación en SBF. La química superficial de todas las muestras se examinó por ángulo de contacto (CA), XPS, XRD y EDX. La topografía y morfología fueron monitoreados por AFM, WLCM y ESEM. La respuesta biológica *in vitro* de los recubrimientos biomiméticos se analizó con la adhesión celular, la diferenciación celular, la biomineralización de las células, y la vitalidad celular observada por CLSM.

Hemos sido capaces de formar películas auto - ensamblados (SAFs) en lugar de SAMs sobre las superficies ultrapulidas de cpTi, según lo revelado por el espesor de la capa medido por elipsometría ($\sim$ 43 - 53 nm), los valores de avance y retroceso de CA y las imágenes de AFM. Las señales XPS de los enlaces $PO-Ti$ y $P=O$ revelaron la presencia de modos de anclaje mono y bidentados de las moléculas alquilfosfonato a las superficies de cpTi. Estas películas revelaron estructuras mixtas ("clusters" / multicapas , monocapas no resueltas , regiones desnudas) dependiendo del grado de heterogeneidad ODPA $<$ PHDA $\sim$ PDDPA. El valor menor de histéresis del ángulo de contacto se encontró en la SAF - ODPA que señala a una película menos heterogénea, esto es porque las energías superficiales del grupo terminal

metilo y de las cadenas hidrocarbonadas son muy similares. Sin embargo, existe una fracción notable de regiones desnudas (defectos hidrófilos, $Ti-OH$) sobre el fondo de la base de carbonos. A partir de los ángulos de contacto de retroceso, llegamos a la conclusión de que la SAF - PDDPA tíene una pequeña fracción de regiones de superficie desnuda, aunque en mayor cantidad que la SAF - PHDA. A partir de los ángulos de contacto de avance, dedujimos que la densidad de las capas desordenadas (dominios hidrófobos) también era pequeña pero diferente entre las SAF - PHDA y PDDPA.

Como era de esperar, se encontró que la nucleación y el crecimiento de HA en las superficies de cpTi fueron dependientes de la SAF subyacente. Los mecanismos de nucleación fueron diferentes con los grupos terminales polares ($Ti-OH$, $-COOH$ y $-PO(OH)_2$) y el apolar ($-CH_3$). La superficie de carga negativa atrae a los iones de calcio positivos y esto aumenta la velocidad de nucleación local de la apatita en la solución de SBF. Debido a la disociación de los grupos hidroxilo, las superficies desnudas de cpTi fueron cargadas negativamente, pero en diferente grado. Sin embargo los enlaces $COO^- - Ca^{2+}$ fueron los más favorables. Para el grupo terminal metilo, la nucleación de apatita ocurrió debido a los dominios desnudos de titanio sobre el fondo de cadenas hidrocarbonadas, aunque la calidad de la cubierta final fué deficiente.

Debido a la propia naturaleza estocástica de la nucleación, el polimorfismo se observó por lo general sobre el recubrimiento de HA para una misma molécula en muestras diferentes. Sin embargo, diferencias notables se encontraron dependiendo de la SAF subyacente. Los resultados mostraron que la SAF - PHDA (terminada en carboxilo) produjo recubrimientos biomiméticos con mayores valores de rugosidad, espesor y una relación Ca/P (1.598), más cercano al valor estequiométrico de la HA (1.67). Todos los recubrimientos biomiméticos (superficies minerales "suaves" a escala de gota) fueron muy hidrófilos ($< 25\ ^{o}$) y su morfología evolucionó con el tiempo de inmersión en SBF hacia una estructura final globular

y agrietada, con varios ciclos de nucleación - crecimiento de por medio. Los ortofosfatos de calcio identificados por XPS revelaron la naturaleza amorfa (ACP) de la capa de fosfato cálcico anterior a la precipitación biomimética, y los valores de la relación Ca/P para los recubrimientos producidos en las superficies hidroxilada, SAF - ODPA y SAF - PDDPA correspondieron a hidroxiapatita deficiente en calcio (CDHA), como ocurre en el hueso natural y los dientes previo a la formación de cristales de apatita. Por caso contrario, el recubrimiento biomimético formado en la SAF - PHDA fue más cristalino.

El recubrimiento biomimético formado sobre la SAF - PHDA reveló la retención de líquido más baja a través de su estructura tortuosa pero interconectada, mientras que para los tres casos restantes (hidroxilado, SAF - ODPA y SAF - PDDPA) la retención de líquidos fué mayor y fluctuante en función de los días de inmersión en SBF. Esto sugiere que el tiempo de incubación en SBF no es único, y que depende de cada SAF. Un tiempo óptimo debería permitir alcanzar un nivel significativo y estable de rugosidad, una baja retención de líquido y un equilibrio entre el grado de amorfismo y de cristalinidad.

El recubrimiento biomimético generado en la SAF - PHDA a un tiempo de incubación corto (2 días), mostró un incremento de la adhesión celular, seguido de la SAF - PDDPA, SAF - ODPA, la superficie de cpTi hidroxilada y finalmente la muestra control sin tratamiento. El recubrimiento formado sobre la superficie cpTi terminada en metilo, mostró mejor adhesión celular que la hidroxilada, porque la formación de la capa de apatita por nucleación heterogénea en la SAF desordenada con unos pocos sitios privilegiados sobre un fondo apolar, se vió favorecida en lugar de la superficie hidroxilada de cpTi con una gran densidad de grupos $Ti-OH$. Sin embargo, la biomineralización fué mejor sobre la superficie hidroxilada de cpTi que para la SAF - PHDA. Esto podría ser debido a que los compuestos amorfos y metaestables como los obtenidos son más solubles que la HA cristalina. La vitalidad celular en el recubrimiento de HA formado en la SAF - PHDA fué mejor. Pero, se sabe que la

fuerza de adhesión de los recubrimientos biomiméticos disminuye con tiempos de inmersión más largos en SBF.

Un recubrimiento cristalino no es óptimo para una rápida curación, pero favorece la estabilidad a largo plazo del biomaterial. Basado en esto y nuestros resultados, postulamos como la mejor opción la molécula difosfonato (PDDPA) que mostró un comportamiento entre la superficie hidroxilada y la molécula carboxilo (PHDA).

El trabajo adicional debe dirigirse a explorar el papel de las SAFs mezcladas patronadas. Esto permitiría la interacción positiva y selectiva con el receptor, para guiar el crecimiento de las células e incluso para acelerar la integración en el hueso y la curación.

APPENDIX A

Effect of sample orientation and nascent calcium phosphate layer during the Biomimetic precipitation

In Chapter 5, in order to reduce the time consuming process of formation of biomimetic coating, we examined the effect of the sample orientation during the incubation in SBF and the previous layer of nascent calcium phosphate for 2 days of SBF immersion. In Fig. A.1 we show the ESEM images of the PHDA - SAF at 4 and 8 days of incubation in SBF without and with the previous nucleation of calcium phosphate layer. For the 4 days of

SBF incubation, the ESEM images were acquired in Large Field Detector (LFD) mode like in the rest of ESEM images shown in other chapters. The ESEM images of samples formed at 8 days in SBF were taken in Solid State Detector (SSD) mode. This mode reveals the chemical composition of the surfaces (see Section 2.4.3). The difference at 4 days is very significant between the sample without the nascent calcium phosphate layer and the sample with it (first row in Fig. A.1). The sample without the previous layer of calcium phosphate produced a very poorly biomimetic layer. The sample without the pre - deposit at 8 days (left - down image Fig. A.1) revealed bright areas that corresponds to bare or nearly coated titanium surface. Instead, the sample with previous nucleation (right - down image in Fig. A.1) showed a complete coverage degree.

Regarding the sample orientation (vertical vs. horizontal) during the SBF incubation, in Fig. A.2 the difference is clearly illustrated with an incubation of 16 days of the PDDPA - SAF. From the vertical incubation, a well defined biomimetic layer is grown over the SAF. Nucleation is enhanced with the vertical orientation. However, ballistic - like deposition is enhanced rather than nucleation with the horizontal orientation of samples. We conclude that the vertical incubation in SBF is recommended to nucleate apatite - like coatings on cpTi surfaces.

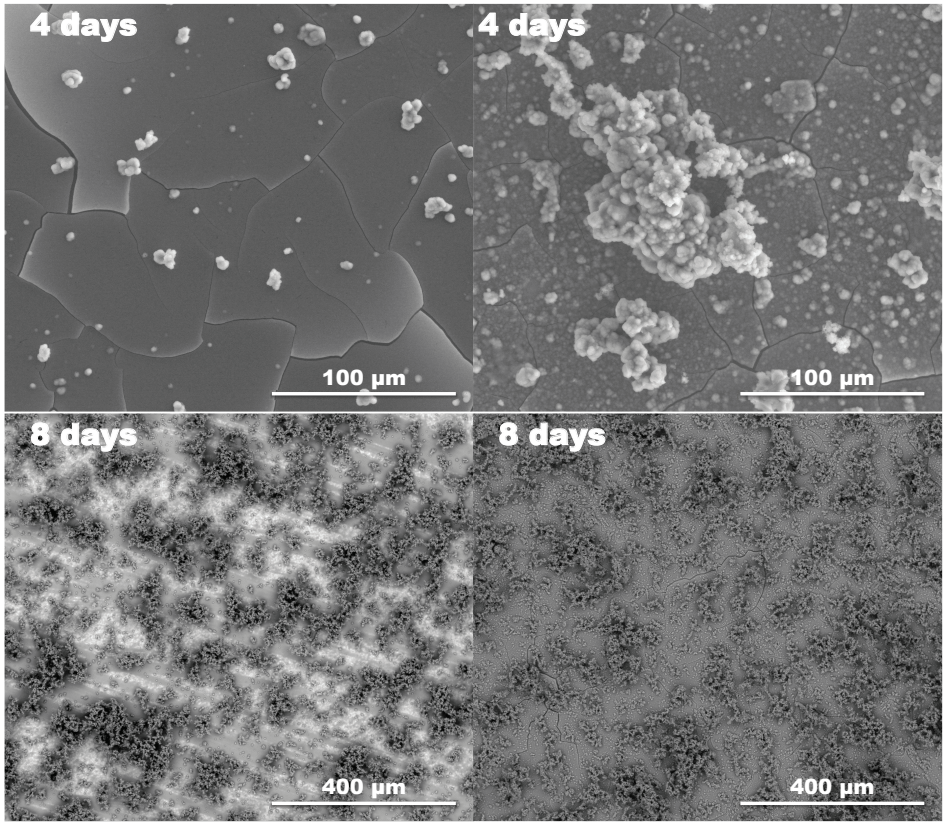

Figure A.1: ESEM micrographs for the PHDA - SAF immersed in SBF. The left images correspond to samples without the nascent layer of calcium phosphate and the right images correspond to samples with the pre-deposit of calcium phosphate. The images for 4 days are shown in LFD mode (topography) and the images for 8 days are shown in SSD mode (chemical composition).

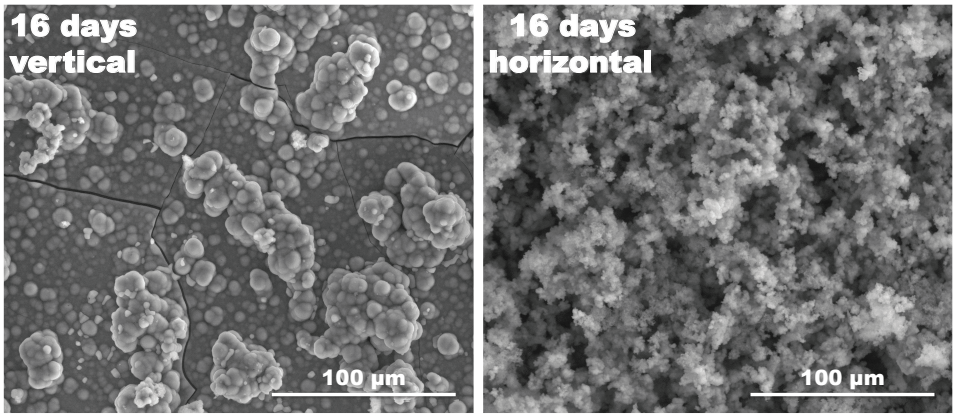

Figure A.2: ESEM micrographs for the PDDPA - SAF immersed for 16 days in SBF in vertical and horizontal position, respectively.

Bibliography

(1) Ratner, B. A Perspective on Titanium Biocompatibility. Titanium in Medicine.*Engineering Materials. Springer Berlin Heidelberg.* **2001** 1–12.

(2) Tossatti., S. G. P. Ph.D. thesis. Functionalized Titanium Surfaces for Biomedical Applications: physico-chemical characterization and biological *in vitro* evaluation. Swiss Federal Institute of Technology Zürich, **2003**.

(3) Jansen., B. L. A.Physicochemistry of Apatite and its Related Calcium Phosphates. *Thin Calcium Phosphate Coatings for Medical Implants. Springer.* **2009** 9–14.

(4) Mao, C.; Li, H.; Cui, F.; Feng, Q.; Wang, H.; Ma, C. Oriented growth of hydroxyapatite on (0001) textured titanium with functionalized self-assembled silane monolayer as template. *J. Mater. Chem.* **1998**, *8*, 2795–2801.

(5) Tanahashi, M.; Matsuda, T. Surface functional group dependence on apatite for-

mation on self-assembled monolayers in a Simulated Body Fluid. *J. Biomed. Mater. Res.* **1997**, *34*, 305–315.

(6) Bothe, R. T.; Beaton, K. E.; Davenport, H., E. Reaction of bone to multiple metallic implants. *Surg. Gynecol. Obstet.* **1940**, *71*, 598–602.

(7) Noort, R. Titanium: The implant material of today. *J. Mater. Sci.* **1987**, *22*, 3801–3811.

(8) Leventhal, G. S. Titanium, a metal for surgery. *J. Bone Joint Surg.* **1951**, *33*, 473–474.

(9) Beder, O. E.; Eade, G. An investigation of tissue tolerance to titanium metal implants in dogs. *Surgery.* **1956**, *39*, 470 – 473.

(10) Parr, G. R.; Gardner, L.; Toth, R. W. Titanium: The mystery metal of implant dentistry. Dental materials aspects. *J. Prosthet. Dent.* **1985**, *54*, 410 – 414.

(11) Tomasi, C.; Wennström, J. L.; Berglundh, T. Longevity of teeth and implants: a systematic review. *J. Oral Rehabil.* **2008**, *35*, 23–32.

(12) Cölfen, H. Biomineralization: A crystal-clear view. *Nat. Mater.* **2010**, *9*, 960–961.

(13) Li, P.; Kangasniemi, I.; de Groot, K.; Kokubo, T. Bonelike Hydroxyapatite Induction by a Gel-Derived Titania on a Titanium Substrate. *J. Am. Ceram. Soc.* **1994**, *77*, 1307–1312.

(14) Dadvinson, J. A.; Gergette, F. State of the art in materials for orthopedic prosthetic devices. *Proceedings of Implant Manufacturing and Materials Technology. Soc. Manufact. Eng.* **1986**, 1 – 26.

(15) Katti, K. S. Biomaterials in total joint replacement. *Colloids Surf., B.* **2004**, *39*, 133 – 142.

(16) Anil, S.; Anand, P. S.; Alghamdi, H.; Jansen, J. A. Dental Implant Surface Enhancement and Osseointegration. *Implant Dentistry - A Rapidly Evolving Practice. InTech.* **2011**, 83 – 109.

(17) Yoshinari, M.; Oda, Y.; Inoue, T.; Matsuzaka, K.; Shimono, M. Bone response to calcium phosphate-coated and bisphosphonate-immobilized titanium implants. *Biomaterials.* **2002**, *23*, 2879 – 2885.

(18) Xu, W.; Hu, W.; Li, M.; Wen, C. Sol/gel derived hydroxyapatite/titania biocoatings on titanium substrate. *Mater. Lett.* **2006**, *60*, 1575 – 1578.

(19) Erdemir, D.; Lee, A. Y.; Myerson, A. S. Nucleation of crystals from solution: Classical and two-step models. *Acc. Chem. Res.* **2009**, *42*, 621 – 629.

(20) Sato, K.; Kumagai, Y.; Tanaka, J. Apatite formation on organic monolayers in simulated body environment. *J. Biomed. Mater. Res.* **2000**, *50*, 16–20.

(21) Kato, K.; Eika, Y.; Ikada, Y. Deposition of a hydroxyapatite thin layer onto a polymer surface carrying grafted phosphate polymer chains. *J. Biomed. Mater. Res.* **1996**, *32*, 687–691.

(22) Liu, Q.; Ding, J.; Mante, F. K.; Wunder, S. L.; Baran, G. R. The role of surface functional groups in calcium phosphate nucleation on titanium foil: a self-assembled monolayer technique. *Biomaterials.* **2002**, *23*, 3103 – 3111.

(23) Textor, M.; Sittig, C.; Frauchiger, V.; Tosatti, S.; Brunette, D. Properties and Biological Significance of Natural Oxide Films on Titanium and Its Alloys. *Titanium in Medicine. Engineering Materials. Springer Berlin Heidelberg.* **2001**, 171–230.

(24) Aparicio, C. Ph.D. thesis. Tratamientos de superficie sobre titanio comercialmente puro para la mejora de la osteointegración de los implantes dentales. Polytechnic University of Catalonia. Biomaterials Department. **2004**.

(25) Fraker, A. C.; Ruff, A. W.; Sung, P.; Van Orden, A. C.; Speck, K. M. Surface preparation and corrosion behavior of titanium alloys for surgical implants. *Titanium alloys in surgical implants. Engineering Materials. ASTM Special Technical Pubblication.* **1983**, 206–219.

(26) Bayati, M. R.; Molaei, R.; Narayan, R. J.; Narayan, J.; Zhou, H.; Pennycook, S. J. Domain epitaxy in $TiO_2/alpha - Al_2O_3$ thin film heterostructures with Ti_2O_3 transient layer. *Appl. Phys. Lett.* **2012**, *100*, 251606 – 251609.

(27) Breme, J.; Biehl, V. *Handbook of Biomaterial Properties. Metallic Biomaterials. Chapman & Hall.* **1998**, 135–144.

(28) Driessens, F. C. M. Mineral Aspects of Dentistry. *Monogr. Oral Sci.* **1982**, *10*, 1–216.

(29) de Groot, K. Bioceramics of calcium phosphate. *CRC Press.***1983**.

(30) LeGeros, R. Z. Calcium Phosphates in Oral Biology and Medicine. *Basel S. Karger.***1991**.

(31) Elliot, J. C. Structure and Chemistry of the Apatites and Other Calcium Orthophosphates. *Stereochemistry of Organometallic and Inorganic Compounds. Studies in Inorganic Chemistry. Elsevier.***1994**.

(32) Chow, L. C.; Eanes, E. D. *Octacalcium Phosphate. Karger.* **2001**.

(33) Daculsi, G.; Passuti, N. Effect of the macroporosity for osseous substitution of calcium phosphate ceramics. *Biomaterials.* **1990**, *11*, 86 – 87.

(34) Daculsi, G.; Passuti, N.; Martin, S.; Deudon, C.; Legeros, R. Z.; Raher, S. Macroporous calcium phosphate ceramic for long bone surgery in humans and dogs. Clinical and histological study. *J. Biomed. Mater. Res.* **1990**, *24*, 379–396.

(35) Passuti, N.; Daculsi, G.; Rogez, J. M.; Martin, S.; Bainvel, J. V. Macroporous calcium phosphate ceramic performance in human spine fusion. *Clin. Orthop. Relat. Res.* **1989**, *248*, 169–176.

(36) Daculsi, G.; Laboux, O.; Malard, O.; Weiss, P. Current state of the art of biphasic calcium phosphate bioceramics. *J. Mater. Sci.: Mater. Med.* **2003**, *14*, 195–200.

(37) Daculsi, G.; Legeros, R. Z.; Nery, E.; Lynch, K.; Kerebel, B. Transformation of biphasic calcium phosphate ceramics in vivo: Ultrastructural and physicochemical characterization. *J. Biomed. Mater. Res.* **1989**, *23*, 883–894.

(38) Daculsi, G.; LeGeros, R.; Heughebaert, M.; Barbieux, I. Formation of carbonate-apatite crystals after implantation of calcium phosphate ceramics. *Calcif. Tissue Int.* **1990**,*46*, 20–27.

(39) Dorozhkin, S. V. Calcium orthophosphates. *J. Mater. Sci.* **2007**, *42*, 1061–1095.

(40) Xia, W.; Lindahl, C.; Lausmaa, J.; Engvist, H. Biomimetic Hydroxyapatite Deposition on Titanium Oxide Surfaces for Biomedical Application. *Advances in Biomimetics. InTech.* **2011**, 429–453.

(41) Ghanaati, S.; Barbeck, M.; Detsch, R.; Deisinger, U.; Hilbig, U.; Rausch, V.; Sader, R.; Unger, R. E.; Ziegler, G.; Kirkpatrick, C. J. The chemical composition of synthetic bone substitutes influences tissue reactions in vivo : histological and histomorphometrical analysis of the cellular inflammatory response to hydroxyapatite, beta-tricalcium phosphate and biphasic calcium phosphate ceramics. *Biomed. Mater.* **2012**, *7*, 015005 – 015018.

(42) Liu, X.; Chu, P. K.; Ding, C. Surface modification of titanium, titanium alloys, and related materials for biomedical applications. *Mat, Sci. Eng. R.* **2004**, *47*, 49 – 121.

(43) Hanawa, T.; Ukai, H.; Murakami, K.; Asaoka, K. Structure of Surface-Modified Layers of Calcium-Ion-Implanted Ti-6Al-4V and Ti-56Ni. *Mater. T. JIM.* **1995**, *36*, 438–444.

(44) Pham, M. T.; Matz, W.; Reuther, H.; Richter, E.; Steiner, G.; Oswald, S. Ion beam sensitizing of titanium surfaces to hydroxyapatite formation. *Surf. Coat. Tech.* **2000**, *128-129*, 313 – 319.

(45) Nayab, S. N.; Jones, F. H.; Olsen, I. Effects of calcium ion implantation on human bone cell interaction with titanium. *Biomaterials.* **2005**, *26*, 4717 – 4727.

(46) Hanawa, T.; Kamiura, Y.; Yamamoto, S.; Kohgo, T.; Amemiya, A.; Ukai, H.; Murakami, K.; Asaoka, K. Early bone formation around calcium-ion-implanted titanium inserted into rat tibia. *J. Biomed. Mater. Res.* **1997**, *36*, 131–136.

(47) Jinno, T.; Kirk, S. K.; Morita, S.; Goldberg, V. M. Effects of calcium ion implantation on osseointegration of surface-blasted titanium alloy femoral implants in a canine total hip arthroplasty model. *J. Arthroplasty.* **2004**, *19*, 102–109.

(48) Xie, Y.; Liu, X.; Chu, P. K.; Ding, C. Nucleation and growth of calcium phosphate on Ca-implanted titanium surface. *Surf. Sci.* **2006**, *600*, 651 – 656.

(49) Yan, L.; Leng, Y.; Weng, L. T. Characterization of chemical inhomogeneity in plasma-sprayed hydroxyapatite coatings. *Biomaterials.* **2003**, *24*, 2585 – 2592.

(50) Herø, H.; Wie, H.; Jørgensen, R. B.; Ruyter, I. E. Hydroxyapatite coatings on Ti produced by hot isostatic pressing. *J. Biomed. Mater. Res.* **1994**, *28*, 343–348.

(51) Kokubo, T.; Kushitani, H.; Sakka, S.; Kitsugi, T.; Yamamuro, T. Solutions able to reproduce in vivo surface-structure changes in bioactive glass-ceramic A-W3. *J. Biomed. Mater. Res.* **1990**, *24*, 721–734.

(52) Jalota, S.; Bhaduri, S.; Tas, A. Effect of carbonate content and buffer type on calcium phosphate formation in SBF solutions. *J. Mater. Sci.: Mater. Med.* **2006**,*17*, 697–707.

(53) Liu, Y.; Li, J.; Hunziker, E.; de Groot, K. Incorporation of growth factors into medical devices via biomimetic coatings. *Philos. T. Roy. Soc. A* **2006**, *364*, 233–248.

(54) Majid, K.; Tseng, M. D.; Baker, K. C.; Reyes-Trocchia, A.; Herkowitz, H. N. Biomimetic calcium phosphate coatings as bone morphogenetic protein delivery systems in spinal fusion. *Spine J.* **2011**, *11*, 560–567.

(55) Bayraktar, D.; Tas, A. C. Chemical preparation of carbonated calcium hydroxyapatite powders at 37^{o}C in urea-containing synthetic body fluids. *J. Eur. Ceram. Soc.* **1999**, *19*, 2573 – 2579.

(56) Maltsev, S. Ph.D. thesis. Structural elucidation of nanocrystalline biomaterials. University of Leipzig, Germany, **2008** .

(57) Hansson, H.; Lindström, J.; Albrektsson, T.; Branemark, P. Osseointegrated titanium implants: Requirements for ensuring a long-lasting, direct bone-to-implant anchorage in man. *Acta Orthop.***1981** *52*, 155–170.

(58) Buser, D. Titanium for Dental Applications (II): Implants with Roughened Surfaces. *Titanium in Medicine. Engineering Materials. Springer Berlin Heidelberg.* **2001**, 875–888.

(59) Mingalyov, P. G.; Lisichkin, G. V. Chemical modification of oxide surfaces with organophosphorus(V) acids and their esters. *Russ. Chem. Rev.* **2006**, *75*, 541 – 557.

(60) Kenausis, G. L.; Vörös, J.; Elbert, D. L.; Huang, N.; Hofer, R.; Ruiz-Taylor, L.; Textor, M.; Hubbell, J. A.; Spencer, N. D. Poly(L-lysine)-g-Poly(ethylene glycol) Layers on Metal Oxide Surfaces: Attachment Mechanism and Effects of Polymer Architecture on Resistance to Protein Adsorption. *J. Phys. Chem. B* **2000**, *104*, 3298–3309.

(61) Hanson, E. L.; Schwartz, J.; Nickel, B.; Koch, N.; Danisman, M. F. Bonding Self-Assembled, Compact Organophosphonate Monolayers to the Native Oxide Surface of Silicon. *J. Am. Chem. Soc.* **2003**, *125*, 16074–16080.

(62) Gawalt, E. S.; Avaltroni, M. J.; Koch, N.; Schwartz, J. Self-Assembly and Bonding of Alkanephosphonic Acids on the Native Oxide Surface of Titanium. *Langmuir* **2001**, *17*, 5736–5738.

(63) Silverman, B. M.; Wieghaus, K. A.; Schwartz, J. Comparative Properties of Siloxane vs Phosphonate Monolayers on A Key Titanium Alloy. *Langmuir* **2005**, *21*, 225–228.

(64) Marcinko, S.; Fadeev, A. Y. Hydrolytic Stability of Organic Monolayers Supported on TiO_2 and ZrO_2. *Langmuir* **2004**, *20*, 2270–2273.

(65) Dubey, M.; Weidner, T.; Gamble, L. J.; Castner, D. G. Structure and Order of Phosphonic Acid-Based Self-Assembled Monolayers on Si(100). *Langmuir* **2010**, *26*, 14747–14754.

(66) Krise, J.; Stella, V. Prodrugs of phosphates, phosphonates and phosphinates. *Adv. Drug Deliv. Rev.* **1996**, *19*, 287–310.

(67) Mastrangelo, F.; Fioravanti, G.; Quaresima, R.; Vinci, R.; Gherlone, E. Self-Assembled Monolayers (SAMs): Which Perspectives in Implant Dentistry? *J. Biomater. Nanobiotechnol.* **2011**, *2*, 533 – 543.

(68) Barney, R. Ph.D. thesis. Synthesis and biological evaluation of novel phosphonates. University of Iowa. **2010**.

(69) Kanta, A.; Sedev, R.; Ralston, J. The formation and stability of self-assembled monolayers of octadecylphosphonic acid on titania. *Colloids Surf., A* **2006**, *291*, 51 – 58.

(70) Liao, K. Ph.D. thesis. Molecular design to control device behavior of organic electronics. University of Princeton. **2012**.

(71) Paz, Y. Self-assembled monolayers and titanium dioxide: From surface patterning to potential applications. *Beilstein J. Nanotech.* **2011**, *2*, 845–861.

(72) Dey, A.; Bomans, P.; Müller, F.; Will, J.; Frederik, P.; With, G.; Sommerdijk, N. The role of prenucleation clusters in surface-induced calcium phosphate crystallization. *Nat. Mater.* **2010** *9*, 1010–1014.

(73) Beniash, E.; Metzler, R.; Lam, R.; Gilbert, P. Transient amorphous calcium phosphate in forming enamel.*J. Struct. Biol.* **2009** *166*, 133–143.

(74) Mahamida, J.; Aichmayerb, B.; Shimonic, E.; Ziblata, R.; Lib, C.; Siegelb, S.; Parisd, O.; Fratzlb, P.; Weinera, S.; Addadia, L. Mapping amorphous calcium phosphate transformation into crystalline mineral from the cell to the bone in zebrafish fin rays.*P.N.A.S.* **2010** *14*, 6316–6321.

(75) Barrére., F. Ph.D. thesis. Biomimetic Calcium Phosphate Coatings: Physicochemistry and Biological Activity. University of Twente, Saint-Gaudens, France. **2002**.

(76) Mullin., J. W. Nucleation.*Crystallization. Butterworth-Heinemann.***1993**.

(77) Yamashita, K.; Oikawa, N.; Umegaki, T. Acceleration and Deceleration of Bone-Like Crystal Growth on Ceramic Hydroxyapatite by Electric Poling. *Chem. Mater.* **1996**, *8*, 2697–2700.

(78) Tarasevich, B.; Chusuei, C.; Allara, D. Nucleation and Growth of Calcium Phosphate from Physiological Solutions onto Self-Assembled Templates by a Solution-Formed Nucleus Mechanism. *J. Phys. Chem. B* **2003**, *107*, 10367–10377.

(79) Yang, B.; Weng, J.; Li, X.; Zhang, X. The order of calcium and phosphate ion deposition on chemically treated titanium surfaces soaked in aqueous solution. *J. Biomed. Mater. Res.* **1999**, *47*, 213–219.

(80) Gawalt, E. S.; Avaltroni, M. J.; Koch, N.; Schwartz, J. Self-Assembly and Bonding of Alkanephosphonic Acids on the Native Oxide Surface of Titanium. *Langmuir* **2001**, *17*, 5736–5738.

(81) Lim, M. S.; Smiley, K. J.; Gawalt, E. S. Thermally driven stability of octadecylphosphonic acid thin films grown on SS316L. *Scanning* **2010**, *32*, 304–311.

(82) Moraila Martínez, C. L.; Rodríguez Valverde, M. A.; Cabrerizo Vílchez, M. A. The role of the electrostatic double layer interactions in the formation of nanoparticle ring-like deposits at driven receding contact lines. *Soft. Matter.* **2013**, *9*, 1664–1673.

(83) Sin, J. C.; Lam, S. M.; Mohamed, A. R.; Lee, K. T. Degrading Endocrine Disrupting Chemicals from Wastewater by TiO_2 Photocatalysis: A Review. *Int. J. Photoenergy* **2012**, *2012*, 167–190.

(84) Pujari, S. P.; Andel, E. V.; Yaffe, O.; Cahen, D.; Weidner, T.; Rijn, C. J. M. V.; Zuilhof, H. Mono-Fluorinated Alkyne-Derived SAMs on Oxide-Free Si(111) Surfaces:

Preparation, Characterization and Tuning of the Si Workfunction. *Langmuir* **2013**, *29*, 570–580.

(85) Hamd, W.; Kerlidou, M. C.; Fize, J.; Müller, G.; Leyris, A.; Matheron, M.; Courtin, E.; Fontecave, M.; Sánchez, C.; Artero, V.; Robert, C. Dye-sensitized nanostructured crystalline mesoporous tin-doped indium oxide films with tunable thickness for photoelectrochemical applications. *J. Mater. Chem. A* **2013**, *1*, 8217–8225.

(86) Lou, Y.; Yuan, S.; Zhao, Y.; Hu, P.; Wang, Z.; Zhang, M.; Shi, L.; Li, D. Molecular-scale interface engineering of metal nanoparticles for plasmon-enhanced dye sensitized solar cells. *Dalton Trans.* **2013**, *42*, 5330–5337.

(87) Hotchkiss, P. J.; Jones, S. C.; Paniagua, S. A.; Sharma, A.; Kippelen, B.; Armstrong, N. R.; Marder, S. R. The Modification of Indium Tin Oxide with Phosphonic Acids: Mechanism of Binding, Tuning of Surface Properties, and Potential for Use in Organic Electronic Applications. *Acc. Chem. Res.* **2012**, *45*, 337–346.

(88) Addadi, L.; Moradian, J.; Shay, E.; Maroudas, N.; Weiner, S. A chemical model for the cooperation of sulfates and carboxylates in calcite crystal nucleation: relevance to biomineralization. *Proc. Natl. Acad. Sci.* **1987**, *84*, 2732–2736.

(89) Mann, S.; Archibald, D.; Didymus, J.; Douglas, T.; Heywood, B.; Meldrum, F.; Reeves, N. Crystallisation at inorganic-organic interfaces: Biominerals and biomimetic synthesis. *Science* **1993**, *261*, 1286–1292.

(90) Aizenberg, J.; Black, A. J.; Whitesides, G. M. Control of crystal nucleation by patterned self-assembled monolayers. *Nature* **1999**, *398*, 495–498.

(91) Queffélec, C.; Petit, M.; Janvier, P.; Knight, D. A.; Bujoli, B. Surface Modification Using Phosphonic Acids and Esters.*Am. Chem. Soc.* **2012**, *112*, 3777–3807.

(92) Chen, X.; Luais, E.; Darwish, N.; Ciampi, S.; Thordarson, P.; Gooding, J. J. Studies on the Effect of Solvents on Self-Assembled Monolayers Formed from Organophosphonic Acids on Indium Tin Oxide. *Langmuir* **2012**, *28*, 9487–9495.

(93) Earle, W. R.; Schilling, E. L.; Stark, T. H.; Straus, N. P.; Brown, M. F.; Shelton, E. Production of Malignancy in Vitro. IV. The Mouse Fibroblast Cultures and Changes Seen in the Living Cells. *J. Natl. Cancer Inst.* **1943**, *4*, 165–212.

(94) Hanks, J. H.; Wallace, R. E. Relation of Oxygen and Temperature in the Preservation of Tissues by Refrigeration. *Exp. Biol. Med.* **1949**, *71*, 196–200.

(95) Ringer, S. A further Contribution regarding the influence of the different Constituents of the Blood on the Contraction of the Heart. *J. Physiol.* **1883**, *4*, 29–42.

(96) Kokubo, T. Surface chemistry of bioactive glass-ceramics. *J. Non-Cryst. Solids* **1990**, *120*, 138 – 151.

(97) Kokubo, T. Apatite formation on surfaces of ceramics, metals and polymers in body environment. *Acta Mater.* **1998**, *46*, 2519 – 2527.

(98) Kokubo, T.; Kim, H.-M.; Kawashita, M.; Nakamura, T. Review. Bioactive metals: preparation and properties. *J. Mater. Sci.: Mater. Med.* **2004**, *15*, 99–107.

(99) Kim, H. M.; Takadama, H.; Miyaji, F.; Kokubo, T.; Nishiguchi, S.; Nakamura, T. Formation of bioactive functionally graded structure on Ti-6Al-4V alloy by chemical surface treatment. *J. Mater. Sci.: Mater. Med.* **2000**, *11*, 555–559.

(100) Tas, A. C. Synthesis of biomimetic Ca-hydroxyapatite powders at 37°C in synthetic body fluids. *Biomaterials* **2000**, *21*, 1429 – 1438.

(101) Dorozhkina, E. I.; Dorozhkin, S. V. Surface mineralisation of hydroxyapatite in modified Simulated Body Fluid (mSBF) with higher amounts of hydrogencarbonate ions.

Colloids and Surfaces A: Physicochemical and Engineering Aspects **2002**, *210*, 41 – 48.

(102) Oyane, A.; Onuma, K.; Ito, A.; Kim, H.-M.; Kokubo, T.; Nakamura, T. Formation and growth of clusters in conventional and new kinds of Simulated Body Fluids. *J. Biomed. Mater. Res. A* **2003**, *64A*, 339–348.

(103) Greish, Y. E.; Brown, P. W. Characterization of bioactive glass - reinforced HAP - polymer composites. *J. Biomed. Mater. Res.* **2000**, *52*, 687–694.

(104) Rhee, S. H.; Tanaka, J. Effect of citric acid on the nucleation of Hydroxyapatite in a Simulated Body Fluid. *Biomaterials* **1999**, *20*, 2155 – 2160.

(105) Habibovic, P.; Barrére, F.; Van Blitterswijk, C. A.; de Groot, K.; Layrolle, P. Biomimetic Hydroxyapatite Coating on Metal Implants. *J. Am. Ceram. Soc.* **2002**, *85*, 517–522.

(106) Tas, A. C.; Bhaduri, S. B. Rapid coating of Ti6Al4V at room temperature with a calcium phosphate solution similar to 10x simulated body fluid. *J. Mater. Res.* **2004**, *19*, 2742–2749.

(107) Chikara, O. How to prepare the simulated body fluid (SBF) and its related solutions. *Proposed by Kokubo and his colleagues.* http://www.apchem,nagoya-u.ac.jp/ketsu5/SBF/index.html.

(108) Weng, J.; Liu, Q.; Wolke, J.; Zhang, X.; de Groot, K. Formation and characteristics of the apatite layer on plasma-sprayed hydroxyapatite coatings in simulated body fluid. *Biomaterials* **1997**, *18*, 1027 – 1035.

(109) Weng, J.; Liu, Q.; Wolke, J.; Zhang, D.; De Groot, K. The role of amorphous

phase in nucleating bone-like apatite on plasma-sprayed hydroxyapatite coatings in Simulated Body Fluid. *J. Mater. Sci. Lett.* **1997** *16*, 335–337.

(110) Kato, K.; Eika, Y.; Ikada, Y. Deposition of a hydroxyapatite thin layer onto a polymer surface carrying grafted phosphate polymer chains. *J. Biomed. Mater. Res.* **1996**, *32*, 687–691.

(111) Claxton, N. S.; Fellers, T. J.; Davidson, M. W. *Laser Scanning Confocal Microscopy* http://www.olympusconfocal.com/theory/LSCMIntro.pdf

(112) Egerton., R. F. *Physical principles of electron microscopy : an introduction to TEM, SEM, and AEM. Springer.* **2005**.

(113) Reimer, L. *Scanning electron microscopy : physics of image formation and micro-analysis. Springer.* **1998**.

(114) Clarke., A. R. *Microscopy techniques for materials science. CRC Press.***2002**.

(115) Briggs, D.; Grant, J. T. *Surface Analysis by Auger and X-ray Photoelectron Spectroscopy. IM Publications, Chichester.* **2003**.

(116) Briggs, D.; Seah, M. *Practical surface analysis. Auger and XPS. Wiley.* **1990**.

(117) Reiner, T.; Klinger, L. M.; Gotman, I. Biomimetic Calcium Phosphate Growth over Differently Shaped Ti Substrates: Modeling the Effect of Surface Curvature. *Cryst. Growth Des.* **2011**, *11*, 190–195.

(118) Rodríguez-Valverde, M.; Cabrerizo-Vílchez, M.; Rosales-López, P.; Páez-Dueñas, A.; Hidalgo-Álvarez, R. Contact angle measurements on two (wood and stone) non-ideal surfaces. *Colloids Surf. A* **2002**, *206*, 485 – 495.

(119) Montes-Ruiz-Cabello, F. J.; Rodríguez-Valverde, M. A.; Cabrerizo-Vílchez, M. A. Contact Angle Hysteresis on Polymer Surfaces: An Experimental Study. *J. Adhes. Sci. Technol.* **2011**, *25*, 2039–2049.

(120) Krasovitski, B.; Marmur, A. Drops down the hill: Theoretical study of limiting contact angles and the hysteresis range on a tilted plate.*Langmuir* **2005**, *21*, 3881–3885.

(121) Pierce, E.; Carmona, F. J.; Amirfazli, A. Understanding of Sliding and Contact Angle Results in Tilted Plate Experiments. *Colloids Surf.* **2008**, *323*, 73–82.

(122) Fernández-Rodríguez, M. A.; Rodríguez-Valverde, M. A.; Cabrerizo-Vílchez, M. A. Selective desorption of organophosphonates on chemically functionalized titanium by Direct Laser Patterning. *Colloids Surf.* **2013**, *441*, 899–904 .

(123) Fernández-Rodríguez, M. A.; Sánchez-Treviño, A. Y.; Luna-Bertos, E.; Ramos-Torrecillas, J.; García-Martínez, O.; Ruiz, C.; Rodríguez-Valverde, M. A.; Cabrerizo-Vílchez, M. A. Wettability and osteoblastic cell adhesion on ultrapolished commercially pure titanium surfaces: the role of the oxidation and pollution states. *J. Adhes. Sci. Technol.* **2014** .

(124) Billiau, A.; Edy, V. G.; Heremans, H.; Van Damme, J.; Desmyter, J.; Georgiades, J. A.; De Somer, P. Human Interferon: Mass Production in a Newly Established Cell Line, MG-63. *Antimicrob. Agents Chemother.* **1977**, *12*, 11–15.

(125) Rodan, S. B.; Imai, Y.; Thiede, M. A.; Wesolowski, G.; Thompson, D.; Bar-Shavit, Z.; Shull, S.; Mann, K.; Rodan, G. A. Characterization of a Human Osteosarcoma Cell Line (Saos-2) with Osteoblastic Properties. *Cancer Res.* **1987**, *47*, 4961–4966.

(126) Bilbe, G.; Roberts, E.; Birch, M.; Evans, D. B. PCR phenotyping of cytokines,

growth factors and their receptors and bone matrix proteins in human osteoblastlike cell lines.*Bone* **1996**, *19*, 437–445.

(127) Morra, M.; Cassinelli, C. Report on in-vitro cell adhesion to titanium dental implants.

(128) Díaz-Rodríguez, L.; García-Martínez, O.; Arroyo-Morales, M.; Reyes-Botella, C.; Ruíz, C. Phenotype and Phagocytic Capacity of MG-63 Osteosarcoma Line. *Ann. N. Y. Acad. Sci.* **2009**, *1173*, E46–E54.

(129) Gerbettaz, S. B.; Merigo, E.; Rocca, J. P.; Carle, G. F.; Rochet, N. Effects of low-level laser therapy on proliferation and differentiation of murine bone marrow cells into osteoblasts and octeoclasts. *Lasers Surg. Med.* **2009**, *41*, 291–297.

(130) Eriksson, C.; Lausmaa, J.; Nygren, H. Interactions between human whole blood and modified TiO_2-surfaces: influence of surface topography and oxide thickness on leukocyte adhesion and activation. *Biomaterials* **2001**, *22*, 1987 – 1996.

(131) Martin, J. Y.; Schwartz, Z.; Hummert, T. W.; Schraub, D. M.; Simpson, J.; Lankford, J.; Dean, D. D.; Cochran, D. L.; Boyan, B. D. Effect of titanium surface roughness on proliferation, differentiation, and protein synthesis of human osteoblast-like cells (MG63). *J. Biomed. Mater. Res.* **1995**, *29*, 389–401.

(132) Mani, G.; Johnson, D. M.; Marton, D.; Dougherty, V. L.; Feldman, M. D.; Patel, D.; Ayon, A. A.; Agrawal, C. M. Stability of Self-Assembled Monolayers on Titanium and Gold. *Langmuir* **2008**, *24*, 6774–6784.

(133) Adden, N.; Gamble, L. J.; Castner, D. G.; Hoffmann, A.; Gross, G.; Menzel, H. Phosphonic Acid Monolayers for Binding of Bioactive Molecules to Titanium Surfaces. *Langmuir* **2006**, *22*, 8197–8204.

(134) Zorn, G.; Gotman, I.; Gutmanas, E. Y.; Adadi, R.; Salitra, G.; Sukenik, C. N. Surface Modification of Ti45Nb Alloy with an Alkylphosphonic Acid Self-Assembled Monolayer. *Chem. Mater.* **2005**, *17*, 4218–4226.

(135) Viornery, C.; Chevolot, Y.; Léonard, D.; Aronsson, B. O.; Péchy, P.; Mathieu, H. J.; Descouts, P.; Grätzel, M. Surface Modification of Titanium with Phosphonic Acid To Improve Bone Bonding: Characterization by XPS and ToF-SIMS. *Langmuir* **2002**, *18*, 2582–2589.

(136) Atuchin, V. V.; Kesler, V. G.; Pervukhina, N. V.; Zhang, Z. Ti 2p and O 1s core levels and chemical bonding in titanium-bearing oxides. *J. Electron Spectrosc. Relat. Phenom.* **2006**, *152*, 18 – 24.

(137) Demri, B.; Hage-Ali, M.; Moritz, M.; Kahn, J.; Muster, D. X-ray photoemission study of the calcium/titanium dioxide interface. *Appl. Surf. Sci.* **1997**, *108*, 245 – 249.

(138) Fusi, M.; Maccallini, E.; Caruso, T.; Casari, C.; Bassi, A. L.; Bottani, C.; Rudolf, P.; Prince, K.; Agostino, R. Surface electronic and structural properties of nanostructured titanium oxide grown by pulsed laser deposition. *Surf. Sci.* **2011**, *605*, 333 – 340.

(139) Diebold, U.; Shinn, N. D. Adsorption and thermal stability of Mn on TiO_2(110): 2p X-ray absorption spectroscopy and soft X-ray photoemission. *Surf. Sci.* **1995**, *343*, 53 – 60.

(140) Wang, R.; Sakai, N.; Fujishima, A.; Watanabe, T.; Hashimoto, K. Studies of surface wettability conversion on TiO_2 single-crystal surfaces. *J. Phys. Chem. B* **1999**, *103*, 2188–2194.

(141) Wang, L. Q; Baer, D. R; Engelhard, M. H.; Shultz, A. N. The adsorption of liquid and vapor water on TiO_2 (110) surfaces: the role of defects. *Surf. Sci.* **1995**, *344*, 237–250.

(142) Woodbridge, C. M.; Gu, X. J.; Langell, M. A. Extra-atomic relaxation energies and auger parameters of titanium compounds. *Surf. Interface Anal.* **1999**, *27*, 816–824.

(143) Carley, A. F.; Chalker, P. R.; Riviere, J. C.; Roberts, M. W. The identification and characterisation of mixed oxidation states at oxidised titanium surfaces by analysis of X-ray photoelectron spectra. *J. Chem. Soc.* **1987**, *83*, 351–370.

(144) Takadama, H.; Kim, H.-M.; Kokubo, T.; Nakamura, T. XPS study of the process of apatite formation on bioactive Ti-6Al-4V alloy in simulated body fluid. *Sci.Technol. Adv. Mater.* **2001**, *2*, 389–396.

(145) Vanoni, C. Ph.D. thesis. Production and Physiochemical Characterization of Self-Assembled Monolayers on Titanium Surfaces and their Influence on Fibroblast Behavior. Laboratory for Surface Science and Technology, ETH Zürich Faculty of Dentistry, UBC Vancouver. **2000**.

(146) Ni, Y.; Feng, B.; Wang, J.; Lu, X.; Qu, S.; Weng, J. Decyl bis phosphonate - protein surface modification of $Ti-6Al-4V$ via a layer - by - layer technique. *J. Mater. Sci.* **2009**, *44*, 4031–4039.

(147) Kochanowski, A.; Hoene, A.; Patrzyk, M.; Walschus, U.; Finke, B.; Luthringer, B.; Feyerabend, F.; Willumeit, R.; Lucke, S.; Schlosser, M. Examination of the inflammatory response following implantation of titanium plates coated with phospholipids in rats. *J. Mater. Sci.: Mater. Med.* **2011**, *22*, 1015–1026.

(148) Dupraz, A.; Nguyen, T.; Richard, M.; Daculsi, G.; Passuti, N. Influence of a cellulosic

ether carrier on the structure of biphasic calcium phosphate ceramic particles in an injectable composite material. *Biomaterials* **1999**, *20*, 663 – 673.

(149) Yan, C. X.; Cavell, R. G. Gas phase phosphorus (1s and 2p) binding energy and auger shifts in some polarizable phosphorus compounds. *J. Electron Spectrosc. Relat. Phenom.* **1987**, *42*, 49 – 60.

(150) Raj, K. J. A.; Shanmugam, R.; Mahalakshmi, R.; Viswanathan, B. XPS and IR spectral studies on the structure of phosphate and sulphate modified titania - A combined DFT and experimental study. *Indian J. Chem.* **2010**, *49*, 9–17.

(151) Mana, N.; Shahab, F. Mouse bone marrow-derived mesenchymal stem cell response to nanostructured titanium substrates produced by high-pressure torsion *Surf. Inter. Anal.* **2013**, *45*, 619–627.

(152) Cai, K.; Frant, M.; Bossert, J.; Hildebrand, G.; Liefeith, K.; Jandt, K. D. Surface functionalized titanium thin films: Zeta-potential, protein adsorption and cell proliferation. *Colloids Surf. B* **2006**, *50*, 1 – 8.

(153) Sun, Y. T.; Yu, C. Y.; Lin, J. C. Synthesis, Surface Characterization and In Vitro Blood Compatibility Studies of the Self-assembled Monolayers (SAMs) Containing Lipid-like Phosphorylethanolamine Terminal Group. *13th International Conference on Biomedical Engineering. ICBME Proceedings* **2009**, *23*, 1413–1417 .

(154) Ishizaki, T.; Teshima, K.; Masuda, Y.; Sakamoto, M. Liquid phase formation of alkyl- and perfluoro-phosphonic acid derived monolayers on magnesium alloy {AZ31} and their chemical properties. *J. Colloid Interface Sci.* **2011**, *360*, 280 – 288.

(155) Azzaroni, O.; Vela, M. E.; Martin, H.; Creus, A. H.; Andreasen, G.; Salvarezza, R. C. Electrodesorption Kinetics and Molecular Interactions at Negatively Charged Self-

Assembled Thiol Monolayers in Electrolyte Solutions. *Langmuir* **2001**, *17*, 6647–6654.

(156) McIntyre, N. S.; Nie, H. Y.; Grosvenor, A. P.; Davidson, R. D.; Briggs, D. XPS studies of octadecylphosphonic acid (OPA) monolayer interactions with some metal and mineral surfaces. *Surf. Interface Anal.* **2005**, *37*, 749–754.

(157) Fusi, M.; Maccallini, E.; Caruso, T.; Casari, C.; Bassi, A. L.; Bottani, C.; Rudolf, P.; Prince, K.; Agostino, R. Surface electronic and structural properties of nanostructured titanium oxide grown by pulsed laser deposition. *Surf. Sci.* **2011**, *605*, 333 – 340.

(158) Pelavin, M.; Hendrickson, D. N.; Hollander, J. M.; Jolly, W. L. Phosphorus 2p electron binding energies. Correlation with extended Hueckel charges. *J. Phys. Chem.* **1970**, *74*, 1116–1121.

(159) Sosulnikov, M. I. Y. T. XPS study of calcium, strontium, barium and their oxides. *DAN SSSR* **1991**, *317*, 418.

(160) Selvam, P.; Viswanathan, B.; Srinivasan, V. XPS studies of the surface properties of CaNi5. *J. Electron Spectrosc. Relat. Phenom.* **1989**, *49*, 203 – 211.

(161) Silva, C. C.; Pinheiro, A. G.; Miranda, M. A. R.; Góes, J. C.; Sombra, A. S. B. Structural properties of hydroxyapatite obtained by mechanosynthesis*Solid State Sci.* **2003**, *5*, 553–558.

(162) Chusuei, C. C.; Goodman, D. W. Calcium Phosphate Phase Identification Using XPS and Time-of-Flight Cluster SIMS. *Anal. Chem.* **1999**, *71*, 149–153.

(163) Feng, Q. L.; Cui, F. Z.; Wang, H.; Kim, T. N.; Kim, J. O. Influence of solution

conditions on deposition of calcium phosphate on titanium by NaOH-treatment. *J. Cryst. Growth* **2000**, *210*, 735–740.

(164) Wachter, S.; Moseke, C.; Groll, J.; Gbureck, U. Emulsion synthesis of dicalcium phosphate particles for the preparation of calcium phosphate cements with improved compressive strengths and reduced setting times. *BioNanoMat* **2013**, *14*, 81–87.

(165) Park, J.; Lee, Y. K.; Kim, K. M.; Kim, K. N. Bioactive calcium phosphate coating prepared on H2O2-treated titanium substrate by electrodeposition. *Surf. Coat. Technol.* **2005**, *195*, 252–257.

(166) Park, J.; Lee, D. Y.; Yaek Oh, K.; Lee, Y. K.; Kim, K. M.; Kim, K. N. Bioactivity of calcium phosphate coatings prepared by electrodeposition in a modified simulated body fluid. *Mater. Lett.* **2006**, *60*, 2573–2577.

(167) Guehennec, L.; Soueidan, A.; Layrolle, P.; Amouring, Y. Surface treatments of titanium dental implants for rapid osseointegration. *Dent. Mater.* **2007**, *23*, 844–854.

(168) Chen, J.; Yang, X.; Myerson, A. Nucleation on engineered surfaces: Concomitant polymorphism and nano-crystal formation. *Handbook of Industrial Crystallization. Butterworth-Heinemann : Massachusetts.* **2001**.

(169) Rodríguez-Valverde, M. A.; Ramon-Torregrosa, P. J.; Cabrerizo-Vílchez, M. A. Estimation of percolation threshold of acid-etched titanium surfaces using Minkowski functionals. *Microscopy: Science, Technology, Applications and Education* **2010**, *4*, 1978–1983.

(170) Schmäehling, J. Ph.D. thesis. Statistical characterization of technical surface microstructure. University of Heidelberg. **2006**.

(171) Chung, R. J.; Hsieh, M. F.; Panda, R. N.; Chin, T. S. Hydroxyapatite layers deposited from aqueous solutions on hydrophilic silicon substrate. *Surf. Coat. Technol.* **2003**, *165*, 194–200.